

Modelling of fuel droplet heating and evaporation: recent results and unsolved problems

Sergei S Sazhin

*Sir Harry Ricardo Laboratories, Advanced Engineering Centre, School of Computing,
Engineering and Mathematics, University of Brighton, Brighton, BN2 4GJ, UK*

Abstract

The most recent developments in the modelling of heating and evaporation of fuel droplets, the results of which were published in 2014-2016, are reviewed, and the most important unsolved problems are identified. Basic principles of power law and polynomial approximations and the heat balance method for modelling the heating of non-evaporating droplets are discussed. Several approaches to modelling the heating of evaporating droplets, predicting different heating and evaporation characteristics, are compared. New results in modelling heating and evaporation of spheroidal droplets are identified. Basic principles of the Discrete Component (DC) model and its application to biodiesel fuel droplets are summarised. Main ideas of the Multi-dimensional Quasi-discrete (MDQD) model and its applications to Diesel and gasoline fuel droplets are discussed. New developments in gas phase evaporation models for multi-component fuel droplets are presented. A self-consistent kinetic model for droplet heating and evaporation is described. New approaches to the estimation of the evaporation coefficient, including those taking into account quantum-chemical effects, are summarised. Among unsolved problems, the effects of non-spherical droplets, limitations of the ETC/ED model, effects of the interaction between droplets, effects of the moving interface due to evaporation, modelling of complex multi-component droplets, modelling of droplet heating and evaporation in near- and super-critical conditions, development of advanced kinetic and molecular dynamics models and effective approximation of the kinetic effects are discussed.

Keywords:

Droplets, fuel, biodiesel, Diesel, gasoline, heating, evaporation, radiation, kinetic modelling

1. Introduction

The modelling of droplet heating and evaporation has been extensively studied since the beginning of the last century, and the results of these studies have been summarised in numerous reviews and monographs including those published by the author [1, 2]. The main stimulus for these studies has been linked with engineering, environmental and pharmaceutical applications of the results of this modelling. For example, droplet heating and evaporation is an integral part of the processes leading to autoignition of the automotive fuel vapour/air mixture in Diesel engines [3]. The scope of the present review is more limited compared with most previously published reviews and monographs, including [1, 2]. It will focus primarily on the modelling of automotive fuel droplets (although some results may have a much wider range of application) and results not included in monograph [2] (although there will be some overlap with the results presented in this monograph; on some occasions the same topics as in [2] will be considered but using different approaches from those described in [2]). As in [1, 2], some topics related to droplet heating and evaporation will not be covered in this review, including heating and evaporation of droplets during their interaction with walls and the Soret effect (see [4] for a recent review of the latter phenomenon). The analysis of purely experimental papers focused on the study of droplet heating and evaporation and papers focused on multi-dimensional simulations of heated and evaporating sprays will be very limited. This review is intended to be complementary to recently published reviews [5, 6], where the main focus is on ignition and combustion of individual droplets and arrays of droplets, rather than fuel droplet heating and evaporation.

The overall structure of the review is similar to that of [1] and [2]. The approaches to modelling of non-evaporating droplets are reviewed in Section 2. The models for droplet heating and evaporation of mono-component droplets are discussed in Section 3. The heating and evaporation models for more realistic multi-component droplets are reviewed in Section 4. Section 5 focuses on kinetic and molecular dynamics models. The main unsolved problems are summarised and discussed in Section 6.

2. Heating of non-evaporating droplets

This section consists of two parts. Firstly the models described in [2] will be briefly summarised with some of the most recent relevant references added. Secondly, the discussion will focus on new models, not previously described in [2].

2.1. Background research into modelling the heating of non-evaporating droplets

In this subsection the models for heating of non-evaporating droplets, described in [2], are briefly summarised. The original references, mentioned in [2], will not be reproduced in most cases, but relevant new references will be added. Since most of the material presented in this section is described in detail in [2], references to this monograph will be omitted in most cases. As in [1, 2], the models for convective and radiative heating will be described separately.

2.1.1. Convective heating of non-evaporating droplets

The most widely used model for droplet heating, for both non-evaporating and evaporating droplets, is the one based on the assumption that liquid thermal conductivity is infinitely large. This model predicts that there is no temperature gradient inside droplets and the evolution of droplet temperature with time is inferred from the energy balance equation: all heat transferred from the ambient gas is spent on raising droplet temperature. Despite the simplicity of this model, it is almost universally used in research and commercial Computational Fluid Dynamics (CFD) and many original investigations of the problem of droplet heating, including the most recent ones (see Section 3.1).

In the case of stationary spherical droplets, the effects of temperature gradient within them were taken into account based on the solution to the one-dimensional (1D) heat transfer equation, assuming that the heating process is also spherically symmetric. This equation was solved either numerically (e.g. [7]) or analytically (see [2]). Two types of boundary conditions at the surface of the droplet were considered. Firstly, these were Robin boundary conditions assuming that the convection heat transfer coefficient is constant at least during a short time step used in calculations. Secondly, it was assumed that the heat flux approaching the droplet from the gas phase is equal to the one entering the droplet; the former heat flux was obtained based on the solution to the same 1D equation but in the gas phase. It was shown

that the analytical solution to this equation in the liquid phase with the first type of boundary condition is particularly useful for practical applications in Computational Fluid Dynamic codes. This model was implemented into ANSYS Fluent using User-Defined Functions (UDF) [8]. The predictions of ANSYS Fluent with the new model were verified against the results predicted by in-house research code for an n-dodecane droplet heated and evaporated in hot air.

The above-mentioned solution for the stationary droplets was generalised to the case of moving droplets based on the so called Effective Thermal Conductivity (ETC) model. In this model, the effects of droplet movement on the heat transfer processes inside the droplet were taken into account by replacing the liquid thermal conductivity (k_l) with the so called effective thermal conductivity (k_{eff}). These two conductivities were linked by the simple relation $k_{\text{eff}} = \chi_T k_l$, where χ_T is a function of the Peclet number, based on liquid properties and the velocity of liquid near the droplet surface; the values of χ_T varied from 1 for almost stationary droplets to 2.72 for fast moving droplets. This model could not predict the distribution of temperature inside moving droplets, but was shown to be able to predict accurately the average surface temperature of the droplets. It is necessary to emphasise that this model was tested for a very limited range of Peclet numbers and the range of its applicability is still open to question. This fact has been almost universally ignored and the model has been applied to the analysis of droplet heating/cooling without further investigation of this range. In the limiting case where liquid thermal conductivity is infinitely large, the effects of temperature gradient inside droplets and the effect of recirculation can be ignored. In this case the model is known as the Infinite Thermal Conductivity (ITC) model.

As follows from the analysis of the solution to the 1D heat transfer equation for stationary spherical droplets, the dependence of temperature on the distance from the droplet centre is close to parabolic except at the very beginning of the heating process. This allows us to assume from the very beginning that this dependence is parabolic and is characterised by two temperatures: the temperature at the centre of the droplet and the one at the surface of the droplet. The model based on this assumption is widely known as the parabolic model. The values of these temperatures can be obtained from analysis of the energy balance equation at the surface of the droplet. The corrections were introduced to this model to make it applicable both at the beginning of the heating process (when the conventional parabolic model cannot be applied) and at times when the temperature profiles inside

droplets are indeed close to parabolic.

Regardless of the liquid phase model used in the analysis, the heat supplied to the droplets from the gas phase is characterised by convection heat transfer coefficient h . In the case of stationary droplets $h = k_g/R_d$, where k_g is gas thermal conductivity, R_d is the droplet radius (in this case the convective heating/cooling of droplets reduces to purely conductive heating/cooling). In many practically important cases the convective heating of droplets is described by the dimensionless Nusselt number $Nu = 2hR_d/k_g$. In the case of stationary droplets, $Nu = 2$. Several correlations were suggested for the estimation of Nu for the moving droplets. The most widely used correlation can be presented as:

$$Nu = 2 + \beta_c Re^{1/2} Pr^{1/3}, \quad (1)$$

where Re and Pr are Reynolds and Prantl numbers based on gas properties and the relative velocity of droplets. Perhaps the most widely used values of β_c in this correlation are $\beta_c = 0.6$ (Ranz and Marchall correlation) and $\beta_c = 0.552$ (Frossling correlation) (see [9] for the discussion of other correlations based on (1)). The main limitation of (1) is that it predicts unphysical infinitely fast growth of Nu with Re at $Re = 0$. An alternative correlation for Nu was suggested by Clift et al [10]:

$$Nu = 1 + (1 + RePr)^{1/3} \max [1, Re^{0.077}] \quad (2)$$

for $Re \leq 400$. Correlation (2) was recommended in a well known paper by Abramzon and Sirignano [11].

2.1.2. Radiative heating of non-evaporating droplets

The simplest and most widely used model for radiative heating of droplets is based on the assumption that droplets are opaque grey spheres, characterised by emissivity ϵ . In this case, the effect of radiative heating of droplets can be considered as a surface phenomenon and radiative heat fluxes are added to the convective heat fluxes hitting the droplet surface. This approach is used in all Computational Fluid Dynamics (CFD) codes that are known to us.

The problem with this model can be recognised based on the simple observation that most fuels are almost transparent in the visible part of the spectrum (e.g. one can see the bottom of a glass filled with Diesel or gasoline fuel). One might also anticipate that these fuels are at least partially

transparent in the infra-red part of the spectrum. Thus the droplets should be considered semi-transparent rather than grey opaque bodies and one would expect that droplet radiative heating takes place not at their surface (as in the case of convective heating) but via the absorption of thermal radiation penetrating inside the droplets.

The most rigorous approach to the calculation of absorption of external thermal radiation inside fuel droplets is based on the solution to the Maxwell equations, with boundary conditions at the droplet's surface. These boundary conditions are continuity of the normal component of the wave electric field and the jump in its tangential components controlled by the complex index of refraction of the liquid. This solution was obtained in the well-known Mie theory. Direct application of the formulae predicted by this theory is limited by the complexity of relevant calculations, and their incorporation into CFD codes is not feasible. In most practical applications, however, we are primarily interested not in the details of the distribution of thermal radiation absorption inside droplets but in the integral absorption of this radiation in the whole volume of droplets. This integral absorption is characterised by the efficiency factor of absorption Q_a , defined as the ratio of radiative power absorbed in a droplet to the power of thermal radiation illuminating that droplet.

The results of Mie calculations of Q_a for thermal radiation at a certain wave length λ for a typical Diesel fuel were approximated by the expression

$$Q_a = \frac{4n}{(n+1)^2} [1 - \exp(-2\tau_0)], \quad (3)$$

where $n \equiv n_\lambda \approx 1.46$ is the index of refraction, $\tau_0 = a_\lambda R_d$ is the optical thickness of droplets, a_λ is the absorption coefficient, R_d is the droplet radius.

Assuming that the thermal radiation illuminating the droplet is that of a black body and n is constant, the average efficiency factor of absorption of thermal radiation in a certain range of wavelengths \overline{Q}_a was calculated. Using the experimentally measured values of the index of absorption $\kappa_\lambda = a_\lambda \lambda / (4\pi)$ it was found that a reasonably good approximation of \overline{Q}_a in the ranges $5 \mu\text{m} \leq R_d \leq 50 \mu\text{m}$ and $1000 \text{ K} \leq \theta_R \leq 3000 \text{ K}$ can be approximated by the following expression:

$$\overline{Q}_a = a R_d^b, \quad (4)$$

where a and b are polynomials (quadratic function in most cases) of the radiative temperature θ_R (external temperature in the case of optically thin media), R_d is droplet radius in μm .

Approximation (4) appears to be particularly useful for implementation into CFD and research numerical codes (e.g. [12]). In fact it allows us to take into account the effect of semi-transparency of droplets on droplet heating and evaporation without using any extra computer resources. As was shown in [13], the predictions of typical droplet heating and evaporation based on (4) are very close to those based on a more complex model taking into account the difference in thermal radiation absorption in different areas inside droplets. \overline{Q}_a predicted by (4) cannot exceed 1.

Note that classical Mie theory can be applied to spherical droplets only. In the case of illumination of droplets of more complex shapes, including spheroidal droplets, more advanced mathematical tools are needed. These include the generalised Lorenz-Mie theories [14]. The models of droplet radiative heating based on these theories have yet to be developed.

The accuracy of calculation of coefficients a and b strongly depends on the accuracy of measurements of κ_λ . Only very preliminary measurements of this parameter have been performed so far; the errors and reliability of the results have not yet been investigated to the best of my knowledge (the values of κ_λ strongly depend on the type of automotive fuel used in the analysis).

Despite considerable progress in developing models taking into account volumetric absorption of thermal radiation in droplets, more basic models in which the absorption of thermal radiation in droplets is considered as a surface phenomenon are still widely used (e.g. [15, 16]).

2.2. Recent developments in modelling the heating of non-evaporating droplets

2.2.1. Power law and polynomial approximations

Well known limitations of the previously mentioned parabolic model and the complexity of the model based on the rigorous analytical/numerical solutions to the heat transfer equation inside droplets stimulated efforts to develop new models. These were more accurate than the parabolic model and more simple than the models based on the rigorous solutions to the above-mentioned heat transfer equation. One such model, known as the power law approximation, was suggested by Brereton [17] and further investigated by Snegirev [18]. This model is based on the assumption that the temperature profile inside the droplet can be approximated as:

$$T(R) = c_{p0} + c_{pp} \left(\frac{R}{R_d} \right)^p, \quad (5)$$

where R is the distance from the droplet centre, p is the model parameter adjusted to replicate temperature profile at small times, constants c_{p0} and c_{pp} are determined from the values of the heat flux at the surface of the droplets and their average temperature. For $p = 2$, Expression (5) describes the parabolic temperature profile.

To describe the transient heating of a spherical droplet it was assumed that p depends on time. At the initial stage of heating the values of p were shown to be very high (typically in the range 10 to 100), and then these values rapidly decreased with time. Since, the parabolic model is known to describe adequately the temperature distribution inside a droplet in a long time limit, it was assumed that $p \geq 2$ at all times. The power law approximation was shown to describe the heating of non-evaporating droplets in gas with fixed temperature, both in short and long time limits, reasonably accurately.

The model developed in [19] is also based on (5) but with $c_{p0} = T_c$ and $c_{pp} = T_s - T_c$, where T_c and T_w are temperatures at the centre of the droplet and at its surface, respectively. An empirical formula for n was obtained based on the temperature distribution predicted by the rigorous 1D model.

The main limitation of this approximation is that it can predict only monotonic temperature profiles. This limitation was overcome by the so called polynomial approximation, originally suggested in [20] (although for a different problem), and investigated in detail in [18]. In this approximation the temperature profile inside the droplet is presented as:

$$T(R) = c_{p0} + c_{p2} \left(\frac{R}{R_d} \right)^2 + c_{pp} \left(\frac{R}{R_d} \right)^p, \quad (6)$$

where $p > 2$.

Approximation (6) allows one to overcome the above-mentioned limitation of the model based on (5). It was shown that the polynomial approximation can adequately describe non-evaporating droplet heating for arbitrary dependence of the external heat flux on time [18] (this was demonstrated for the cases of stepwise and smooth periodic surface heat flux).

Intrinsic limitation of the power law (including parabolic model) and polynomial approximations stems from the assumption that the temperature profile (either parabolic or higher order polynomial) is instantly established in the whole droplet volume. At the same time, one would expect (and this is confirmed by a rigorous analytical/numerical solution to the heat transfer

problem inside droplets) that initially only a thin layer close to the droplet surface is affected by the external heat supplied to the droplet; then this heat gradually penetrates inside the droplet up to its centre. These processes are taken into account in the model described below.

2.2.2. Heat balance integral method

The heat balance integral method, originally described in [21, 18], is based on the introduction of the thermal layer of thickness $\delta(t)$, which is assumed to be time-dependent in the general case. Inside this layer temperature is approximated by the parabolic profile, and the initial temperature is set unchanged outside the layer:

$$T(t) \begin{cases} c_{h0} + c_{h2} \left(\frac{R - (R_d - \delta)}{R_d} \right)^2, & R_d - \delta < R \leq R_d \\ T_0 & 0 \leq R \leq R_d - \delta \leq R. \end{cases} \quad (7)$$

Expression (7) describes the parabolic model when $\delta = R_d$.

Having found the droplet average temperature from the heat balance equation for the whole droplet, the thickness δ can be estimated by iterations of the following equation:

$$\delta^{(i)} = R_d \sqrt{\frac{2k_{\text{eff}} (T_0 - \bar{T})}{q_s R_d} \left[1 - \frac{1}{2} \frac{\delta^{(i-1)}}{R_d} + \frac{1}{10} \left(\frac{\delta^{(i-1)}}{R_d} \right)^2 \right]^{-1}} \quad (8)$$

where $i = 1, 2, 3, \dots$ is the iteration number, q_s is the heat flux at the droplet surface, k_{eff} is the droplet effective thermal conductivity defined earlier. Note that in the case when $\bar{T} > T_0$ we expect that $q_s < 0$.

In the limiting case when $\delta^{(i)} = \delta^{(i-1)} = R_d$, Equation (8) reduces to:

$$T_0 = \bar{T} + \frac{3q_s R_d}{10k_{\text{eff}}}. \quad (9)$$

This expression coincides with the one predicted by the parabolic model for $R = R_d$. It was shown that the thermal layer expands to $\delta = R_d$ when the Fourier number $\text{Fo} = k_{\text{eff}} t / (c_l \rho_l R_d^2)$, where c_l and ρ_l are specific liquid heat capacity and density respectively, reaches 1/10.

As demonstrated in [18], the heat balance integral method can predict the time evolution of the surface temperature of a non-evaporating droplet much more accurately than the parabolic model. Note, however, that this method,

as well as the power law and polynomial approximations, were verified in [18] based on the analytical solution to the heat transfer equation inside a droplet using the Neumann boundary condition (fixed external heat flux). The limits of applicability of this solution have not been investigated. This could be done based on the comparison of this solution with the solution to this equation using the Robin boundary condition (used in [2]).

All approaches to droplet heating discussed so far are based on the assumption that the heat conduction equation is linear. Possible approaches to solving non-linear heat conduction problems are discussed in [22, 23, 24, 25]. The heat transfer problem in an orthotropic sphere (difference in heat conductivities in different directions was taken into account) was considered in [26]. This generalisation seems not to be relevant to the problem of fuel droplet heating and evaporation. The analysis of non-Fourier models of heat transfer is beyond the scope of this review (see [27, 28, 29, 30, 31, 32, 33] for the details).

Note that the problem of heating of non-evaporating spheroidal droplets, using the Dirichlet boundary conditions, was solved analytically by Niven [34] more than a century ago. There has been no further progress in this direction to the best of my knowledge.

3. Droplet heating and evaporation (mono-component droplets)

As in the case of Section 2, this section will include two parts. Firstly the models described in [2] will be briefly summarised with some of the most recent relevant references added. Secondly, the discussion will focus on new models, not previously described in [2].

3.1. Background research into the modelling of mono-component droplets

In a series of our earlier papers summarised in [2] the effect of evaporation on droplet heating was taken into account by replacing the ambient gas temperature in the analytical solution to the heat transfer equation inside droplets with the so-called effective temperature defined as:

$$T_{\text{eff}} = T_g + \frac{\rho_l L \dot{R}_d}{h}, \quad (10)$$

where the value of \dot{R}_d (the derivative of the droplet radius with respect to time) was taken from the previous time step.

Using the classical Stefan-Fuchs model, the effect of evaporation on the Nusselt number, corresponding to the convection heat transfer coefficient h in (10), for stationary droplets can be described by the following equation:

$$\text{Nu} = \text{Nu}_0 \frac{\ln(1 + B_T)}{B_T}, \quad (11)$$

where $\text{Nu}_0 = 2h_0 R_d k_g = 2$, $h_0 = k_g/R_d$ is the convective heat transfer coefficient for a non-evaporating sphere, B_T is the Spalding heat transfer number

$$B_T = \frac{c_{pv}(T_g - T_s)}{L(T_s) - (|\dot{q}_d|/\dot{m}_d)}, \quad (12)$$

c_{pv} is specific heat capacity of fuel vapour at constant pressure, T_s is the droplet surface temperature, $L(T_s)$ is specific heat of evaporation, $|\dot{q}_d|$ is heat spent on raising droplet internal energy, \dot{m}_d is the droplet evaporation rate (note that $\dot{m}_d \leq 0$).

Using the same above-mentioned Stefan-Fuchs model, the value of \dot{m}_d for stationary droplets can be estimated as:

$$\dot{m}_d = -4\pi R_d D_v \rho_{\text{total}} \ln(1 + B_M), \quad (13)$$

where D_v is the binary diffusion coefficient of fuel vapour in air, $\rho_{\text{total}} = \rho_v + \rho_g$ is the density of the mixture of vapour (subscripts v) and ambient gas (air; subscripts g), B_M is the Spalding mass transfer number defined as

$$B_M = \frac{\rho_{vs} - \rho_{v\infty}}{\rho_{gs}}, \quad (14)$$

where subscript s refers to the surface of the droplet, subscript ∞ refers to ambient conditions. When deriving (13) both the contribution of molecular diffusion of vapour relative to air and bulk motion of vapour together with air (Stefan flow) were taken into account. In the limit when $B_M \ll 1$ the effect of Stefan flow can be ignored. Also, when deriving (13) it was assumed that ρ_{total} does not depend on the distance from the surface of the droplet. This is a reasonable assumption for weakly evaporating droplets when ρ_{total} is controlled mainly by ambient gas density, but is expected to be a serious limitation of the model for strongly evaporating droplets with high surface temperatures. A model in which this assumption is relaxed was developed by Tonini and Cossali [35].

Note that ρ_{vs} is controlled by the droplet surface temperature. This leads to a strong link between Expression (13) and the corresponding equation for droplet heating. A simplified version of Equation (13) for vacuum flash evaporation cooling (without the Stefan flow) is given in [36, 37].

Using the analogy with the convective heat transfer coefficient, we can introduce the convective mass transfer coefficient h_m such that

$$\dot{m}_d = 4\pi R_d^2 h_m (\rho_{g\infty} - \rho_{gs}). \quad (15)$$

Comparing (13) and (15) we can find an explicit expression for h_m :

$$h_m = \frac{h_{m0} \rho_{\text{total}} \ln(1 + B_M)}{\rho_{gs} B_M}, \quad (16)$$

where $h_{m0} = D_v/R_d$. Assuming that $\rho_{gs} \approx \rho_{\text{total}}$ (this is compatible with the assumption that $\rho_{\text{total}} = \text{const}$), we can write:

$$h_m = h_{m0} \frac{\ln(1 + B_M)}{B_M}. \quad (17)$$

Introducing the Sherwood number $\text{Sh} = 2h_m R_d/D_v$ we can rewrite Formula (17) as:

$$\text{Sh} = \text{Sh}_0 \frac{\ln(1 + B_M)}{B_M}, \quad (18)$$

where $\text{Sh}_0 = 2h_{m0} R_d/D_v = 2$ (see the analogy with the Nusselt number for non-evaporating droplets). Using Sh , Expression (13) can be presented in a more compact form:

$$\dot{m}_d = -2\pi R_d D_v \rho_{\text{total}} \text{Sh} B_M. \quad (19)$$

An alternative expression for \dot{m}_d for stationary droplets was derived in the form:

$$\dot{m}_d = -\frac{4\pi k_m R_d}{c_{pv}} \ln(1 + B_T), \quad (20)$$

where k_m is thermal conductivity of the mixture of ambient gas and fuel vapour (in the case of weak evaporation, $k_m \approx k_g$), B_T is defined by (12).

Abramzon and Sirignano [11] suggested that Expressions (11), (13), (18) and (20) could be generalised to the case of moving evaporating droplets using the so called ‘film theory’. The key concepts of this theory are film thicknesses

δ_T and δ_M , the expressions for which were derived from the requirements that the rates of a purely molecular transport by thermal conduction or diffusion through the film must be equal to the actual intensity of the convective heat or mass transfer between the droplet surface and the external flow. Ignoring the Stefan flow for estimation of δ_T and δ_M , this requirement can be presented as:

$$\frac{2}{1 - \frac{R_d}{R_d + \delta_{T0}}} = \text{Nu}_0, \quad \frac{2}{1 - \frac{R_d}{R_d + \delta_{M0}}} = \text{Sh}_0, \quad (21)$$

where subscripts $_0$ at δ_T and δ_M indicate that the effects of the Stefan flow were ignored. Equations (21) can be rearranged to the form presented in [11]:

$$\delta_{T0} = \frac{2R_d}{\text{Nu}_0 - 2}, \quad \delta_{M0} = \frac{2R_d}{\text{Sh}_0 - 2}. \quad (22)$$

For stationary droplets $\text{Nu}_0 = \text{Sh}_0 = 2$. Hence, $\delta_{T0} = \delta_{M0} = \infty$.

The effect of droplet motion on Nu_0 for non-evaporating droplets is described by Eqs. (1) and (2) (subscripts $_0$ in these equations need to be added to indicate non-evaporating droplets). Similar expressions were obtained for Sh_0 [11]:

$$\text{Sh}_0 = 2 + \beta_c \text{Re}^{1/2} \text{Sc}^{1/3}, \quad (23)$$

$$\text{Sh}_0 = 1 + (1 + \text{ReSc})^{1/3} \max[1, \text{Re}^{0.077}] \quad (24)$$

for $\text{Re} \leq 400$, where $\text{Sc} = \nu_m/D_v$, ν_m is the kinematic viscosity of the mixture of gas and vapour. Correlation (24) was recommended in [11].

δ_{T0} and δ_{M0} , defined by (22), can also be considered as thicknesses of the thermal and diffusional boundary layers. One can draw a parallel between these boundary layers and the conventional hydrodynamic laminar boundary layer [38]. It is known that surface blowing results in the thickening of the latter layer. One would expect that a similar thickening takes place for the thermal and diffusion boundary layers due to the effect of the Stefan flow. This thickening was described by parameters F_T and F_M defined as [11]:

$$F_T = \delta_T/\delta_{T0}, \quad F_M = \delta_M/\delta_{M0}. \quad (25)$$

To estimate F_T and F_M , a model problem of the laminar boundary layer flow past an evaporating edge was considered in [11]. The following correlations were suggested in the ranges $0 \leq (B_T, B_M) \leq 20$ and $1 \leq (\text{Pr}, \text{Sc}) \leq 3$:

$$F_{T,M} = (1 + B_{T,M})^{0.7} \frac{\ln(1 + B_{T,M})}{B_{T,M}}. \quad (26)$$

$F_{T,M}$ increases from 1 to 1.285 when $B_{T,M}$ increases from 0 to 8, and remains almost constant for larger $B_{T,M}$.

Using film theory, we would expect that an increase in the film thicknesses, described by (25) and (26), would lead to a corresponding decrease in Nu_0 and Sh_0 . The new decreased values of Nu_0 and Sh_0 , called ‘modified’ Nusselt and Sherwood numbers in [11] (Nu^* and Sh^*), were found from (21), in which δ_{T0} and δ_{M0} were replaced with $\delta_T = \delta_{T0}F_T$ and $\delta_M = \delta_{M0}F_M$:

$$\frac{2}{1 - \frac{R_d}{R_d + F_T \delta_{T0}}} = \text{Nu}^*, \quad \frac{2}{1 - \frac{R_d}{R_d + F_M \delta_{M0}}} = \text{Sh}^*. \quad (27)$$

Equations (27) can be rearranged to the form presented in [11]:

$$\text{Nu}^* = 2 + \frac{\text{Nu}_0 - 2}{F_T}, \quad \text{Sh}^* = 2 + \frac{\text{Sh}_0 - 2}{F_M}. \quad (28)$$

Note that while Nu_0 and Sh_0 have clear physical meaning as the Nusselt number for non-evaporating droplets, and Sherwood number for evaporating droplets in the limit $B_M \ll 1$ (the contribution of the Stefan flow can be ignored), the physical meaning of Nu^* and Sh^* is less clear. These parameters allow us to present the expressions for the actual Nusselt and Sherwood numbers for moving and evaporating droplets as:

$$\text{Nu} = \text{Nu}^* \frac{\ln(1 + B_T)}{B_T}, \quad \text{Sh} = \text{Sh}^* \frac{\ln(1 + B_M)}{B_M}. \quad (29)$$

The introduction of Nu^* and Sh^* allows one to generalise Expressions for \dot{m}_d , given by (13) and (20), to [11]:

$$\dot{m}_d = -2\pi R_d D_v \rho_{\text{total}} \text{Sh}^* \ln(1 + B_M), \quad (30)$$

$$\dot{m}_d = -\frac{2\pi k_m R_d}{c_{pv}} \text{Nu}^* \ln(1 + B_T). \quad (31)$$

After dividing both sides of (30) by the corresponding sides of (31) the following relation between B_T and B_M can be obtained [11]:

$$B_T = (1 + B_M)^\varphi - 1, \quad (32)$$

where

$$\varphi = \left(\frac{c_{pv}}{c_{pg}} \right) \left(\frac{\text{Sh}^*}{\text{Nu}^*} \right) \frac{1}{\text{Le}}, \quad (33)$$

$Le = k_m / (D_v \rho_{\text{total}} c_{pg})$ is the gas Lewis number but with thermal conductivity equal to that of a mixture of air and vapour and density equal to that of a mixture of air and vapour.

Possible modification of the model described above was suggested in [39] (see Section 4.2.3 of [2]). The evaporation process leads to the inward movement of the droplet surface (liquid/vapour interface). The effect of this movement on droplet heating was considered in a series of our papers summarised in Section 4.4 of [2]. The physical nature of this effect seems to be similar to that of the exchange of energy when a ball hits the back of a moving lorry. The quantitative characteristics of this exchange at the molecular level have yet to be investigated.

The model based on the combination of the Abramzon and Sirignano model for the gas phase [11] and the analytical solution to the heat transfer equation for the liquid phase was extensively validated mainly based on the experimental results obtained at the University of Lorraine (one of the latest comparisons is presented in [40]).

Note that despite considerable progress in developing advanced models of droplet heating and evaporation, the simplest models based on the assumption that there is no temperature gradient inside droplets are still widely used in the modelling of these processes (e.g. [41, 42, 43, 44, 45, 46, 47, 48, 49, 50, 51]). Some authors used an even simpler droplet evaporation model based on the assumption that droplet temperature does not change over time, which leads to the well known d^2 -model (e.g. [52, 53]). In [54] a modified version of Eq. (13) was used assuming that $k_g/C_{pg} = \rho_{\text{total}} D_v$ and $c_{pg} = c_{pv}$. The validity of these assumptions is far from obvious.

3.2. Various new approaches to modelling the heating of evaporating droplets

Remembering (12) and (32), one can obtain the heat rate supplied to the droplet to raise (or reduce) its temperature (internal energy) in the form:

$$\dot{q}_d = -\dot{m}_d \left[\frac{c_{pv}(T_g - T_s)}{B_T} - L(T_s) \right] = -\dot{m}_d \left[\frac{c_{pv}(T_g - T_s)}{(1 + B_M)^\varphi - 1} - L(T_s) \right], \quad (34)$$

where $\dot{q}_d > 0$ when the droplet is heated. We restrict our analysis to stationary droplets for the time being for which $\varphi = \left(\frac{c_{pv}}{c_{pg}} \right) \frac{1}{Le}$.

Since the pioneering paper by Abramzon and Sirignano [11], Expression (34) has been widely used for modelling the heating of evaporating droplets, in combination with Equation (13) for modelling droplet evaporation. An

obvious limitation of Expression (34) is that the value of \dot{q}_d is not affected by the thermal conductivity of liquid, which seems to contradict the physical nature of \dot{q}_d , as discussed later in the paper.

An alternative approach to the calculation of \dot{q}_d could be based on the analysis of temperature distribution inside droplets, inferred from the direct analysis of convective heating of evaporated droplets (see [2] for the details). This approach is restricted to the case when liquid thermal conductivity is finite, which can be expected for any realistic liquid. Using this approach, \dot{q}_d can be estimated as

$$\dot{q}_d = 4\pi R_d^2 k_l \left. \frac{\partial T}{\partial R} \right|_{R=R_d-0}, \quad (35)$$

where $T(R)$ can be inferred from the analytical solution to the heat transfer equation inside the droplet for a fixed convection heat transfer coefficient; this solution was extensively discussed in [2]. Having substituted this solution into (34) we obtain:

$$\begin{aligned} \dot{q}_d = 4\pi R_d k_l \sum_{n=1}^{\infty} \left\{ q_n \exp[-\kappa_R \lambda_n^2 t] - \frac{\sin \lambda_n}{\|v_n\|^2 \lambda_n^2} \mu_0(0) \exp[-\kappa_R \lambda_n^2 t] - \right. \\ \left. - \frac{\sin \lambda_n}{\|v_n\|^2 \lambda_n^2} \int_0^t \frac{d\mu_0(\tau)}{d\tau} \exp[-\kappa_R \lambda_n^2 (t - \tau)] d\tau \right\} [-1 - h_0] \sin \lambda_n, \end{aligned} \quad (36)$$

where λ_n are solutions to the equation:

$$\lambda \cos \lambda + h_0 \sin \lambda = 0, \quad (37)$$

$$\begin{aligned} \|v_n\|^2 &= \frac{1}{2} \left(1 - \frac{\sin 2\lambda_n}{2\lambda_n} \right) = \frac{1}{2} \left(1 + \frac{h_0}{h_0^2 + \lambda_n^2} \right), \\ q_n &= \frac{1}{R_d \|v_n\|^2} \int_0^{R_d} \tilde{T}_0(R) \sin \left[\lambda_n \left(\frac{R}{R_d} \right) \right] dR, \\ \kappa_R &= \frac{k_l}{c_l \rho_l R_d^2}, \quad \mu_0(t) = \frac{h T_g(t) R_d}{k_l}, \end{aligned}$$

$h_0 = (h R_d / k_l) - 1$, $\tilde{T}_0(R) = R T_{d0}(R) / R_d$. The solution to Equation (37) gives a set of positive eigenvalues λ_n numbered in ascending order, ($n = 1, 2, \dots$).

Once the value of \dot{q}_d has been found, the evaporation rate can be found from Equation (20). Remembering the definition of B_T this equation can be rewritten as:

$$\dot{m}_d = -\frac{4\pi k_g R_d}{c_{pv}} \ln \left(1 + \frac{c_{pv}(T_g - T_s) \dot{m}_d}{L(T_s) \dot{m}_d - \dot{q}_d} \right). \quad (38)$$

Thus we have two approaches to modelling heating and evaporation of stationary droplets. The first one is based on Equations (13) and (34) (conventional approach originally suggested in [11], Model 1), and the approach based on Equations (36) and (38) (Model 2). In what follows a comparative analysis of these approaches will be presented following [55].

Expression (36) is applicable to any time step with $t = 0$ referring to the beginning of the time step; t refers to the end of the time step. The values of \dot{q}_d at the beginning of each time step are equal to the values of \dot{q}_d at the end of the previous time step or the start of the heating process. Hence, without loss of generality we can assume that $t = 0$ in Expression (36). The values of \dot{q}_d predicted by Expression (36) were shown to coincide within the accuracy of plotting with those predicted by Expression (35) using the numerical differentiation of the temperature predicted by the analytical solution to the heat transfer equation inside the droplet.

Note that in contrast to Expression (13), Equation (38) is a non-linear equation for \dot{m}_d . It has two solutions, $\dot{m}_d = 0$ (non-evaporating droplet) and $\dot{m}_d < 0$ (evaporating droplet), when

$$\frac{4\pi k_g R_d (T_g - T_s)}{\dot{q}_d} > 1, \quad (39)$$

and only one trivial solution $\dot{m}_d = 0$ (non-evaporating droplet) when Condition (39) is not satisfied.

In the limiting case when $B_T \ll 1$, Equation (38) has the analytical solution:

$$\dot{m}_d = \frac{1}{L(T_s)} [\dot{q}_d - 4\pi k_g R_d (T_g - T_s)]. \quad (40)$$

This solution does not have physical meaning unless Condition (39) is satisfied. Expression (13) can still be used in this approach if

$$B_M = (1 + B_T)^{1/\varphi} - 1. \quad (41)$$

All thermodynamic and transport properties for liquid and gas were assumed constant during each time step but their changes from one time step to another due to the corresponding changes in temperature were taken into account. The effects of thermal swelling were taken into account.

The model was applied to the analysis of heating of an evaporating n-dodecane droplet in air at a pressure of 30 bar and temperature 700 K. Thermodynamic and transport properties of n-dodecane are mainly taken

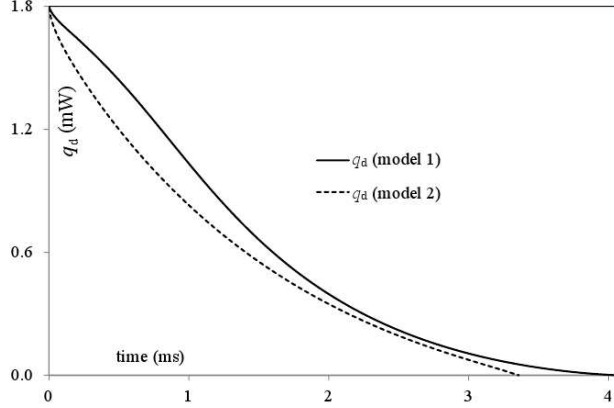


Figure 1: Plots of \dot{q}_d versus time predicted by Model 1 and Model 2 for an evaporating n-dodecane droplet heated in air at a pressure of 30 bar and temperature 700 K. The initial droplet temperature and radius are assumed to be equal to 300 K and 10 μm respectively. Reprinted from International Communications in Heat and Mass Transfer, Volume 57, Sazhin et al., Two approaches to modelling the heating of evaporated droplets, Pages 353-356, Copyright Elsevier (2014).

to be the same as in [56], except for the diffusion coefficient for n-dodecane vapour in air which was taken from [13]. The initial droplet temperature and radius are assumed equal to 300 K and 10 μm respectively. The results predicted by Model 2 were compared with those predicted by Model 1. In both cases the finite thermal conductivity of liquid was taken into account.

The values of \dot{q}_d , predicted by these two approaches are shown in Fig. 1. Note that at the very final stages of droplet evaporation the values of \dot{q}_d predicted by Model 2 became negative (although close to zero) which eventually led to the situation where Equation (38) had no real solutions. To avoid this situation the distribution of temperature inside droplets was frozen at the moment when $\dot{q}_d = 0$. Also, at the very final stage of droplet evaporation, the predicted droplet temperature could approach the critical temperature and even exceed it. This was partly remedied by assuming that once T_{eff} has reached its minimal value it remains at this level until the droplet fully evaporates. These assumptions are expected to produce minor effects on the predicted surface temperatures and radii of droplets which are not important for practical applications. The problems with modelling

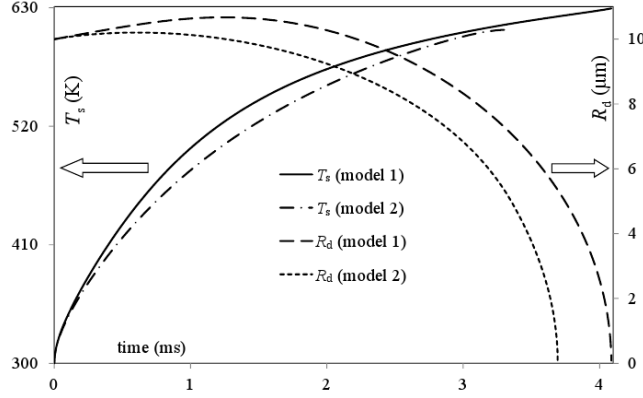


Figure 2: The same as in Fig. 1 but for droplet surface temperatures (T_s) and radii (R_d). Reprinted from International Communications in Heat and Mass Transfer, Volume 57, Sazhin et al., Two approaches to modelling the heating of evaporated droplets, Pages 353-356, Copyright Elsevier (2014).

droplet heating and evaporation at the final stages of droplet evaporation when $dR_d/dt \rightarrow \infty$ were recognised in our previous studies (e.g. [57]).

As one can see from Fig. 1, the time dependence trends for \dot{q}_d , predicted by both approaches, are rather similar, but the actual values of \dot{q}_d are noticeably different. This difference in the values of \dot{q}_d leads to rather large differences in the corresponding values of droplet radii and surface temperatures versus time, as shown in Fig. 2. As follows from the latter figure, Model 2 predicts lower droplet surface temperatures and shorter evaporation times than Model 1. Lower droplet surface temperatures predicted by Model 2 compared with Model 1 are expected to lead to lower values of the heat fluxes at the surface of the droplet. This is consistent with the predicted values of \dot{q}_d shown in Fig. 1. Similar trends in time evolution of the parameters predicted by both models allow us to use them for qualitative analysis of droplet evaporation, but their reliability for quantitative analysis of the processes remains unclear. One of the reasons for the differences between the predicted results might lie in the fact that both approaches to the calculation of the evaporation rate are based on the quasi-steady-state approximation. The limitations of this approximation for the case of non-evaporating droplet heating were discussed in [2].

The model suggested and developed in [58, 59] is essentially based on the coupled solutions to heat and mass transfer equations in the gas and liquid phase for stationary droplets (this model was called by the authors ‘a complete model’). This problem is rather similar to the one considered in [2] (see Section 3.1.1). In contrast to [2], the focus of the analysis of [58, 59] was not on finding and analysing the solutions to the coupled equations, but on finding simplified solutions to these equations in some limiting cases. A simplified version of the complete model, called the quasi-homogeneous model, was developed using an asymptotic analysis in the limiting case when the so called homogenization time ($\tau_{\text{hom},l} = R_d^2/\alpha_l$, R_d is the droplet radius, α_l is liquid diffusivity) is much less than the droplet evaporation time [59]. The quasi-homogeneous model was further simplified to the fully quasi-steady-state model (time dependence of the liquid surface temperature can be ignored). A simple formula was suggested to evaluate the relative difference between the droplet evaporation times predicted by the complete model and those predicted by the fully quasi-steady-state model. The application of this formula together with the fully quasi-steady-state model enables one to estimate the droplet evaporation time given by the complete model.

The models discussed so far have focused only on spherical droplets. Recent developments in modelling the heating and evaporation of spheroidal droplets are discussed in the next section.

3.3. Heating and evaporation of spheroidal droplets

The models described so far were based on the assumption that droplets are perfect spheres. At the same time the shapes of most actually observed droplets in engineering and environmental applications are far from spherical ([60, 61]. It is not possible to develop a general theory for heating and evaporation of droplets of arbitrary shapes except by performing numerical modelling for specific shapes. In most cases the effects of non-sphericity of droplets have been investigated assuming that droplet shapes can be approximated by prolate or oblate spheroids.

The heat conduction equation inside a spheroidal body (droplet) was first (to the best of my knowledge) solved analytically more than 135 years ago [34]. This solution, however, turned out to be too complex for most practical applications. In most cases this problem (and the related problem of mass transfer inside the body) has been investigated based on the numerical solutions to the heat transfer (and mass diffusion) equations [62, 63].

The problem of heat/mass transfer inside spheroidal bodies, considered in the above-mentioned papers, is complementary to the problem of heat/mass transfer from/to ambient fluid (gas) to/from a spheroidal body, taking into account the relative velocity between the gas and the body, in the general case. The latter problem has been considered in numerous papers based on the numerical solutions to momentum and heat transfer equations in the ambient fluid (gas) in the ellipsoidal coordinate system. The analysis of [64, 65, 66, 67, 68] was based on the assumption that the body surface was fixed. Juncu [69] took into account changes in body temperature with time, while assuming that there is no temperature gradient inside the body (the thermal conductivity of the body was assumed infinitely high).

These approaches are equally applicable to solid bodies and droplets. In the case of droplets, however, apart from heating, the evaporation processes should also be taken into account in the general case. Grow [70] was perhaps the first to solve the problem of heat and mass transfer in the vicinity of spheroidal particles assuming that their relative velocities are equal to zero, although she considered coal chars rather than droplets. One of the main limitations of this paper is that both mass and heat transfer equations were presented in the form of Laplace equations, which implies that the effects of Stefan flow from the surface of the particles were ignored. The latter effects were taken into account in the exact solutions to the mass and heat transfer equations in the gas phase around a spheroidal droplet suggested in [71]. In that paper it was assumed that the temperatures at all points at the surface of a droplet are the same and constant, and the droplet's shape remains spheroidal. A combined problem of spheroidal droplet heating and evaporation, similar to the one studied in [71], was considered in [72]. As in [71], the authors of [72] based their analysis on the solution to the species conservation equation in the gas phase and assumed that the thermal conductivity of droplets is infinitely large. In contrast to [71], the authors of [72] took into account the relative velocities of droplets, assuming that the dependencies of the Nusselt and Sherwood numbers on the Reynolds and Prantle numbers are the same as those for the spherical droplets. Also, they took into account the time dependence of droplet temperatures and sizes, although their analysis focused on oblate droplets only.

As follows from a brief overview of the models described above, the general problem of heating and evaporation of spheroidal droplets is far from resolved. We believe, however, that the results presented in [71] could be considered a starting point for constructing a model at least for spheroids which are

only slightly deformed. The main ideas of the model described in [71] are summarised below.

3.3.1. The Tonini and Cossali model (spheroidal droplets)

The analysis of [71] focused on exact solutions to the mass and heat transfer equations in the gas phase around a spheroidal droplet. The droplet was assumed to be a mono-component droplet and the following steady-state equation for the vapour mass fraction (Y_v) was solved in the gas phase:

$$\nabla (\rho_{\text{tot}} \mathbf{U} Y_v - \rho_{\text{tot}} D_v \nabla Y_v) = 0, \quad (42)$$

where ρ_{tot} is the density of the mixture of vapour and ambient gas, \mathbf{U} is the Stefan velocity of the mixture of vapour and air, D_v is the diffusion coefficient of vapour in air.

Eq. (42) was solved in ellipsoidal coordinates ξ, u, φ remembering that all processes are axially symmetric; z was chosen as the axis of symmetry. In this case these coordinates are linked with Cartesian coordinates x, y, z by the following equations:

$$\left. \begin{aligned} x &= a\Phi_-(\xi) \sin(u) \cos(\varphi) \\ y &= a\Phi_-(\xi) \sin(u) \sin(\varphi) \\ x &= a\Phi_+(\xi) \cos(u) \end{aligned} \right\} \quad (43)$$

where

$$\Phi_{\pm}(\xi) = \frac{e^{\xi} \pm s(\varepsilon)e^{\xi}}{2}, \quad s(\varepsilon) = \text{sign}(\varepsilon - 1), \quad \varepsilon = a_z/a_r,$$

$2a_z$ and $2a_r$ are the sizes of the spheroid along and perpendicular to z -axis, respectively ($\varepsilon > 1$ and $s = 1$ for prolate spheroids, $\varepsilon < 1$ and $s = -1$ for oblate spheroids).¹ Assuming that the volume of a spheroid is equal to that of a perfect sphere of radius R_0 , the following relations were obtained, valid for both prolate and oblate spheroids:

$$\xi_0 = \ln \sqrt{\frac{\varepsilon^s + 1}{\varepsilon^s - 1}}; \quad a = R_0 \frac{|1 - \varepsilon^2|^{1/2}}{\varepsilon^{1/3}}, \quad (44)$$

where $\xi = \xi_0$ corresponds to the surface of the spheroid.

¹Note that in [67, 68] prolate and oblate spheroids were defined as those with $\varepsilon < 1$ and $\varepsilon > 1$ respectively; it seems that the same definition is used in Fig. 1 of [66]

The authors of [71] solved Eq. (42) assuming that the values of Y_v and all other scalar properties are the same along the whole surface of the droplet and equal to $Y_v = Y_{vs}$, and Stefan velocity and diffusive fluxes are perpendicular to the droplet surface ($\mathbf{U} = (U_\xi, 0, 0)$). These assumptions allowed them to simplify Eq. (42) to:

$$\rho_{\text{tot}} U_\xi \frac{dY_v}{d\xi} = \frac{D_v}{aS^2} \frac{d}{d\xi} \left[\rho_{\text{tot}} \Phi_-(\xi) \frac{dY_v}{d\xi} \right], \quad (45)$$

where

$$S^2 \equiv S^2(\xi, u) = \Phi_-(\xi) [\Phi_-^2(\xi) \cos^2 u + \Phi_+^2(\xi) \sin^2 u]^{1/2}. \quad (46)$$

When deriving Eq. (45) the mass conservation equation

$$\frac{d}{d\xi} [S^2 \rho_{\text{tot}} U_\xi] = 0, \quad (47)$$

where S^2 is defined by Eq. (46), was used.

Note that Eq. (45) is different from the one on which the analysis of [72] was based (see their Eq. (10)). The latter equation is the Laplace-type equation which is valid only when the Stefan flow is ignored.

Note that, although in the original paper [71] Eq. (45) was derived under the assumption that Y_v is the same along the whole surface of the droplet, it can be shown that this equation remains valid under an alternative assumption, that the directions of the gradients of Y_v are close to the ξ -directions. This assumption is expected to be valid in the case when the sphericity of the droplet ε is reasonably close to 1. The original assumption that Y_v is the same along the whole surface of the droplet implied that there is no temperature gradient at the surface of the droplet, which follows from another assumption made by [71] that droplet thermal conductivity is infinitely large.

Assuming the validity of the condition $\rho_{\text{tot}} = \rho_v + \rho_a = \text{const}$, and that at large distances from the droplet $Y_v = Y_{v\infty} = \text{const}$, the solutions to Eqs. (45) and (47) were obtained as [71]:

$$Y_v = 1 - (1 - Y_{vs}) \begin{cases} \left(\frac{1 - Y_{v\infty}}{1 - Y_{vs}} \right)^{\frac{\arctan e^\xi - \arctan e^{\xi_0}}{(\pi/2) - \arctan e^{\xi_0}}} & \text{oblate} \\ \left(\frac{1 - Y_{v\infty}}{1 - Y_{vs}} \right)^{1 - \frac{\ln(e^\xi + 1) - \ln(e^\xi - 1)}{\ln(e^{\xi_0} + 1) - \ln(e^{\xi_0} - 1)}} & \text{prolate} \end{cases} \quad (48)$$

$$\frac{d\dot{m}_{\text{ev}}}{dA} = \rho_{\text{tot}} U_\xi(\xi_0) = \frac{\rho_{\text{tot}} D_v}{R_0} \Gamma(\varepsilon) \ln \frac{1 - Y_{v\infty}}{1 - Y_{vs}}, \quad (49)$$

where

$$\Gamma(\varepsilon) = \frac{|1 - \varepsilon^2|^{1/2}}{\varepsilon^{1/3}} \begin{cases} \frac{1}{\pi - 2 \arctan\left(\sqrt{\frac{1+\varepsilon}{1-\varepsilon}}\right)} & \text{oblate} \\ \frac{1}{\ln\left(\sqrt{\frac{1+\varepsilon}{\varepsilon-1}}+1\right) - \ln\left(\sqrt{\frac{1+\varepsilon}{\varepsilon-1}}-1\right)} & \text{prolate} \end{cases} \quad (50)$$

$\frac{d\dot{m}_{ev}}{dA}$ is the evaporation flux. The derivation of Eq. (49) was based on the assumption that ξ -directions near the droplet surface are close to the radial directions, which is satisfied for spheroids with ε reasonably close to 1 (the validity of this is assumed throughout the whole review).

In the original paper [71] it was assumed that $Y_{vs} = \text{const}$. In the general case these formulae could be applied to the case when $Y_{vs} = Y_{vs}(u)$ provided that the spheroid can be considered as a slightly deformed sphere (ε is close to 1). This implies that the evaporation flux can be a function of u in the general case, while in the original paper [71] this flux did not depend on u . Also, in the original paper [71] the expression for the evaporation rate, rather than the evaporation flux was presented. This evaporation rate could be found only in the case when the temperatures at all point on the droplet surface are the same. The validity of Expression (49) does not depend upon this assumption.

The assumption $\rho_{\text{tot}} = \rho_v + \rho_a = \text{const}$ was relaxed in [35]. The generalisation of the approach suggested in [35] to the case of spheroidal droplets has not been considered to the best of my knowledge.

The analysis of Eq. (42) in [71] was complemented by the analysis of the heat transfer equation:

$$\rho_{\text{tot}} \mathbf{U} c_p \nabla T = k_g \nabla^2 T, \quad (51)$$

where c_p is the specific heat capacity at constant pressure and k_g is the thermal conductivity of gas (mixture of fuel vapour and air in the general case).

In [71], Eq. (51) was solved using assumptions and boundary conditions similar to those which were used for the solution to Eq. (42). Namely, it was assumed that the temperatures at all points along the droplet surface are the same and the temperature gradients are perpendicular to the surfaces $\xi = \text{const}$. These assumptions, alongside the assumption that the temperature as a large distance from the droplet is equal to $T_\infty = \text{const}$, allowed the authors of [71] to simplify Eq. (51) and present its solution as:

$$T = \frac{T_\infty - T_s}{1 - \eta} [\eta^{\zeta(\xi, \varepsilon)} - \eta] + T_s, \quad (52)$$

where

$$\eta = \exp \left[-\frac{1}{\text{Le}} \ln \frac{1 - Y_{v\infty}}{1 - Y_{vs}} \right], \quad (53)$$

$$\zeta(\xi, \varepsilon) = \begin{cases} \frac{\pi - 2 \arctan(e^\xi)}{\pi - 2 \arctan\left(\sqrt{\frac{1+\varepsilon}{1-\varepsilon}}\right)} & \text{oblate} \\ \frac{\ln(e^\xi + 1) - \ln(e^\xi - 1)}{\ln(\varepsilon + \sqrt{\varepsilon^2 - 1})} & \text{prolate} \end{cases} \quad (54)$$

$\text{Le} = k_g / (\rho_{\text{tot}} c_p D_v)$ is the Lewis number.

If the assumption that $T_s = \text{const}$ made in [71] is relaxed then η becomes a function of u in the general case (recall that $Y_{vs} = Y_{vs}(T_s)$).

Expression (52) allows us to find the local convective heat transfer coefficient h based on the following formula:

$$h = -\frac{\left| -k_g \nabla T|_{\xi=\xi_0} \right|}{|T_\infty - T_s|}. \quad (55)$$

Although the value of h was not explicitly calculated in [71], this calculation follows in a straightforward way from a previous analysis by these authors. Hence, we consider this calculation as part of the Tonini and Cossali model. Having substituted Expression (52) into Formula (55) the following expression for h can be obtained:

$$h = \frac{k_g \eta}{R_0 (1 - \eta)} \begin{cases} \frac{\varepsilon^{1/3}}{\left[\pi - 2 \arctan\left(\sqrt{\frac{1+\varepsilon}{1-\varepsilon}}\right) \right] \sqrt{\left(\frac{1}{1-\varepsilon^2} - \sin^2 u\right)}} & \text{oblate} \\ \frac{\varepsilon^{1/3}}{\left[\ln(\varepsilon + \sqrt{\varepsilon^2 - 1}) \right] \sqrt{\left(\frac{1}{\varepsilon^2 - 1} - \sin^2 u\right)}} & \text{prolate} \end{cases} \quad (56)$$

where η is defined by Expression (53).

It can be shown that the coordinate u is linked with $\theta = \arctan \left[\sqrt{x^2 + y^2} / z \right]$ by the following relation;

$$\tan u = \varepsilon \tan \theta \quad (57)$$

valid for both prolate and oblate spheroids.

The model described above was generalised to the case of oscillating droplets under the assumption that the process can be considered quasi-steady-state [73]. The model was able to predict the instantaneous and average mass and heat transfer rates over an oscillation period. Both these

rates were functions of the oscillating frequency and droplet deformation. The results were compared with the predictions by the approximate model described by Mashayek [74]. The model was able to capture different evaporating mechanisms from oblate and prolate drops. It predicted an increment in the average evaporation rate and heat transfer rate due to droplet oscillation, of up to 20% for a maximum excess surface area equal to 100%. The model was shown to be valid for small, highly volatile liquid drops, evaporating in gas at high temperatures.

The results of the generalisation of the model described above to the case of triaxial ellipsoidal droplets are presented in [75]. In this paper, a new analytical model for heat and mass transfer from deformed droplets was developed, based on the solutions to the species and energy conservation equations under steady-state conditions. Explicit equations to predict the vapour mass fraction and temperature distribution, the local vapour flux, and heat and evaporation rates were suggested. It was shown that the droplet deformation enhances both the total and local mass and heat transfer. The evaporation rate from deformed droplets, having the same volume and surface, was shown to be at a maximum for the prolate droplet and at a minimum for the oblate droplet, while intermediate values of evaporation rate were found for triaxial ellipsoidal droplets. For this class of droplet shapes the local vapour flux was found to be proportional to the fourth root of the surface Gaussian curvature.

Purely numerical investigation of fluid flow and heat transfer from heated spheroids was conducted in [76].

The problem of heating and evaporation of non-spherical droplets in homogeneous gas is complementary to the problem of heating and evaporation of spherical droplets but in non-homogeneous gas. In the case when this heating and evaporation takes place in the presence of a temperature gradient in the ambient gas, the well known Marangoni effect is expected. This effect on droplet heating and evaporation has been studied in numerous papers, including the most recent ones [77, 78, 79].

Asymmetric liquid-liquid droplet heating in a laminar boundary layer was considered in [80]. The analysis of these authors focused on the influences of Weber, Prandtl, and Reynolds numbers on the system evolution. They performed simulations with a coupled Eulerian-Lagrangian interface capturing methodology, alongside a Eulerian solver for the NavierStokes equations. As a result, they predicted the spatial and temporal evolution of the temperature and velocity fields for the droplet and the surrounding fluid.

4. Droplet heating and evaporation (multi-component droplets)

As in the case of Sections 2 and 3, this section will include two parts. Firstly the models described in [2] will be briefly summarised. Secondly, the discussion will focus on new models/results, not previously described in [2].

4.1. Background research into the modelling of multi-component droplets

All models for mono-component droplets discussed in the previous section remain valid for multi-component droplets. In addition to the processes considered in the previous section, however, for multi-component droplets we need to take into account that different components evaporate at different rates, creating concentration gradients in the liquid phase. The latter leads to the liquid phase mass diffusion of species described by the diffusion equation for the mass fractions of each component. The simplest form of this equation, when only the radial diffusion is accounted for, can be presented as [2]:

$$\frac{\partial Y_{l,i}}{\partial t} = D_l \left(\frac{\partial^2 Y_{l,i}}{\partial R^2} + \frac{2}{R} \frac{\partial Y_{l,i}}{\partial R} \right), \quad (58)$$

where subscripts l and i indicate liquid phase and particular type of species respectively. It was assumed that the diffusion coefficient D_l is the same for all liquid components (a more rigorous approach to the calculation of this coefficient is presented in [81]).

This equation needs to be solved subject to the boundary condition at the surface of the droplet:

$$\left. \frac{\partial Y_{l,i}}{\partial R} \right|_{R=R_d-0} = \frac{D_v \rho_{\text{total}} \ln(1 + B_M)}{D_l \rho_l R_d} (Y_{l,i} - \varepsilon_i), \quad (59)$$

where

$$\varepsilon_i = \frac{Y_{vis}}{\sum_i Y_{vis}}, \quad (60)$$

subscript v indicates the vapour phase. This needs to be supplemented by the conditions at the droplet centre:

$$\left. \frac{\partial Y_{l,i}}{\partial R} \right|_{R=0} = 0 \quad (61)$$

and the relevant initial conditions. Note that, as in the case of the equation for temperature inside droplets, Condition (61) can be replaced by a

more general requirement that $Y_{l,i}(R, t)$ are twice continuously differentiable functions at $R \leq R_d$.

In the equilibrium state, the partial pressure of the i th vapour species at the surface of the droplet can be found from the equation:

$$p_{v,i} = \gamma_i X_{l,i} p_{v,i}^*, \quad (62)$$

where $X_{l,i}$ is the molar fraction of the i th species in the liquid near the droplet surface, $p_{v,i}^*$ is the partial vapour pressure of the i th species in the case when $X_{l,i} = 1$, γ_i is the activity coefficient. In some applications the latter coefficient can be assumed equal to 1. In this case Equation (62) leads to Raoult's law:

$$p_{v,i} = X_{l,i} p_{v,i}^*. \quad (63)$$

In most engineering applications, a solution to Equation (58) was not considered and the diffusivity of species (D_l) was considered to be either infinitely small (multi-component droplets were modelled as mono-component ones) or infinitely large (perfect mixing of species). As will be shown later, both these simplified approaches can lead to unacceptably large errors in predicted droplet temperatures and droplet evaporation times compared with the prediction of the model taking into account finite species diffusion rate inside droplets. Where species diffusion was taken into account, this was mainly performed based on the numerical solution to Equation (58). In contrast to this approach, in a series of our papers, the results of which are summarised in [2], a new approach to this problem based on the analytical solution to (58), subject to boundary condition (59), was suggested. Assuming that $R_d = \text{const}$, this solution for a short time step, subject to the initial condition $Y_{li}(t = 0) = Y_{li0}(R)$ was obtained in the form [2]:

$$Y_{li} = \epsilon_i + \frac{1}{R} \left\{ \left[\exp \left[D_l \left(\frac{\lambda_0}{R_d} \right)^2 t \right] [q_{Yi0} - Q_{Y0} \epsilon_i] \sinh \left(\lambda_0 \frac{R}{R_d} \right) + \sum_{n=1}^{\infty} \left[\exp \left[-D_l \left(\frac{\lambda_n}{R_d} \right)^2 t \right] [q_{Yin} - Q_{Yn} \epsilon_i] \sin \left(\lambda_n \frac{R}{R_d} \right) \right] \right] \right\}, \quad (64)$$

where λ_0 and λ_n ($n \geq 1$) are solutions to equations

$$\tanh \lambda = -\frac{\lambda}{h_{Y0}} \quad \text{and} \quad \tan \lambda = -\frac{\lambda}{h_{Y0}},$$

respectively, $h_{Y0} = -\left(1 + \frac{\alpha_m R_d}{D_l}\right)$,

$$Q_{Yn} = \begin{cases} -\frac{1}{||v_{Y0}||^2} \left(\frac{R_d}{\lambda_0}\right)^2 (1 + h_{Y0}) \sinh \lambda_0 & \text{when } n = 0 \\ \frac{1}{||v_{Yn}||^2} \left(\frac{R_d}{\lambda_n}\right)^2 (1 + h_{Y0}) \sin \lambda_n & \text{when } n \geq 1 \end{cases} \quad (65)$$

$$q_{Yin} = \frac{1}{||v_n||^2} \int_0^{R_d} R Y_{li0}(R) v_{Yn}(R) dR, \quad (66)$$

$n \geq 0$,

$$v_{Y0}(R) = \sinh\left(\lambda_0 \frac{R}{R_d}\right), \quad v_{Yn}(R) = \sin\left(\lambda_n \frac{R}{R_d}\right), \quad n \geq 1,$$

$$||v_{Y0}||^2 = \int_0^{R_d} v_{Y0}^2(R) dR = -\frac{R_d}{2} \left[1 + \frac{h_{Y0}}{h_{Y0}^2 - \lambda_n^2}\right], \quad (67)$$

$$||v_{Yn}||^2 = \int_0^{R_d} v_{Yn}^2(R) dR = \frac{R_d}{2} \left[1 + \frac{h_{Y0}}{h_{Y0}^2 + \lambda_n^2}\right], \quad n \geq 1, \quad (68)$$

$Y_{lis} = Y_{lis}(t)$ are liquid components' mass fractions at the droplet's surface,

$$\alpha_m = \frac{|\dot{m}_d|}{4\pi \rho_l R_d^2} = \text{const.} \quad (69)$$

In the case of moving droplets, the distribution of mass fractions of species can be described by the same Solution (64), but with D_l replaced by the effective diffusivity D_{eff} defined as:

$$D_{\text{eff}} = \chi_Y D_l, \quad (70)$$

where the coefficient χ_Y can be approximated as:

$$\chi_Y = 1.86 + 0.86 \tanh \left[2.225 \log_{10} (\text{Re}_{d(l)} \text{Sc}_l / 30)\right], \quad (71)$$

$\text{Sc}_l = \nu_l / D_l$ is the liquid Schmidt number, ν_l is the liquid kinematic viscosity. As in the case of k_{eff} , liquid fuel transport properties and the liquid velocity just below the droplet surface were used to calculate $\text{Re}_{d(l)}$. The model based on Equations (70) and (71) is known as the Effective Diffusivity (ED) model. The model, based on the assumption that species diffusivity is infinitely fast ($D_{\text{eff}} = \infty$) is referred to as the Infinite Diffusivity (ID) model.

As in the case of the heat transfer equation inside droplets, Solution (64) was generalised to the case of time-dependent droplet radii during the time step. Also, as in the case of mono-component droplets, the model based on Solution (64) was validated based on the experimental results obtained at the University of Lorraine (see [40]).

The model based on Equation (58) or its solution (64) is known as the Discrete Component Model (DCM). It is typically applicable only in the case when the number of components in the droplets is small which is not the case in most realistic fuels, including automotive fuels. An alternative approach is based on the probabilistic analysis of a large number of components (e.g. Continuous Thermodynamics approach and the Distillation Curve Model). In this family of models a number of additional simplifying assumptions were used, including the assumption that species inside droplets mix infinitely quickly. The limitations of this assumption will be discussed later in the analysis.

A new approach to modelling heating and evaporation of multi-component droplets, suitable for the case when a large number of components is present in the droplets, was suggested in [82, 56]. In contrast to the previously suggested models, designed for large numbers of components, the new model takes into account the diffusion of liquid species and thermal diffusion as in the classical Discrete Component Models. This model was called the quasi-discrete model. As in the case of the Continuous Thermodynamics approach, the quasi-discrete model is based on the distribution function with respect to a particular property. This function was approximated as:

$$f_m(n) = C_m(n_0, n_f) \frac{(M(n) - \gamma)^{\alpha-1}}{\beta^\alpha \Gamma(\alpha)} \exp \left[- \left(\frac{M(n) - \gamma}{\beta} \right) \right], \quad (72)$$

where $n_0 \leq n \leq n_f$, subscripts $_0$ and $_f$ stand for initial and final (the smallest and the largest values of n (carbon number)), M is the molar mass, $\Gamma(\alpha)$ is the Gamma function, α and β are parameters that determine the shape of the distribution, γ determines the original shift,

$$C_m(n_0, n_f) = \left\{ \int_{n_0}^{n_f} \frac{(M(n) - \gamma)^{\alpha-1}}{\beta^\alpha \Gamma(\alpha)} \exp \left[- \left(\frac{M(n) - \gamma}{\beta} \right) \right] dn \right\}^{-1}. \quad (73)$$

This choice of C_m assures that

$$\int_{n_0}^{n_f} f_m(n) dn = 1.$$

Assuming that fuel includes only alkanes, M (in kg/kmole) and n can be linked by the following expression:

$$M = 14n + 2. \quad (74)$$

As follows from the analysis presented in [2], the transport and thermodynamic properties of alkanes are weak functions of n . In this case, one can assume that their properties in a certain narrow range of n are close, and replace the continuous distribution (72) with a discrete one, consisting of N_f quasi-components with carbon numbers

$$\bar{n}_j = \frac{\int_{n_{j-1}}^{n_j} n f_m(n) dn}{\int_{n_{j-1}}^{n_j} f_m(n) dn}, \quad (75)$$

and molar fractions

$$X_j = \int_{n_{j-1}}^{n_j} f_m(n) dn, \quad (76)$$

where j is an integer in the range $1 \leq j \leq N_f$. The choice of n_j can be arbitrary. In our model we assume that all $n_j - n_{j-1}$ are equal, i.e. all quasi-components have the same range of values of n . For the case when $N_f = 1$ the analysis of multi-component droplets is reduced to that of mono-component droplets. These new quasi-components are not the actual physical hydrocarbon components (\bar{n}_j are not integers in the general case). Hence, this model is called the quasi-discrete model. These quasi-components are treated as actual components in the conventional Discrete Component Model (DCM), including taking into account diffusion of liquid species in droplets. This model is expected to be particularly useful when N_f is much less than the number of actual species in the hydrocarbon mixture. All thermodynamic and transport properties of quasi-components were determined for $n = \bar{n}_j$. For example, partial pressures of individual quasi-components were estimated as (Raoult's law is assumed to be valid):

$$p_v(\bar{n}_j) = X_{lsi}(\bar{n}_j) p^{\text{sat}}(\bar{n}_j), \quad (77)$$

where X_{lsi} is the molar fraction of liquid quasi-components at the surface of the droplet.

The main limitation of the quasi-discrete model is that it is based on the assumption that fuels consist only of alkanes. The same model could be

applied to the case when alkanes are replaced by another family of components. It cannot, however, be directly applied to the case of most realistic fuels, for which the contributions of various groups of components should be taken into account. This can be done in the generalised version of the quasi-discrete model, called the Multi-dimensional Quasi-discrete Model which will be considered later in this section.

Chen et al. [83] compared the predictions of three heat and mass transfer models: the ITC/ID model (known as the well-mixed (WM) model), the frozen evaporation (FZ) model and the DC ETC/ED model (referred to as the diffusion controlled (DC) model) for multi-component droplet heating and evaporation. For the frozen evaporation (FZ) model, at any time in the evaporation, the temperature and the composition of the droplets were equal to their initial values. The test fuels were mixtures of n-decane (a surrogate fuel for kerosene) and alcohol (ethanol or butanol) with differing volumetric ratios. The predictions of the models were validated against experimental data. The ITC/ID model was shown to be suitable for predicting slow evaporation processes with low injection pressures.

Despite the progress in the development of the models for heating and evaporation of multi-component droplets, the ITC/ID model is still widely used for modelling these processes (e.g. [84]). The results of recent experimental studies of heating and evaporation of multi-component droplets are discussed in [85, 86, 87].

Note that the approaches to modelling heating and evaporation of multi-component droplets, discussed above, are different from the ones used for modelling heating and evaporation of droplets containing insoluble particles or saline water droplets. See [88, 89, 90, 91, 92, 93, 94] for a discussion of the latter problems.

Another problem with modelling multi-component droplets, that is beyond the scope of this review, is modelling micro-explosions in droplets, which is defined as the sudden evaporation of water droplets inside the continuous phase (see [95, 96, 97, 98] for further details).

The discussion of the new models/results, not previously described in [2], will focus on the application of the Discrete Component Model to biodiesel fuels (Section 4.2) and the description of the new Multi-dimensional Quasi-discrete Model and its application to Diesel (Section 4.3) and gasoline (Section 4.4) fuels. Recent developments in gas phase evaporation models for multi-component droplets are discussed in Section 4.5.

Methyl Ester	Abbreviation	Fatty Acids																	
		C8:0	C10:0	C12:0	C14:0	C16:0	C17:0	C18:0	C20:0	C22:0	C24:0	C16:1	C18:1	C20:1	C22:1	C24:1	C18:2	C18:3	Other
Tallow	TME	-	-	0.20	2.50	27.90	-	23.00	0.40	0.40	-	2.50	40.00	0.30	0.30	-	2.00	-	0.50
Lard	LME	-	-	-	1.00	26.00	-	14.00	-	-	-	2.80	44.00	2.00	2.00	-	8.00	-	0.20
Butter	BME	5.19	2.80	3.40	10.99	31.66	-	10.79	0.40	0.40	-	2.40	36.37	1.00	1.00	-	3.00	0.60	-
Coconut	CME	6.00	0.00	50.00	15.00	9.00	-	3.00	-	-	-	-	7.00	-	-	-	2.00	-	-
Palm Kernel	PMK	2.00	4.00	50.00	17.00	9.00	-	1.70	1.50	1.50	-	0.40	12.00	-	-	-	1.30	-	-
Palm	PME	-	-	0.26	1.29	45.13	-	4.47	0.35	0.17	-	0.21	38.39	-	-	-	9.16	0.19	0.38
Safflower	SFE	-	-	-	-	5.20	-	2.30	-	-	-	-	76.38	-	-	-	16.22	-	-
Peanut	PTE	-	-	-	0.50	9.00	-	4.00	7.00	7.00	-	1.50	49.00	-	-	-	23.00	-	-
Cottonseed	CSE	-	-	-	2.00	19.00	-	2.00	-	-	-	-	31.00	2.50	2.50	-	41.00	-	-
Corn	CNE	-	-	-	1.00	9.00	-	2.50	-	-	-	1.50	40.00	1.00	1.00	-	44.00	-	-
Sunflower	SNE	-	-	-	-	5.92	-	4.15	1.38	1.38	-	-	18.46	-	-	-	68.41	0.30	-
Tung	TGE	-	-	-	-	3.64	-	2.55	-	13.14	-	-	10.10	0.81	-	-	13.75	51.64	4.37
Hemp1	HME1	-	-	-	-	6.63	0.21	2.66	0.45	0.25	0.23	0.33	11.88	0.27	0.17	0.15	56.71	38.67	-
Soybean	SME	-	-	-	0.38	10.90	-	4.40	0.40	-	-	-	34.00	-	-	-	25.80	7.20	-
Linseed	LNE	-	-	-	0.20	6.20	-	0.60	-	-	-	-	18.00	-	-	-	16.00	59.00	-
Hemp2	HME2	-	-	-	-	6.51	-	2.46	0.90	-	-	-	11.88	0.90	-	-	54.82	20.07	2.46
Canola seed	CAN	-	-	-	4.48	0.14	1.99	0.62	0.35	0.16	0.36	59.66	1.49	0.42	-	20.89	9.44	-	-
Waste oil	WME	-	-	0.20	0.67	15.69	0.20	6.14	0.39	0.44	0.30	0.73	42.84	0.56	0.15	-	29.36	2.03	0.30
Rapeseed	RME	-	-	-	-	4.93	-	1.66	0.56	-	-	-	26.61	-	22.32	0.77	24.75	9.70	8.70

Table 1: Types of biodiesel fuels, their abbreviations, acid codes and molar fractions of the components (pure methyl esters). Symbols M for the acid codes are omitted. Reprinted from Fuel, Volume 154, Al Qubeissi et al., Modelling of biodiesel fuel droplet heating and evaporation: Effects of fuel composition, Pages 308-318, Copyright Elsevier (2015).

4.2. Discrete Component Model: application to biodiesel fuel droplets

The preliminary results of modelling biodiesel fuel droplet heating and evaporation, using the Discrete Component Model, were presented in [99]. The analysis of that paper was based on only five types of biodiesel fuel and it was concluded that the predictions of the Discrete Component Model are very close to those based on the assumption that biodiesel fuel can be approximated by a single component with averaged characteristics (the droplet evaporation times predicted by these models differed by less than about 5.5% for typical Diesel engine-like conditions). In [100], an analysis, similar to the one presented in [99], is performed but for a much wider range of biodiesel fuels (19 types altogether) and more realistic engine conditions. In what follows the main results obtained in [100] are presented and discussed.

The following types of biodiesel fuels were used in [100]: Tallow Methyl Ester (TME), Lard Methyl Ester (LME), Butter Methyl Ester (BME), Coconut Methyl Ester (CME), Palm Kernel Methyl Ester (PMK), Palm Methyl Ester (PME), Safflower Methyl Ester (SFE), Peanut Methyl Ester (PTE), Cottonseed Methyl Ester (CSE), Corn Methyl Ester (CNE), Sunflower Methyl Ester (SNE), Tung Methyl Ester (TGE), Hemp-oil Methyl Ester, produced from Hemp seed oil in the Ukraine (HME1), Soybean Methyl Ester (SME), Linseed Methyl Ester (LNE), Hemp-oil Methyl Ester, produced in the European Union (HME2), Canola seed Methyl Ester (CAN), Waste cooking-oil Methyl Ester (WME) and Rapeseed Methyl Ester (RME). The molar frac-

Fatty Acids	Acid code	Molecular Formula	Molar Mass (g/mol)	Boiling Point (K)
Methyl octanoate	C8:0 M	C ₉ H ₁₈ O ₂	144.212	467.5
Methyl decanoate	C10:0 M	C ₁₁ H ₂₂ O ₂	172.265	501.1
Methyl dodecanoate	C12:0 M	C ₁₃ H ₂₆ O ₂	214.338	530.42
Methyl tetradecanoate	C14:0 M	C ₁₅ H ₃₀ O ₂	242.39	554.20
Methyl palmitate	C16:0 M	C ₁₇ H ₃₄ O ₂	270.442	577.98
Methyl heptadecanoate	C17:0 M	C ₁₈ H ₃₆ O ₂	284.468	589.87
Methyl stearate	C18:0 M	C ₁₉ H ₃₈ O ₂	298.494	601.76
Methyl eicosanoate	C20:0 M	C ₂₁ H ₄₂ O ₂	326.546	625.55
Methyl docosanoate	C22:0 M	C ₂₃ H ₄₆ O ₂	354.598	649.33
Methyl tetracosanoate	C24:0 M	C ₂₅ H ₅₀ O ₂	382.65	673.11
Methyl palmitoleate	C16:1 M	C ₁₇ H ₃₂ O ₂	268.426	577.57
Methyl oleate	C18:1 M	C ₁₉ H ₃₆ O ₂	296.478	601.31
Methyl eicosenoate	C20:1 M	C ₂₁ H ₄₀ O ₂	324.53	625.05
Methyl erucate	C22:1 M	C ₂₃ H ₄₄ O ₂	352.582	648.79
Methyl nervonate	C24:1 M	C ₂₅ H ₄₈ O ₂	380.634	672.53
Methyl linoleate	C18:2 M	C ₁₉ H ₃₄ O ₂	294.462	601.3
Methyl linolenate	C18:3 M	C ₁₉ H ₃₂ O ₂	292.446	601.58
Others	—	—	296.478	601.31

Table 2: Names, acid codes, molecular formulae, molar masses and boiling points of the components (pure methyl esters). Reprinted from Fuel, Volume 154, Al Qubeissi et al., Modelling of biodiesel fuel droplet heating and evaporation: Effects of fuel composition, Pages 308-318, Copyright Elsevier (2015).

tions of the components of these fuels (in percentages) are shown in Table 1. The meaning of symbols of components, presented in Table 1, and their acid codes, molecular formulae, molar masses and boiling temperatures are shown in Table 2. The transport and thermodynamic properties of all components shown in Tables 1 and 2 were taken from Appendix B of [99]. The properties of unidentified additives (others) were assumed to be identical to those of C18:1M .

The predictions of the following models were compared:

(1) a model taking into account the contributions of all components of biodiesel fuels, their realistic diffusion, temperature gradient, and recirculation within the droplet, in the case of moving droplets (using the Effective Thermal Conductivity/Effective Diffusivity (ETC/ED) model); this model is referred to as the ‘ME’ model;

(2) a model taking into account the contribution of all components of biodiesel fuels, but assuming that the diffusivity of species in droplets is infinitely fast and the liquid thermal conductivity is infinitely large (using the Infinite Thermal Conductivity/Infinite Diffusivity (ITC/ID) model); this model is referred to as the ‘MI’ model;

(3) a model ignoring transient diffusion of species (treating all species as a single component with properties depending only on temperature, which was updated at each time step) and assuming that the liquid thermal conductivity is infinitely large (ITC model); this model is referred to as the ‘SI’ model.

The initial droplet radius is assumed equal to $R_{d0} = 12.66 \mu\text{m}$. A droplet of initial temperature $T_{d0} = 360 \text{ K}$ is assumed to be moving through air at constant velocity of $U_d = 28 \text{ m/s}$. Ambient temperature and pressure are assumed equal to 700 K and 3.2 MPa respectively.

The plots of time evolution of droplet surface temperature (T_s) and radius (R_d) for Butter Methyl Ester (BME) are presented in Fig. 3. As one can see from this figure, the ME model predicts longer evaporation times compared with the MI and SI models. This error for the SI model was found to be 25.2%. The importance of this result lies in the fact that it contradicts one of the main conclusions drawn in our previous paper [99], based on the analysis of Palm Methyl Ester, Hemp Methyl Esters, Rapeseed oil Methyl Ester, and Soybean oil Methyl Ester. In [99] it was concluded that the droplet evaporation times predicted by the SI model differ by less than about 5.5% (note that the analysis of [99] was based on different values of input parameters compared with the current paper).

To provide a deeper understanding of the processes taking place during

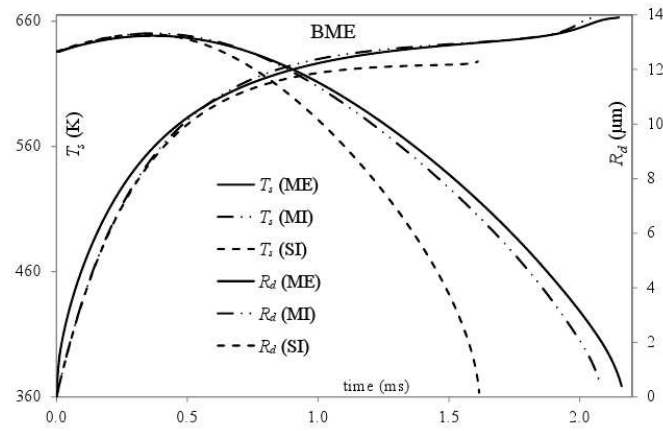


Figure 3: The plots of time evolution of a droplet's surface temperature (T_s) and radius (R_d) for Butter Methyl Ester (BME) predicted by the multi-component ETC/ED model (ME), single-component (zero diffusivity)/ITC model (SI), and multi-component ITC/ID model (MI). The droplet is assumed to have initial radius $12.66 \mu\text{m}$ and is moving at 28 m/s in still air at temperature and pressure equal to 700 K and 3.2 MPa , respectively. Reprinted from Fuel, Volume 154, Al Qubeissi et al., Modelling of biodiesel fuel droplet heating and evaporation: Effects of fuel composition, Pages 308-318, Copyright Elsevier (2015).

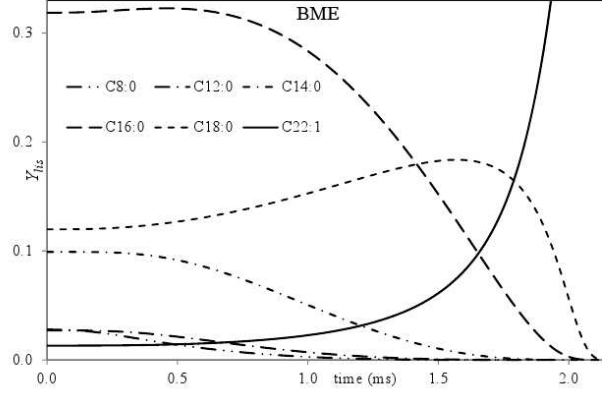


Figure 4: The plots of time evolution of surface mass fractions of C8:0M, C12:0M, C14:0M, C16:0M, C18:0M and C22:1M for a Butter Methyl Ester (BME) droplet for the same conditions as in Fig. 3. Reprinted from Fuel, Volume 154, Al Qubeissi et al., Modelling of biodiesel fuel droplet heating and evaporation: Effects of fuel composition, Pages 308-318, Copyright Elsevier (2015).

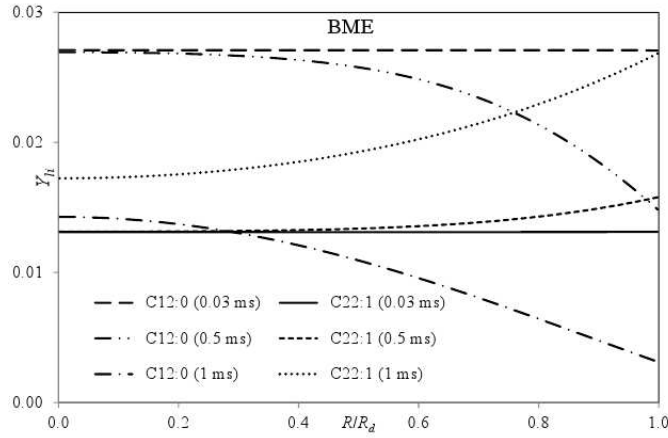


Figure 5: The plots of mass fractions of C12:0M and C22:1M versus normalised distance from the droplet centre at three time instants 0.03 ms, 0.5 ms and 1 ms for a Butter Methyl Ester (BME) droplet for the same conditions as in Figs. 3-4. Reprinted from Fuel, Volume 154, Al Qubeissi et al., Modelling of biodiesel fuel droplet heating and evaporation: Effects of fuel composition, Pages 308-318, Copyright Elsevier (2015).

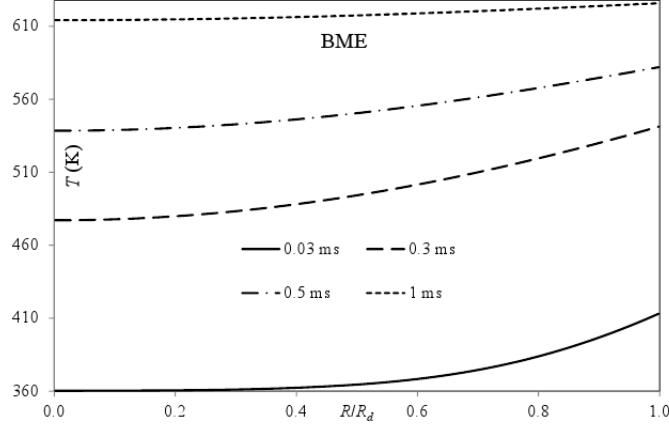


Figure 6: The plots of temperature versus normalised distance from the droplet centre at four time instants 0.03 ms, 0.3 ms, 0.5 ms and 1 ms for a Butter Methyl Ester (BME) droplet for the same conditions as in Figs. 3-5. Reprinted from Fuel, Volume 154, Al Qubeissi et al., Modelling of biodiesel fuel droplet heating and evaporation: Effects of fuel composition, Pages 308-318, Copyright Elsevier (2015).

biodiesel fuel droplet heating and evaporation, in Figs. 4-6 we presented the plots of surface mass fractions of selected components versus time, the plots of mass fractions of selected components versus normalised distance from the droplet centre at various time instants and temperatures versus normalised distance from the droplet centre at various time instants for Butter Methyl Ester (BME). As follows from Fig. 4, the surface mass fractions of the lightest components (C8:0M, C12:0M and C14:0M) monotonically decrease with time. The surface mass fraction of the heaviest component (C22:1M) monotonically increases with time. The surface mass fractions of the intermediate components (C16:0M and C18:0M) first increase and then decrease with time. At the end of the evaporation process, only the heaviest and least volatile component remains at the droplet surface. This component is responsible for prolonged droplet lifetime predicted by the ME model compared with the SI model, and higher surface temperatures at the final stage of droplet evaporation.

As one can see from Fig. 5, the decrease in the surface mass fraction of one of the lightest components (C12:0M) with time is accompanied by a corresponding decrease in the mass fraction of this component in the body of

the droplet. The rate of this decrease, however, reduces in the regions close to the droplet centre. Thus a negative gradient for this mass fraction is formed inside the droplet, which leads to the diffusion of this component from the droplet centre to its surface. As can be inferred from the same figure, the increase in the surface mass fraction of the heaviest components (C22:1M) with time is accompanied by a corresponding increase in the mass fraction of this component in the body of the droplet, although the rate of this increase reduces in the regions close to the droplet centre. Thus positive gradients for this mass fraction are formed inside the droplet, which lead to the diffusion of this component from the droplet surface to its centre. This leads to the formation of a droplet consisting mainly of the heaviest component (C22:1M) at the end of the evaporation process. One can clearly see from Fig. 5 that gradients of mass fractions of the components inside the droplet are initially small but increase with time. This observation shows the limitations of the well-mixed models, including the MI model, widely used for the analysis of multi-component droplet heating and evaporation.

As one can see from Fig. 6, at the initial stage of droplet heating and evaporation (0.03 ms after the start of the process) rather large gradients of temperature inside the droplet close to the droplet surface are formed. In contrast to the case of species molar fractions, however, the gradients of temperature inside droplets decrease with time. These gradients are reasonably small at 1 ms after the start of the process. This means that the Infinite Thermal Conductivity model can be applied to the analysis of droplet heating and evaporation, except at the very beginning of the process, when high accuracy of calculations is not required.

The general shapes of the curves, but for other biodiesel fuels show the same trends as in Figs. 4-6. To summarise the results for all biodiesel fuels under consideration, we were able to show that the SI model under-predicts the droplet evaporation times compared with the ME model (believed to be the most reliable one) by up to about 26%. This result does not support our earlier finding that the deviations between the evaporation times predicted by these models do not exceed about 5.5%. The evaporation times predicted by the MI model were shown to be reasonably close to those predicted by the first model. The MI model under-predicts this time by not more than 4.3% except for Rapeseed Methyl Ester (RME) for which the under-prediction was 15.1%. The multi-component model predicts higher droplet surface temperatures at the final stages of evaporation (in most cases) and longer evaporation times than the single component model. This is related to the fact that at

the final stages of droplet evaporation the mass fraction of heavier species, which evaporate more slowly than the lighter species and have higher boiling temperatures, increases at the expense of lighter species.

The analysis presented in this section has focused predominantly on the functionality testing of the models and no direct comparison between the modelling and experimental results was presented.

The evaporation characteristics of a Palm Methyl Ester (PME) droplet were investigated in [101]. It was shown that PME droplets tend to evaporate much more slowly than Diesel fuel droplets in the same conditions.

4.3. Multi-dimensional Quasi-discrete Model: application to Diesel fuel droplets

4.3.1. Description of the model

Although the usefulness and efficiency of the quasi-discrete model, described in Section 4.1, was clearly demonstrated, this model still has a number of serious limitations the most important of which is that it is based on the assumption that Diesel and gasoline fuels consist only of n-alkanes. At the same time, the total molar fraction of alkanes (n-alkanes and iso-alkanes) is only about 40% of the overall composition of Diesel fuels (a similar conclusion could be drawn for gasoline fuel). Hence, the contribution of other components apart from alkanes cannot be ignored. Also, even if we restrict our analysis to alkanes alone, it does not appear to be easy to approximate this distribution with a reasonably simple distribution function $f_m(n)$, similar to the one given by Expression (72). In [102], the quasi-discrete model was generalised to address both these problems. A realistic composition of Diesel fuels, schematically shown in Fig. 7, reproduced from Fig. 1 of [103], was used in the analysis presented in [102]. In what follows the main features of the model described in [102], called the Multi-dimensional Quasi-discrete Model (MDQDM), are summarised.

The results presented in Fig. 7 were simplified, taking into account that the properties of n-alkanes and iso-alkanes are rather close. Observing that the contributions of tricycloalkanes, diaromatics and phenanthrenes to Diesel fuel are rather small (less than about 1.6% for each of these components) allows us to ignore the dependence of the properties of these components on the number of carbon atoms and replace these three groups with three components, tricycloalkane, diaromatic and phenanthrene, with arbitrary chosen carbon numbers. The molar fraction of tricycloalkanes was estimated to be 1.5647%, while the molar fractions of diaromatics and phenanthrenes were

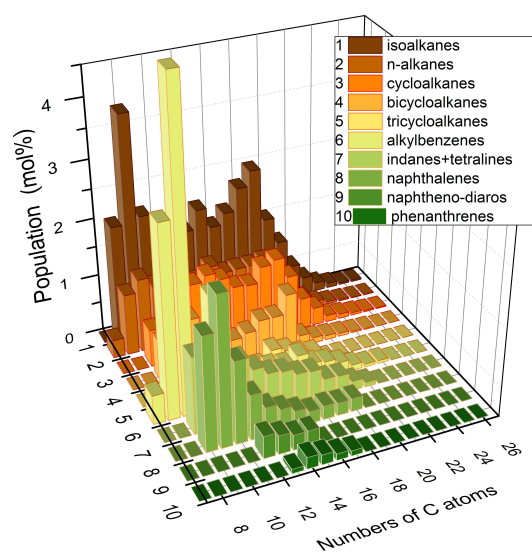


Figure 7: Distribution functions of various hydrocarbons versus the numbers of carbon atoms in molecules in a representative sample of Diesel fuel. Reprinted from Fluid Phase Equilibria, Volume 356, Gun'ko et al., A quantum chemical study of the processes during the evaporation of real-life Diesel fuel droplets, Pages 146-156, Copyright Elsevier (2013).

m	Component
1	Alkanes
2	Cycloalkanes
3	Bicycloalkanes
4	Alkylbenzenes
5	Indanes & tetralines
6	Naphthalenes
7	Tricycloalkane
8	Diaromatic
9	Phenanthrene

Table 3: The relation between parameter m and groups ($m = 1-6$) and components ($m = 7-9$). Reprinted from Fuel, Volume 154, Sazhin et al., A multi-dimensional quasi-discrete model for the analysis of Diesel fuel droplet heating and evaporation, Pages 238-266, Copyright Elsevier (2014).

estimated to be 1.2240% and 0.6577%, respectively. Transport and thermodynamic properties of the components are summarised in Appendices 1-7 of [102] (for most recent estimates of pressures and temperature dependence of volume and viscosity of Diesel fuels see [104]).

In the Multi-dimensional Quasi-discrete Model the focus is shifted from the analysis of the distribution function to the direct analysis of molar fractions of the components. These are described by the matrix X_{nm} , where n refers to the number of carbon atoms, and m refers to the groups (e.g. alkanes) or individual components (tricycloalkane, diaromatic and phenanthrene). The link between the values of m and the components is shown in Table 3.

For each m the values of \bar{n}_{jm} of quasi-components were introduced as

$$\left. \begin{aligned} \bar{n}_{1m} &= \frac{\sum_{n=n_{1m}}^{n=n_{(\varphi_m+1)m}} (nX_{nm})}{\sum_{n=n_{1m}}^{n=n_{(\varphi_m+1)m}} X_{nm}}, \\ \bar{n}_{2m} &= \frac{\sum_{n=n_{(\varphi_m+2)m}}^{n=n_{(2\varphi_m+2)m}} (nX_{nm})}{\sum_{n=n_{(\varphi_m+2)m}}^{n=n_{(2\varphi_m+2)m}} X_{nm}}, \\ \bar{n}_{3m} &= \frac{\sum_{n=n_{(2\varphi_m+3)m}}^{n=n_{(3\varphi_m+3)m}} (nX_{nm})}{\sum_{n=n_{(2\varphi_m+3)m}}^{n=n_{(3\varphi_m+3)m}} X_{nm}}, \\ &\dots\dots\dots \\ \bar{n}_{\ell m} &= \frac{\sum_{n=n_{((\ell-1)\varphi_m+\ell)m}}^{n=n_{k_m}} (nX_{nm})}{\sum_{n=n_{((\ell-1)\varphi_m+\ell)m}}^{n=n_{k_m}} X_{nm}}, \end{aligned} \right\} \quad (78)$$

where $n_{1m}=n_{m(\min)}$ is the minimal value of n for which $X_{nm} \neq 0$, $n_{k_m}=n_{m(\max)}$ is the maximal value of n for which $X_{nm} \neq 0$, $\ell = \text{integer } ((k_m + \varphi_m)/(\varphi_m + 1))$. Parameter φ_m is assumed to be integer; $\varphi_m + 1$ is equal to the number of components to be included into quasi-components, except possibly the last one in the group. φ_m is assumed to be the same for all quasi-components within group m . If $\varphi_m = 0$ then $\ell = k_m$ and the number of quasi-components is equal to the number of actual components. φ_m and k_m depend on m in the general case.

An alternative approach to generation of \bar{n}_{jm} , used in [102], is based on the selection of the number of quasi-components n_q . In this case the number of components in each quasi-component, except possibly the last one, (n_c), is taken equal to the nearest integer of the ratio k_m/n_q . If k_m/n_q is not an integer then the number of components in the last quasi-component (n_{lc}) is either greater than n_c , if $(k_m/n_q) > n_c$, or less than n_c , if $(k_m/n_q) \leq n_c$.

As in the case of the original quasi-discrete model, \bar{n}_{im} are not integers in the general case. Due to the additional dimensions introduced by the subscript m in Equation (78), the new model is called the Multi-dimensional Quasi-discrete Model (MDQDM). MDQDM can be further simplified and approximated by the single-component model. The maximal number of these quasi-components/components, providing the most accurate approximation of Diesel fuel, is 98. In this case, the new model reduces to the conventional Discrete Component Model (DCM). The quasi-components in the MDQDM are treated in the same way as the quasi-components in the conventional quasi-discrete model. Also, the temperature gradient and quasi-components' diffusion inside droplets are taken into account as in the quasi-discrete model.

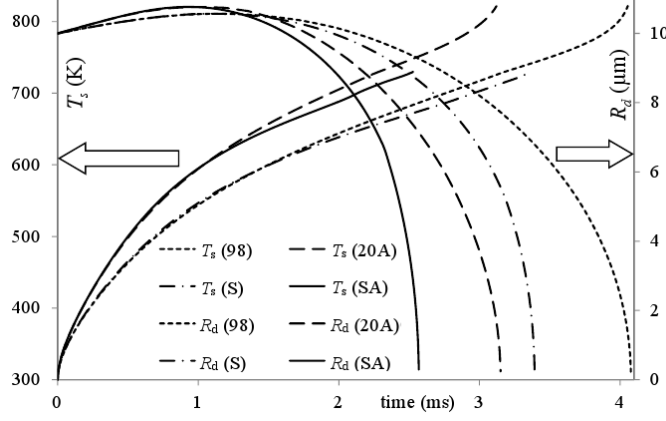


Figure 8: The plots of the droplet surface temperatures T_s and radii R_d versus time for four approximations of Diesel fuel composition (see the text of the paper). Reprinted from Fuel, Volume 154, Sazhin et al., A multi-dimensional quasi-discrete model for the analysis of Diesel fuel droplet heating and evaporation, Pages 238-266, Copyright Elsevier (2014).

In [102] it was investigated by how much the latter number can be reduced, provided that the errors introduced by this reduction are acceptable for practical engineering applications. Some key findings of this paper are summarised in the next section.

4.3.2. Application of the model to Diesel fuel

In [102] the model described in Section 4.3.1 was applied to the analysis of heating and evaporation of a droplet with initial radius $R_{d0} = 10 \mu\text{m}$ in air with density, temperature and pressure equal to: $\rho_a = 11.9 \text{ kg/m}^3$, $T_a = 880 \text{ K}$, $p_a = 30 \text{ bar}$.

The plots of the droplet surface temperatures T_s and radii R_d versus time for a stationary droplet and four approximations of Diesel fuel composition are shown in Fig. 8. These are the approximations used: the contributions of all 98 components are taken into account (indicated as (98)); the contributions of only 20 alkane components are taken into account (standard approximation used in the original quasi-discrete model (indicated as (20A))); the contribution of all 98 components is approximated by a single quasi-component (indicated as (S)); and the contributions of only 20 alkane components are taken into account and these are approximated by a single quasi-component with the average value of the carbon number ($\text{C}_{14.763}\text{H}_{31.526}$;

indicated as (SA)). In the cases when only the contribution of alkanes was taken into account, the mass fractions of the components were recalculated to ensure that the total mass fractions of all alkanes were equal to 1. The same applies to the cases when other components are removed from the analysis.

As follows from Fig. 8, the approximation of 98 actual components by a single quasi-component leads to a noticeable under-estimation of the droplet surface temperature, and an under-estimation of the evaporation time by about 17%. In the case when Diesel fuel was approximated by 20 alkane components, the predicted droplet surface temperatures appeared to be higher and the evaporation time shorter by about 23% than in the case of approximation of Diesel fuel by 98 components. This means that the approximation of Diesel fuel by alkanes, a widely used assumption in the modelling of Diesel fuels, leads to results which are less accurate, compared with the approximation of Diesel fuel by a single quasi-component. The approximation of Diesel fuel by a single alkane quasi-component ($C_{14.763}H_{31.526}$) leads to under-prediction of the evaporation time by about 37% which is not acceptable even for qualitative analysis of the process. This leads us to question the validity of the results of numerous papers where Diesel fuel was approximated by a single alkane component (n-dodecane in most cases).

Note that in all cases shown in Fig. 8 the droplet surface temperatures keep increasing with time until the droplets evaporate. This is consistent with our earlier studies of this process (e.g. [2]). This result questions the applicability of the assumption that the droplet surface temperature remains constant during the evaporation process which is widely used in simplified models of this process (see Section 3.1). The well known d^2 -law is implicitly based on this assumption (see [2]).

The plots of the droplet surface temperatures T_s and radii R_d versus time for the same conditions as in Fig. 8 but for a wider range of approximations of Diesel fuel are shown in Figs. 9 and 10. Only the final stage of droplet heating and evaporation is shown in these figures.

As one can see from Figs. 9 and 10, the plots S and S7 (ignoring the contribution of diaromatic and phenanthrene) for surface temperatures and radii are almost indistinguishable. Also, plots 9 and 7 (ignoring the contribution of diaromatic and phenanthrene) are rather close. The same applies to plots 23 and 21 (ignoring the contribution of diaromatic and phenanthrene). This means that the contribution of diaromatic and phenanthrene can be safely ignored in the approximation of Diesel fuel when modelling the heating and evaporation of fuel droplets in realistic Diesel engine-like conditions. Both

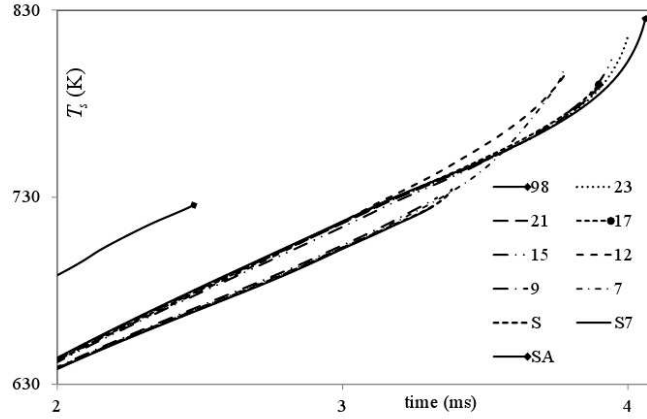


Figure 9: The plots of the droplet surface temperatures T_s versus time for ten approximations of Diesel fuel composition: 98 components (indicated as (98)); 23, 21, 17, 15, 12, 9 and 7 quasi-components/components (numbers near the curves); the contributions of all groups are approximated by single quasi-components, to which the contribution of tricycloalkane is added, leading to 7 quasi-components/components (indicated as (S7)); the contribution of all 98 components is taken into account as that of a single component as in the case shown in Fig. 8 (indicated as (S)) (see the details in the text of [102]); the contributions of only 20 alkane components are taken into account and these are treated as a single component, with the average value of the carbon number ($C_{14.763}H_{31.526}$; indicated as (SA)). The same ambient conditions and model as in the case shown in Fig. 8 were used for the analysis; only the final stage of droplet heating and evaporation is shown. Reprinted from Fuel, Volume 154, Sazhin et al., A multi-dimensional quasi-discrete model for the analysis of Diesel fuel droplet heating and evaporation, Pages 238-266, Copyright Elsevier (2014).

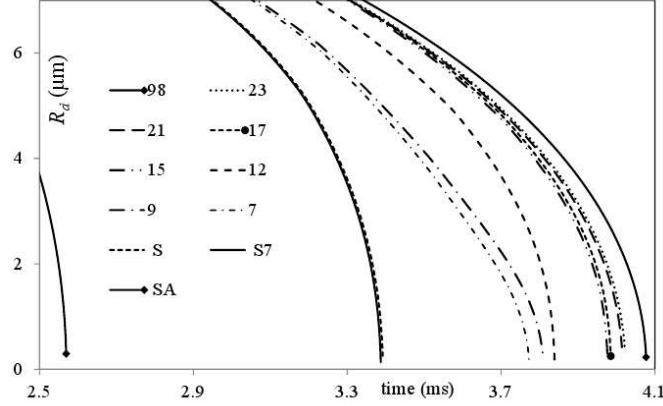


Figure 10: The same as Fig. 9 but for the droplet radii R_d . Reprinted from Fuel, Volume 154, Sazhin et al., A multi-dimensional quasi-discrete model for the analysis of Diesel fuel droplet heating and evaporation, Pages 238-266, Copyright Elsevier (2014).

for droplet surface temperatures and radii, the accuracy of approximations improves as the number of QC/Cs increases. In the case of 15 QC/Cs the droplet evaporation time can be estimated with an error of about 2.5%. In the case of 21 QC/Cs, this error reduces to about 1.5%. This error is comparable with that for the approximation of Diesel fuel with 40 QC/Cs. Thus when balancing simplicity with accuracy of the model we can recommend the approximation of Diesel fuel with 21 QC/Cs if errors less than about 2% can be tolerated. This number of QC/Cs can be reduced to 15 if errors less than about 3% can be tolerated. The latter model requires about 6 times less CPU time compared with the model taking into account the contributions of all 98 components.

4.4. Multi-dimensional Quasi-discrete Model: application to gasoline fuel droplets

The application of the Multi-dimensional Quasi-discrete Model to gasoline fuel droplets is described in [105]. The main results presented in this paper are summarised in this section.

The analysis of [105] focused on FACE-C gasoline fuel (Fuel for Advanced Combustion Engines – C) droplets. Composition of this fuel was simplified by replacing groups of similar components with single components (with

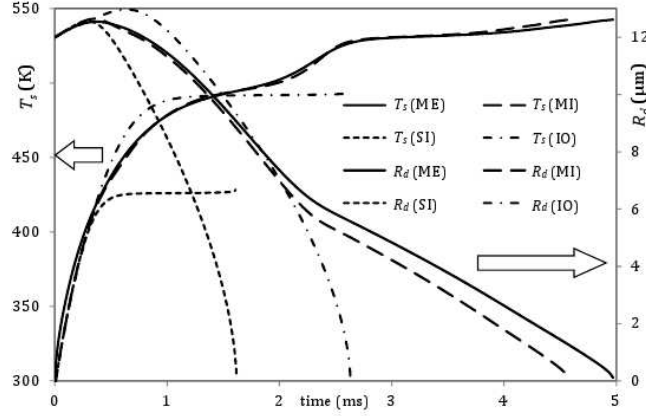


Figure 11: The droplet surface temperatures T_s and radii R_d versus time for the cases when: 1) the contributions of all 20 components are taken into account using the ETC/ED model (ME); 2) the contribution of 20 components are taken into account using the ITC/ID model (MI); 3) the 20 components are approximated by a single component with average thermodynamic and transport properties in combination with the ITC model (SI); 4) gasoline fuel is approximated by iso-octane in combination with the ITC model (IO). Reprinted from Fuel, Volume 159, Al Qubeissi et al., Modelling of gasoline fuel droplets heating and evaporation, Pages 373-384, Copyright Elsevier (2015).

averaged properties, based on averaged molar weights; or the ones with the highest molar contributions in the groups with molar fractions up to 1.5%). This approach allowed the authors of [105] to reduce the number of species in gasoline fuel to 20 components. These components were allocated to 3 groups, n-alkanes (5 components), iso-alkanes (8 components), and aromatics (4 components); and 3 components approximating groups with small molar fractions (indanes/naphthalenes, cycloalkanes and olefins).

The model was applied to modelling FACE-C droplet heating and evaporation in typical gasoline engine conditions. The initial droplet radius and temperature were taken equal to $12 \mu\text{m}$ and 296 K , respectively. The droplet relative velocity was assumed to be fixed and equal to 24 m/s . Ambient air (gas) pressure and temperature were assumed equal to $p = 9 \text{ bar}$ and $T_g = 545 \text{ K}$, respectively.

The plots of the droplet surface temperatures T_s and radii R_d versus time for FACE-C gasoline fuel droplet heating and evaporation are presented in Fig. 11. Four cases are shown in this figure: 1) the contributions of all 20

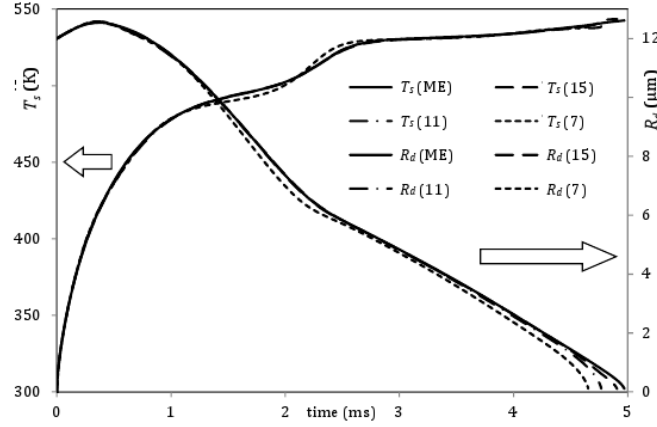


Figure 12: The same as Fig. 11 but for the cases when the ETC/ED model was used taking into account the contributions of all 20 components of gasoline fuel (indicated as ME) and assuming that these components are approximated by 15, 11 and 7 quasi-components/components (QC/Cs) (numbers are indicated near the plots). Reprinted from Fuel, Volume 159, Al Qubeissi et al., Modelling of gasoline fuel droplets heating and evaporation, Pages 373-384, Copyright Elsevier (2015).

components are taken into account using the ETC/ED model (indicated as (ME)); 2) the contributions of 20 components are taken into account using the ITC/ID model (indicated as (MI)); 3) the thermodynamic and transport properties of 20 components are averaged to form a single component and temperature gradient inside the droplet is ignored (ITC model) (indicated as (SI)); and 4) the ITC model in which gasoline fuel is approximated by iso-octane (2,2,4-trimethylpentane; indicated as (IO)) is used. As one can see from Fig. 11, the errors in droplet surface temperatures and evaporation times, predicted by the SI model are 13.6% and 67.5%, respectively. For the IO model these errors reduce to 6.3% and 47.1%, respectively, and reduced further to 4.8% and 8%, respectively, when the MI model was used. Although the accuracy of the latter model might be acceptable in some engineering applications, this model cannot describe adequately the underlying physics of the processes inside droplets (heat conduction and species diffusion).

The same plots as in Fig. 11 but for the cases when 20 components of gasoline fuel are approximated by 15 (3 QC/Cs of n-alkanes, 6 QC/Cs of iso-alkanes, 3 QC/Cs of aromatics, 1 indane/naphthalene, 1 cycloalkane

and 1 olefin), 11 (2 QC/Cs of n-alkanes, 4 QC/Cs of iso-alkanes, 2 QC/Cs of aromatics, 1 indane/naphthalene, 1 cycloalkane and 1 olefin) and 7 (2 QCs of alkanes, 3 QC/Cs of iso-alkanes, and 2 QC/Cs of aromatics) QC/Cs, using the ETC/ED model, are shown in Fig. 12. As can be seen from this figure, the errors in surface temperatures and evaporation times predicted by the model using 15 QC/Cs are 0.3% and 1.3%, respectively. These errors increase to 0.5% and 4%, respectively, when gasoline fuel is approximated by 11 QC/Cs, and further increase to 0.8% and 6.4%, respectively, when gasoline fuel is approximated by 7 QC/Cs. Even in the latter case, however, these errors can be tolerated in some practical engineering applications. This model is more accurate than the MI model, and it describes adequately the underlying physics of the processes in droplets.

Also, it was shown that the approximation of the actual composition of gasoline fuel by 6 quasi-components/components (2 QCs of n-alkanes, 2 QCs of iso-alkanes, and 2 QCs of aromatics), using the MDQD model, leads to errors in estimated droplet surface temperatures and evaporation times of about 0.9% and 6.6% respectively, for the same engine conditions, which can be tolerated in many practical engineering applications. It was shown that the application of the latter model leads to about 70% reduction in CPU time compared to the model taking into account the contributions of all 20 components of gasoline fuel.

Note that the original version of the Multi-dimensional Quasi-discrete Model (MDQDM) was specifically designed to model Diesel and gasoline fuel droplet heating and evaporation but not their ignition characteristics. Several surrogates of these fuels have been developed, specifically to model their ignition characteristics, but none of these surrogates proved suitable for modelling fuel droplet heating and evaporation [106] (the applicability of the recently developed surrogates (see [107, 108, 109, 110, 111]) to modelling multi-component fuel droplet heating and evaporation has not yet been investigated). A new formulation of physical surrogates of FACE-A gasoline fuel, based on heating and evaporation characteristics, was suggested in [112]. These surrogates were developed using an approach similar to that used in the development of the MDQDM, and were shown to be suitable for modelling both heating and evaporation of fuel droplets and the ignition characteristics of a fuel vapour/air mixture. The main ideas of the model developed in [112] are summarised below.

The analysis of [112] focused on FACE-A gasoline fuel. Firstly, four surrogates of FACE-A found in the literature were considered. These surrogates

#	Component	Surr4 (8 Comp)	Surr5 (7 Comp)	Surr6 (6 Comp)
1	n-butane	3.919	3.919	3.919
2	n-heptane	6.652	8.238	8.238
3	iso-pentane	12.784	12.784	12.784
5	3 methyl hexane	25.875	25.875	25.875
7	iso-octane	46.869	46.869	48.063
9	2,6-dimethyloctane	1.194	1.194	0.000
14	1t,2 dimethylcyclopentane	1.585	0.000	0.000
16	1-methyl-2-propylcyclohexane	1.121	1.121	1.121

Table 4: Mass fractions (in %) of three new ‘physical’ surrogates of FACE-A gasoline fuel. Reprinted from Fuel, Volume 176, Elwardany et al., A new formulation of physical surrogates of FACE-A gasoline fuel based on heating and evaporation characteristics, Pages 56-62, Copyright Elsevier (2016).

include the five component surrogate chosen for its ability to match the ignition delay time of the FACE-A gasoline fuel (called Surr1), the primary reference fuel surrogate (PRF84) that matches the research octane number (RON) of FACE-A, the one that matches hydrogen-to-carbon ratio (H/C), RON, density and distillation curve with FACE-A (Surr2), and the one that matches the RON based on molar fraction linear blending (Surr3). It was shown that these surrogates cannot predict adequately the time evolution of surface temperatures and radii of FACE-A droplets. New ‘physical’ surrogates with 8, 7 and 6 components (Surr4, Surr5, and Surr6) were introduced to match the heating and evaporation characteristics of these droplets.

FACE-A gasoline fuel has the following mass fractions for the groups of components: 10.57% n-paraffins, 86.12% iso-paraffins, 0.37% aromatics, 2.49% naphthalenes and 0.45% olefins which represented 66 components. To design surrogates Surr4, Surr5, and Surr6, 66 components of FACE-A were replaced by 19 components to represent this fuel. This reduction in the number of components was based on merging components from the same chemical groups and having the same chemical formula, which have very close thermophysical properties; the components with the highest initial compositions were chosen to be the representative components. The heating and evaporation characteristics of all previously suggested and new surrogates were verified against the results predicted by this 19 component model.

New ‘physical’ surrogates were designed via further simplifications of the above-mentioned 19 component model by retaining the most important components and ignoring the contributions of other components. Mass fractions

Target	FACE A	PRF 84	Surr1	Surr2	Surr3	Surr4	Surr5	Surr6
H/C ratio	2.29	2.26	2.28	2.28	2.26	2.29	2.3	2.3
M (kg/kmol)	97.8	112	101.5	102	106.5	98.6	98.64	98.44
RON	83.5	84	85.3	86.6	85.6	80.3	79	79.5

Table 5: H/C ratio, molecular weight and RON of FACE-A fuel and seven surrogates. Reprinted from Fuel, Volume 176, Elwardany et al., A new formulation of physical surrogates of FACE-A gasoline fuel based on heating and evaporation characteristics, Pages 56-62, Copyright Elsevier (2016).

of components in these surrogates are shown in Table 4.

Firstly, an 8-component surrogate, Surr4, retaining the same mass fractions of n-butane, n-heptane, iso-pentane, and iso-octane as in FACE-A, was suggested. These components contribute more than 70% of the total mass of FACE-A gasoline fuel. It was shown that 2-methylpentane, 3-methylhexane and 2,3-dimethylpentane have similar evaporation behaviour; they were replaced by 3-methylhexane which contributes 25.875% of Surr4. The remaining minor components were replaced by 2,6-dimethyloctane, 1t,2 dimethylcyclopentane and 1-methyl-2-propylcyclohexane. The composition of Surr4 was further simplified in a 7-component surrogate, Surr5, in which n-heptane and 1t,2 dimethylcyclopentane were replaced by n-heptane. Finally in a 6-component surrogate, Surr6, the composition of Surr5 was further simplified by replacing iso-octane and 2,6-dimethyloctane with iso-octane.

The heating and evaporation characteristics of the new surrogates were shown to be much closer to those of the 19 component model, compared to those of the previously suggested surrogates PRF84, Surr1, Surr2 and Surr3. The evaporation time predicted for the Surr6 droplet was shown to be almost identical to that of the FACE-A fuel droplet, while the maximal error in the prediction of the droplet surface temperature did not exceed 2%, which is acceptable in most engineering applications. The evaporation times predicted for Surr4 and Surr5 droplets were shown to be longer than those of the FACE-A droplets by 5%. The difference between the droplet surface temperatures predicted for Surr4 and Surr5 and that for FACE-A did not exceed 13%. It was suggested that Surr5 could be considered an optimal physical surrogate.

To illustrate the ability of the new surrogates to represent FACE-A fuel in engine applications, three additional properties were considered: the H/C ratio, molecular weight, and RON. These are shown in Table 5 alongside similar

properties predicted for surrogates PRF84, Surr1, Surr2 and Surr3. Matching molar masses and H/C ratios of the target fuels indicate both matching diffusivity and flame speed, while matching RONs indicate matching ignition delay time. The values of these properties for FACE-A, PRF84, Surr1, 2 and 3 were taken from the literature (see [112]). The RONs for Surr4, 5 and 6 were calculated following the previously suggested procedure based on the detailed composition of fuels (see [112]). As can be seen from Table 5, compared with the previously suggested surrogates, Surr4, 5 and 6 have values of RON, molar masses, and H/C ratios which are marginally closer to those of FACE-A. Therefore, the new physical surrogates not only improved heating and evaporation prediction, but also have better representations of the H/C ratio, molecular weight, and RON.

Also, Samimi Abiaheh et al. [113] and Su and Chen [114] paid attention to the fact that there was no comprehensive gasoline surrogate that could mimic both the evaporation and combustion of the target gasoline simultaneously with a limited number of components, and suggested new approaches to the design of such surrogates, in a different way to that suggested in [112]. In [113], surrogate components were selected to emulate the hydrogen-to-carbon ratio (H/C), hydrocarbon class distribution, heating value, research and motor octane numbers (RON and MON), density, and distillation curve. Also, their choice was constrained by the availability of kinetic mechanisms. Thus the approach to the selection of surrogates was more stringent than that of [112] where chemical characteristics were concerned and less stringent than that of [112] where physical characteristics were concerned (the analysis of the physical characteristics of surrogates performed in [113] focused only on the distillation curve).

The analysis of [113] led to development of a seven component gasoline surrogate for emulation of the physical and chemical properties of USA non-oxygenated gasoline fuel RD387. It was shown that the surrogate successfully reproduces the distillation curve, H/C, density, and heating value. The surrogate was also shown to be able to adequately reproduce the first stage and total ignition delay times. Finally, the surrogate model reproduced the RCM pressure traces with an acceptable error margin. The laminar flame speeds of the surrogate were also simulated and compared with experimental data for a wide range of pressures and equivalence ratios. A good agreement between the surrogate and gasoline laminar flame speeds was demonstrated, especially for lean to stoichiometric conditions. It was suggested that the surrogate mixture could be used in internal combustion engine modelling.

As in the case of [113], the choice of ‘physical’ surrogate in [114] was based on matching the distillation curves. A new 6-component surrogate mixture composed of i-pentane/n-heptane/toluene/iso-octane/n-propyl cyclohexane/iso-undecane was developed in [114] to match the targeted gasoline in terms of thermophysical properties and experimental distillation curve. This new surrogate also covered the toluene reference fuel components, which are the three basic components for ignition modelling. This allowed the authors to match both physical and chemical characteristics of gasoline fuel using only one surrogate.

In [114] the temperature distribution inside droplets was described by two parameters: surface and core temperatures. This approach is much simpler and less accurate than the one used in MDQDM, where the details of temperature distribution inside droplets were taken into account. In contrast to [112], the authors of [114] took into account the effects of turbulence on liquid thermal diffusivity.

The hybrid multi-component (HMC) model, described in [115], can be considered a simplified version of the MDQDM. In the HMC model, the multi-component fuels (gasoline fuels were considered in [115]) were modelled as several discrete classes, each of which was described by a separate distribution function.

The analysis of heating and evaporation of multi-component droplets thus far described in this section has focused primarily on the liquid phase. It has been assumed that all vapour components in the gas phase behave as a single component. This assumption is relaxed in the next section where recent gas phase evaporation models for multi-component droplets are described.

4.5. Gas phase evaporation models for multi-component droplets

In the classical Stefan-Fuchs theory, Equation (13) for evaporation of mono-component droplets was derived taking into account the conservation of vapour mass flux at any point around a stationary droplet. In the case of multi-component droplets we can impose a similar condition for all individual components in the gas phase. Following [116], this condition can be presented as:

$$\frac{d}{dR} \left(R^2 \rho_{\text{total}} U Y_k - R^2 D^{(k,m)} \rho_{\text{total}} \frac{dY_k}{dR} \right) = 0, \quad (79)$$

where subscript $_k$ refers to ambient gas ($k = 0$) or fuel vapour species ($k = 1, \dots, n$, n is the total number of vapour species), $R \geq R_d$ is the distance from the centre of the droplet in the gaseous phase, $D^{(k,m)}$ is the mass diffusion

coefficient for the species k in the mixture, Y_k are mass fractions of species k , U is the Stefan velocity estimated as

$$U = \frac{\sum_{k=1}^n \dot{m}_d^{(k)}}{4\pi R^2 \rho_{\text{total}}}, \quad (80)$$

$\dot{m}_d^{(k)}$ is evaporation rate of species k (following [116] and in contrast to Equation (13) we assume that $\dot{m}_d^{(k)} \geq 0$ during the evaporation process), ρ_{total} the total density of the mixture, including ambient gas.

The analysis of Equation (79) is very difficult due to the fact that both ρ_{total} and $D^{(k,m)}$ are unknown functions of R . Our further analysis is based on the assumption that ρ_{total} and $D^{(k,m)}$ remain constant for all R (the assumption that ρ_{total} is constant was made when deriving Equation (13)). The values of $D^{(k,m)}$ were estimated in the reference conditions as (Blanc's law):

$$D^{(k,m)} = \left(\sum_{j=0; j \neq k}^n \frac{Y_{j \text{ (ref)}}}{D^{(k,j)}} \right)^{-1}, \quad (81)$$

where

$$Y_{j \text{ (ref)}} = \frac{2Y_{j \text{ (s)}} + Y_{j \text{ (\infty)}}}{3}, \quad (82)$$

$Y_{j \text{ (s)}}$ and $Y_{j \text{ (\infty)}}$ are the mass fractions of species j at the surface of the droplets and in ambient gas, respectively. Expression (82) allows us to consider ρ_{total} under the reference conditions as well ($\rho_{\text{total}} = \rho_{\text{ref}}$).

Having introduced new variable $\zeta = R_d/R$, the general analytical solution to Equation (79) was obtained in the form [116]:

$$Y_k = \alpha_k \exp \left[-\frac{\dot{m}_d^{(\text{total})}}{4\pi \rho_{\text{total}} R_d D^{(k,m)}} \zeta \right] + \varepsilon_k, \quad (83)$$

where $\dot{m}_d^{(\text{total})} = \sum_{k=1}^n \dot{m}_d^{(k)}$,

$$\varepsilon_k = \frac{\dot{m}_d^{(k)}}{\sum_{k=1}^n \dot{m}_d^{(k)}} \quad (84)$$

is the evaporation rate of species k , α_k are unknown constants.

Recalling that $Y_k(\zeta = 0) = Y_{k\infty}$, we find that $\alpha_k = Y_{k\infty} - \varepsilon_k$. This relation for α_k allows us to rewrite Equation (83) for the droplet surface ($\zeta = 1$) as:

$$Y_{ks} = (Y_{k\infty} - \varepsilon_k) \exp \left[-\frac{\dot{m}_d^{(\text{total})}}{4\pi\rho_{\text{total}}R_d D^{(k,m)}} \right] + \varepsilon_k. \quad (85)$$

Equation (83) was rearranged to [116]:

$$\varepsilon_k = \frac{Y_{ks} - Y_{k\infty} \exp \left[-\frac{\dot{m}_d^{(\text{total})}}{4\pi\rho_{\text{total}}R_d D^{(k,m)}} \right]}{1 - \exp \left[-\frac{\dot{m}_d^{(\text{total})}}{4\pi\rho_{\text{total}}R_d D^{(k,m)}} \right]}, \quad (86)$$

$$\sum_{k=1}^n \frac{Y_{ks} - Y_{k\infty}}{\left(1 - \exp \left[-\frac{\dot{m}_d^{(\text{total})}}{4\pi\rho_{\text{total}}R_d D^{(k,m)}} \right] \right)} = 1 = \sum_{k=1}^n Y_{k\infty}. \quad (87)$$

Non-linear Equation (87) was used in [116] to calculate the total evaporation rate $\dot{m}_d^{(\text{total})}$ assuming that the values of all other parameters in this equation are known. Once the value of $\dot{m}_d^{(\text{total})}$ was obtained, the values of ε_k were calculated from Equation (87).

The Stefan-Fuchs equation (79) could be formulated in terms of molar rather than mass fluxes [117]. The latter equation could be solved under the assumption that the molar density of the mixture does not depend on the distance from the droplet surface. The solution to this equation would be rather similar to (86) and (87) and its explicit form was given in [117]. These two equations and their solutions predict slightly different evaporation rates since the conditions of constant total mass density and constant molar density of the mixture are not equivalent.

To take into account the effects of multi-component droplet movement on droplet heating and evaporation, in [116] (as well as in a number of other papers, e.g. [118]) it was assumed that there is no interaction between evaporating species. For each of these species the Abramzon and Sirignano model [11], described in Section 3.1, was applied. The validity of this assumption is not at first evident. This is the reason why, in many papers and books, including [2], the effect of relative motion between species in the gas phase has been ignored altogether.

A comparison between the values of $\dot{m}_d^{(\text{total})}$ inferred from Expression (87) and obtained using a simplified model based on Equation (30) for stationary

droplets was also performed in [116]. In the latter formula it was assumed that $\rho_{\text{total}} = \rho_{\text{ref}}$; B_M was calculated based on the summations of mass fractions of vapour species at the surface of the droplet and ambient conditions. Two approaches to calculation of the diffusion coefficient in (30) were used. Firstly, this coefficient was calculated based on the Wilke and Lee formula (see Formula (45) in [40]) with all input parameters averaged over all species present in the system (this averaging did not take into account different mass fractions of species). Secondly, the coefficient was calculated based on direct averaging of the values of $D^{(k,m)}$ taking into account mass fractions of species:

$$D_v = \frac{\sum_{k=1}^n Y_{k \text{ (ref)}} D^{(k,m)}}{\sum_{k=1}^n Y_{k \text{ (ref)}}}. \quad (88)$$

The models based on the first and second approaches were referred to in [116] as Models 1 and 3. In [116], the predictions of the values of $\dot{m}_d^{(\text{total})}$ inferred from (87) were compared with the predictions of Models 1 and 3 and the predictions of a simplified model described in [119], referred to as Model 2. It was shown that Models 1 and 3 predict values of $\dot{m}_d^{(\text{total})}$ which are almost identical to those inferred from (87), while Model 2 clearly underestimates the evaporation rate. It is anticipated that the predictions of Model 1 would be improved if the averaging of input parameters in the Wilke and Lee formula took into account mass fractions of individual components as in Equation (88). This is expected to provide additional support to the application of a simplified model, where multi-component gas is treated as mono-component, when modelling the evaporation of multi-component fuels (cf. [2]).

The authors of [120, 121, 122, 117] drew attention to the fact that more accurate description of multi-component diffusion, compared with Equation (79), should be based on the Maxwell-Stefan equations. Ignoring the Soret effects, diffusion due to pressure gradients and external forces, these equations can be presented as [123, 117]:

$$\nabla X^{(p)} = \sum_{k=0}^n \frac{1}{C_m D_{pk}} (X^{(p)} \mathbf{N}^{(k)} - X^{(k)} \mathbf{N}^{(p)}), \quad (89)$$

where $X^{(k)}$ is the molar fraction of the k th component, C_m is the molar density of the mixture, $D_{pk} = D_{kp}$ is the binary diffusion coefficient of the p th component into the k th component, $\mathbf{N}^{(p)}$ is the molar flux of the p th component, $k = 0$ refers to ambient gas.

For a multi-component spherical droplet only the radial components of the species molar fluxes can be retained. In this case, Eq. (89) was presented in a similar format to that inferred from Eq. (79). This allowed the authors of [117] to present the solution to (89) in a similar format to (86) and (87), but for molar fractions, assuming that the total molar density does not depend on the distance from the droplet surface.

It was shown that the predictions based on Eq. (79) (Stefan-Fuchs equation) underestimate the total evaporation rate, especially at high ambient gas temperatures, for various droplet compositions. The largest deviation of the absolute values of the evaporation rate, predicted by the Stefan-Fuchs and Maxwell-Stefan equations, was found when none of the species mass fractions was dominant.

4.6. Other approaches to modelling heating and evaporation of multi-component droplets

A new quasi-dimensional multi-component heating and evaporation model for multi-component fuel droplets was suggested in [81]. In contrast to the Discrete Component Model (in [81] this model is referred to as the one-dimensional model) described in Section 4.1 and 4.2, this model is based not on the rigorous solution to heat transfer and species diffusion equations inside droplets, but on the polynomial (quadratic) approximations of the temperature and mass fractions of species distributions inside droplets (in the case of temperature this approach is similar to the one used in the parabolic model discussed in Section 2). As in the case of the Discrete Component Model, the analysis of the quasi-dimensional model is based on the ETC/ED model. Both the ideal gas approach (Raoult's law is assumed to be valid) and the real gas approach were used in the analysis of [81]. The Peng-Robinson equation of state and the van der Waals mixing rule were used. The radiative heating of droplets was taken into account. The authors of [81] believed that their model could be a reasonable compromise between the rigorous Discrete Component Model and a simplistic model in which the temperature and species mass fractions inside droplets were ignored (this model was called the zero-dimensional model in [81]). The model was extensively validated against experimental measurements, and good agreements with these measurements were observed (compared with the prediction of the zero-dimensional model).

When modelling ethanol-blended gasoline fuel droplet evaporation, the authors of [121] relaxed the assumption that Raoult's law is valid and estimated the vapour-liquid equilibrium using quantum chemical *ab initio* de-

scription (see Section 5.3.1). The Maxwell-Stefan diffusion and convection theory (see Eq. (89)) was used for the calculation of gas phase transport characteristics of the components.

A simple relation providing the multi-component diffusion matrix as a power series in terms of the $N - 1$ independent mole fractions in the mixture, where N is the total number of molar fractions, was derived from the kinetic gas theory in [124]. This power series converged quickly for gas mixtures with one major component in which the remaining $N - 1$ species were diluted.

A new reduced multi-component diffusion model for the gas phase was suggested in [125] for application to premixed flames. The main ideas of this model could be applied to the problem of diffusion of components in a multi-component fuel although this has not yet been investigated to the best of my knowledge.

5. Kinetic and molecular dynamics models for droplet heating and evaporation

As in the case of Sections 2 – 4, there are two parts to this section. Firstly the models described in [2] will be summarised. Then the discussion will shift to new models/results, not previously described in [2].

5.1. Background research into kinetic and molecular dynamics modelling

In the models discussed so far the modelling of droplet heating and evaporation processes has been based on the hydrodynamic approximation. In this approximation, vapour at the droplet surface is assumed to be saturated and the evaporation is modelled as the diffusion of vapour from the droplet surface to the ambient gas [2]. The limitations of this approximation have been well known since the pioneering papers published more than 100 years ago (see [126] and the references therein). In a number of studies, summarised in [2], the heating and evaporation of n-dodecane ($C_{12}H_{26}$) (a crude approximation for Diesel fuel) and a mixture of n-dodecane (approximating alkanes in Diesel fuel) and p-dipropylbenzene (approximating aromatics in Diesel fuel) droplets was studied and a new model combining the kinetic and hydrodynamic approaches based on the Boltzmann equations for vapour and air (kinetic region) was developed (an approximation of Diesel fuel by a mixture of n-dodecane and m-xylene was considered in [127], but the implications of this approximation for kinetic modelling have not been investigated). In the immediate vicinity of droplet surfaces (up

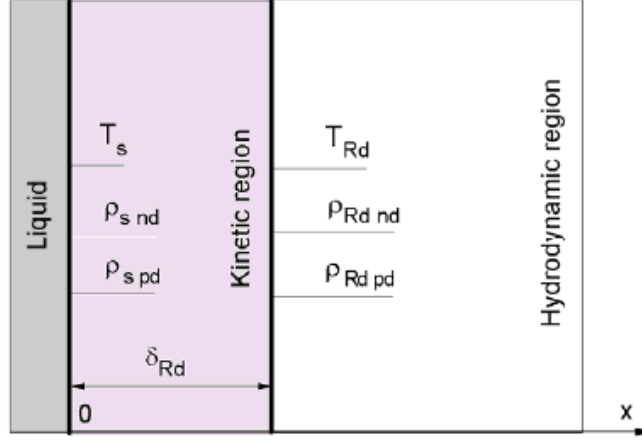


Figure 13: Liquid, kinetic and hydrodynamic regions near the surface of the droplet. T_s is the droplet surface temperature, $\rho_{s(n,p)}$ are n-dodecane (n) and p-dipropylbenzene (p) vapour densities in the immediate vicinity of the droplet surface, T_{Rd} and $\rho_{Rd(n,p)}$ are the temperature and n-dodecane (n) and p-dipropylbenzene (p) vapour densities at the outer boundary of the kinetic region. Reprinted from International Journal of Heat and Mass Transfer, Volume 93, Sazhin et al., A self-consistent kinetic model for droplet heating and evaporation, Pages 1206-1217, Copyright Elsevier (2016).

to about one hundred molecular mean free paths), the vapour and ambient gas dynamics were studied, while at larger distances the analysis was based on the hydrodynamic equations (hydrodynamic region). Mass, momentum and energy fluxes were conserved at the interface between these regions and between the kinetic region and liquid. The modelling took into account the contributions of up to three components in the kinetic region (up to two components approximating Diesel fuel, and air approximated by nitrogen). The above-mentioned three regions in the vicinity of the droplet surface are schematically shown in Fig. 13.

In kinetic modelling inelastic collisions between molecules were taken into account using a simplified model, the main ideas of which are described below. Let us consider two colliding molecules. Regardless of the nature of the collision between them, their centre of mass is not affected by this collision. The state of the molecules after the collision is described in the reference system linked with this centre of mass. In this system, each of these molecules has three translational and a certain number of internal degrees of freedom,

so that the total number of degrees of freedom of both molecules is equal to N . During the collisions, the energies of each molecule are redistributed between the degrees of freedom, but the total number of degrees of freedom remains the same. Also, it is assumed that none of these degrees of freedom predominates. This assumption implies that we should focus our attention on the systems close to thermodynamic equilibrium.

The assumption that none of the degrees of freedom predominates allows us to consider the redistribution of energy between these degrees of freedom during the collision process as random with uniform probability distribution (we are not interested in any specific details of these collisions). For each of these degrees of freedom one dimension in the N -dimensional space, describing all degrees of freedom, is allocated. Once this has been done, we can consider a sphere in this space with its centre at the origin (where energies of all degrees of freedom are equal to zero) and radius given by the following expression:

$$r = \sqrt{\sum_{i=1}^{i=N} E_i}, \quad (90)$$

where E_i is the energy of the i th degree of freedom (translational or internal). Since r^2 gives the total energy of the system E_f , Equation (90) can be considered as an equation of the conservation of energy at the surface of the sphere. The redistribution of energy following an inelastic collision was described as a random motion along the surface of the sphere defined by (90). In the case of elastic collisions this sphere becomes three dimensional ($N = 3$).

It was assumed that the distribution function of evaporated molecules is Maxwellian and vapour pressure at the droplet surface is saturated and obeys Raoult's law (in the case of bi-component droplets). The mass flux of evaporated molecules was controlled by the evaporation coefficient β , which is the ratio of the actual mass flux of molecules leaving the droplet surface and the maximal possible mass flux. The values of this coefficient were inferred from molecular dynamic simulations of the evaporation of n-dodecane presented in [128]. The analysis presented in [128] was based on the United Atom Model and led to the following approximation of the evaporation coefficient for n-dodecane:

$$\beta(T_s) = 7 \times 10^{-6} T_s^2 - 9.8 \times 10^{-3} T_s + 3.7215. \quad (91)$$

where T_s is the droplet surface temperature.

Note that the United Atom Model is based on the Force Field (FF) approximation, when quantum mechanics effects due to the contribution of electron shells are not taken into account (the contributions of these effects will be discussed later in Section 5.3).

The boundary condition at the interface between the kinetic and hydrodynamic regions was inferred based on the requirement of the conservation of heat and mass fluxes at this interface. The hydrodynamic heat and mass fluxes were calculated based on the simplifying assumptions that the temperature at the outer boundary of the kinetic region is equal to the droplet surface temperature and vapour pressure at this boundary is equal to the saturated vapour pressure at temperature equal to the droplet surface temperature. The requirement of the conservation of heat and mass fluxes at this interface allowed us to find the corrected values of temperature and vapour density. The main problem with this approach is that the heat and mass fluxes in the hydrodynamic region, calculated based on these corrected values of temperature and vapour density, are not equal to the heat and mass fluxes in the hydrodynamic region used to find these corrected values, in the general case. This problem was resolved in our recent paper [129], the main results of which are summarised in the next section.

5.2. A self-consistent kinetic model for droplet heating and evaporation

As in the previous approaches, the analysis of [129] was based on finding the values of temperature and vapour density at the outer boundary of the kinetic region. These were inferred from the requirement that both heat flux and mass flux of vapour (or vapour components) in the kinetic and hydrodynamic regions in the vicinity of the interface between these regions should be equal. Initially, these fluxes in the hydrodynamic region were calculated based on the values of temperature and vapour density at the surface of the droplet. Then the values of temperature and vapour density at the outer boundary of the kinetic region, obtained following the above-mentioned procedure, were used to calculate the corrected values of hydrodynamic heat and mass fluxes. In this procedure, the corrected values of temperature and vapour density (or densities in the case of bi-component droplets) at the outer boundary of the kinetic region were used to calculate the corrected values of hydrodynamic heat and mass fluxes. The latter in their turn led to new corrected values of temperature and vapour density at the outer boundary of the kinetic region. One would expect that if this process converges then one would obtain self-consistent values for both heat and mass fluxes. The

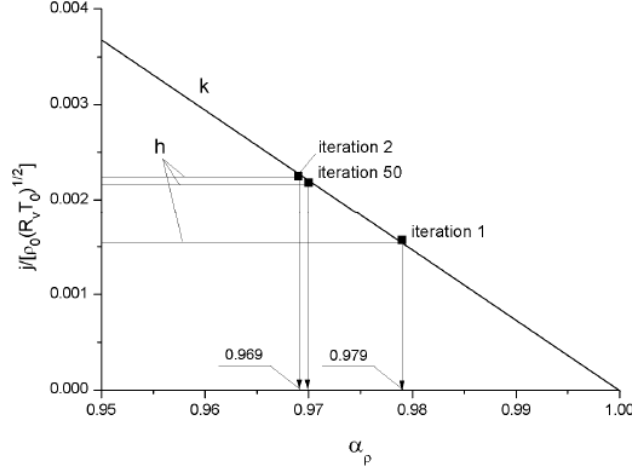


Figure 14: The plots of normalised mass fluxes $\tilde{j} \equiv j/(\rho_0 \sqrt{R_v T_0})$ predicted by the kinetic (line ‘k’) and hydrodynamic (lines ‘h’) models for an n-dodecane droplet moving with velocity 10 m/s versus $\alpha_\rho \equiv \rho_{Rd}/\rho_s$ (normalised vapour density at the outer boundary of the kinetic region). Droplet surface and gas temperatures are assumed equal to 600 K and 1000 K respectively. Reprinted from International Journal of Heat and Mass Transfer, Volume 93, Sazhin et al., A self-consistent kinetic model for droplet heating and evaporation, Pages 1206-1217, Copyright Elsevier (2016).

hydrodynamic and kinetic models used in [129] are similar to the ones described in Sections 5.1, 3 and 4.1, except that the evaporation coefficient was assumed equal to 1 for both n-dodecane and p-dipropylbenzene (the effect of the evaporation coefficient on the results was shown to be small).

The above-mentioned iterative procedure is illustrated in Figs. 14 and 15 for the calculation of density and temperature at the interface between the kinetic and hydrodynamic regions. It was assumed that Diesel fuel is approximated by n-dodecane, a droplet was moving with relative velocity equal to 10 m/s and its surface temperature was equal to 600 K; gas temperature and pressure were taken equal to 1000 K and 30 bar respectively. The plots of $\tilde{j}_k \equiv j_{k,n}/(\rho_0 \sqrt{R_v T_0})$ versus α_ρ and $\tilde{q}_k \equiv q_k/(p_0 \sqrt{R_v T_0})$ versus α_T are shown in Figs. 14 and 15, respectively (lines indicated as ‘k’). In the same figures, the plots of $\tilde{j}_h \equiv j_{h,n}/(\rho_0 \sqrt{R_v T_0})$ versus α_ρ and $\tilde{q}_h \equiv q_h/(p_0 \sqrt{R_v T_0})$ versus α_T , assuming that $\alpha_\rho = 1$ and $\alpha_T = 1$, are also shown (lines marked ‘h’, iteration 1). The intersection between these two pairs of lines gave the values

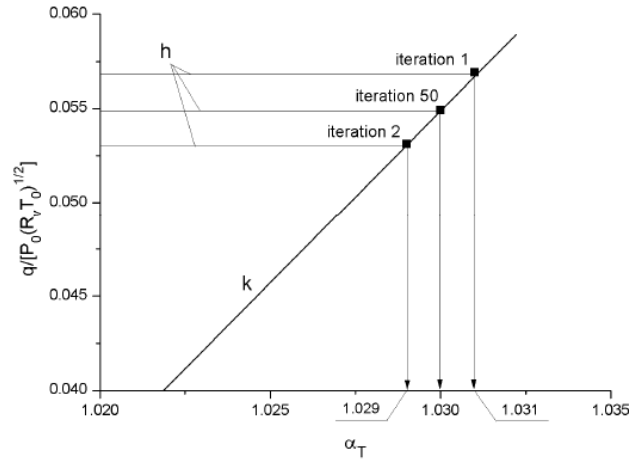


Figure 15: The plots of normalised heat fluxes $\tilde{q} \equiv q/(p_0 \sqrt{R_v T_0})$ predicted by the kinetic (line ‘k’) and hydrodynamic (lines ‘h’) models for an n-dodecane droplet moving with velocity 10 m/s versus $\alpha_T \equiv T_{Rd}/T_s$ (normalised temperature at the outer boundary of the kinetic region). Droplet surface and gas temperatures are assumed equal to 600 K and 1000 K respectively. Reprinted from International Journal of Heat and Mass Transfer, Volume 93, Sazhin et al., A self-consistent kinetic model for droplet heating and evaporation, Pages 1206-1217, Copyright Elsevier (2016).

$\alpha_\rho = 0.979$ and $\alpha_T = 1.031$.

In the analysis presented in [2] these corrections were directly used for calculation of mass and heat fluxes, taking into account the kinetic effects. In the new model described in [129], these corrections were used to update the values of \tilde{j}_h and \tilde{q}_h , and the updated values of these fluxes are shown in Figs. 14 and 15 as the lines marked ‘h’, iteration 2. The intersections of these new lines with lines \tilde{j}_k and \tilde{q}_k provide us with updated values $\alpha_\rho = 0.969$ and $\alpha_T = 1.029$. Further iterations up to iteration 50 lead to visible changes in these corrections, as shown in the same Figs. 14 and 15. The difference in the values of α_ρ and α_T inferred from consecutive iterations decreases with increasing iteration number, so that the differences between these values inferred from the 49th iteration were almost indistinguishable from those inferred from the 50th iteration. Note that, in contrast to the previously used non-self-consistent model, the new approach does not rely on the observation that \tilde{q}_k is almost independent of α_ρ and \tilde{j}_k is almost independent of α_T .

The same analysis as presented in Figs. 14 and 15 was repeated for other droplet surface temperatures in the range 300-650 K and gas temperatures 800 K, 1000 K and 1200 K. Also, the same analysis was repeated for bi-component droplets (80% n-dodecane and 20% p-dipropylbenzene mixture) for droplet surface temperatures in the range 300-650 K and gas temperature equal to 1000 K. The predictions of the kinetic model at temperatures close to the critical temperature of n-dodecane ($T_{cr} = 659$ K) proved to be unreliable and it was assumed that the values of α_ρ and α_T at $T_s > 650$ K are the same as at $T_s = 650$ K. This assumption is expected to affect the very final stage of droplet evaporation, and has limited effect on the overall picture of droplet heating and evaporation.

The results of the above-mentioned analyses are presented in the form of the plots of α_ρ and α_T versus droplet surface temperatures T_s for gas temperatures and pressure equal to 1000 K and 30 bar, respectively, and n-dodecane droplet velocity 10 m/s, shown in Figs. 16 and 17. As can be seen from Fig. 16, the values of α_ρ decrease with increasing T_s . The values of α_ρ inferred from iteration 2 are lower than those inferred from iteration 1; these values for the 3rd iteration are almost indistinguishable from those inferred from all the following iterations up to iteration 50. The behaviour of the curve α_T versus T_s , shown in Fig. 17, appears to be more complex than that of α_ρ versus T_s . For low temperatures α_T increases with increasing T_s , at intermediate temperatures α_T decreases with increasing T_s , and at temperatures close to 650 K, α_T again increases with increasing T_s . As in the

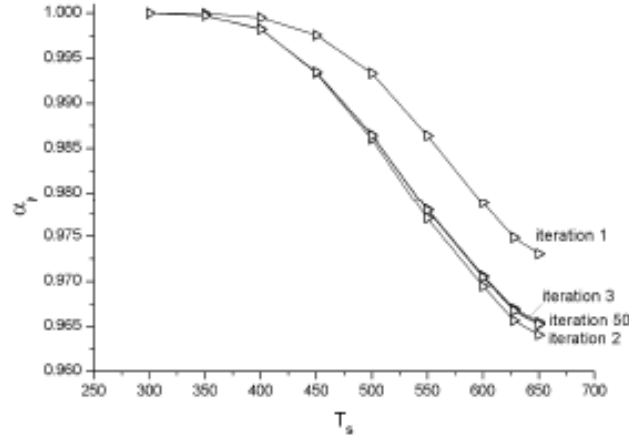


Figure 16: The plots of α_ρ versus T_s for an n-dodecane droplet moving with velocity 10 m/s in gas (air) at temperature equal to 1000 K. Reprinted from International Journal of Heat and Mass Transfer, Volume 93, Sazhin et al., A self-consistent kinetic model for droplet heating and evaporation, Pages 1206-1217, Copyright Elsevier (2016).

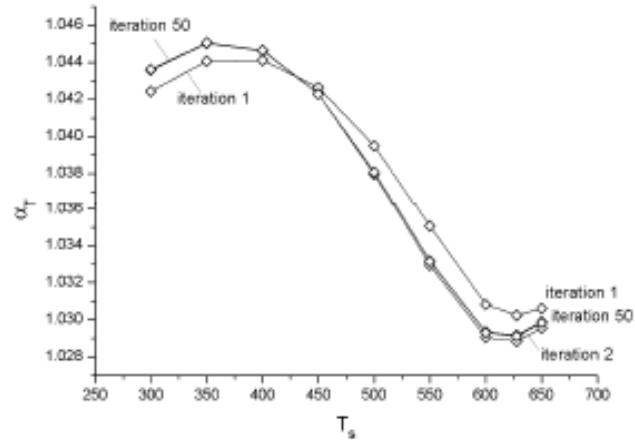


Figure 17: The plots of α_T versus T_s for an n-dodecane droplet moving with velocity 10 m/s in gas (air) at temperature equal to 1000 K. Reprinted from International Journal of Heat and Mass Transfer, Volume 93, Sazhin et al., A self-consistent kinetic model for droplet heating and evaporation, Pages 1206-1217, Copyright Elsevier (2016).

case of α_ρ , the values of α_T inferred from iteration 3 and higher iterations are almost indistinguishable. These values are slightly higher than those inferred from iteration 1 for low T_s and slightly lower than those inferred from iteration 1 for high T_s . In our analysis, the values inferred from iteration 50 are assumed to describe adequately the self-consistent heat and mass fluxes in the vicinity of the surfaces of heated and evaporating droplets.

The general shapes of the curves for other values of gas temperatures and approximations of Diesel fuel turned out to be similar to the ones shown in Figs. 16 and 17. The new model was applied to the analysis of heating and evaporation of Diesel fuel droplets with initial radii and temperature equal to 5 μm and 300 K, immersed into gas with temperatures equal to 800 K, 1000 K and 1200 K and pressure equal to 30 bar. Droplets were stationary or moving with fixed velocity equal to 10 m/s. It was shown that in all cases the kinetic effects led to a decrease in droplet surface temperature and an increase in the evaporation time. This increase was shown to be more visible for higher gas temperatures and moving droplets. The addition of p-dipropylbenzene was shown to decrease the kinetic effects on the droplet evaporation time.

5.3. *New approaches to the estimation of the evaporation coefficient*

As mentioned in Section 5.1, the solution to the Boltzmann equation in the kinetic region requires formulation of the boundary condition at the liquid/gas interface. This boundary condition is essentially controlled by the evaporation coefficient. The approximation of the results molecular dynamics calculations of this coefficient, using the United Atom Model, is given by Equations (91).

One of the main limitations of the United Atom Model, used for approximation (91), is that in this model the interaction between individual molecules was described using the force field (FF) methods, which simplify both inter- and inner-molecular interactions by ignoring electrons *per se*. The applicability of this approach is far from obvious, as the dynamics of individual molecules in the vicinity of droplet surfaces are essentially quantum mechanical processes. The quantum mechanical (quantum-chemical (QC)) models describing the processes at and in the vicinity of Diesel fuel droplet surfaces are described in [103, 130, 131, 132, 133]. Note that papers [103, 130, 131, 132] primarily address the quantum chemistry community. The importance of the results presented in these papers might have been overlooked by a wider engineering audience. The main objective of [133] was

to summarise the main results reported in [103, 130, 131, 132], but in a format that can be easily understood by the engineering community interested in modelling the heating and evaporation of Diesel fuel droplets. The main results of [133] are summarised in this section of the review.

5.3.1. Brief overview of quantum-chemical methods

Although the solution to the Schrödinger equation for the wave function ψ in some simple cases (e.g. isolated hydrogen atom) is well known and described in standard quantum mechanics textbooks, its general solution when many particles need to be analysed simultaneously is still a challenge for quantum mechanical modelling. One of the most widely used simplified methods to solve this equation is known as the Hartree-Fock (HF) method. There are two strategies for application of the HF method for practical calculations. In the semi-empirical methods the integrals used in the HF method are estimated based on experimental data or based on a series of rules which allow us to set certain integrals to zero. In the *ab initio* methods an attempt is made to calculate all these integrals.

Although the HF method is widely used in practical computations, this method is still an approximate one and demands considerable computational effort. This led to the development of alternative approaches to the calculation of electronic systems, including the Density Functional Theory (DFT). This technique focuses on the electron density (ρ_e) rather than on the wave function ψ_e . In this theory it is assumed that the energy of a molecule is a function of the electron density. Since the electron density is a function of position $\rho_e(\mathbf{r})$, this energy appears to be a function of a function, that is functional of density. This approach appears to be not only much less demanding computationally compared with the HF method, but in some cases it can lead to more accurate results compared with the latter method.

On some occasions various approximations of the energy functional in the DFT, that incorporate parts of the exact exchange from the HF theory, have been suggested. One such approach is known as B3LYP (Becke, 3-parameter, Lee-Yang-Parr). Various semi-empirical quantum chemistry methods, mentioned earlier, are important for dealing with large molecules where the full HF method without the approximations (*ab initio* approach) and DFT are too expensive. In these methods a range of fitting parameters are typically used to produce the results that best agree with experimental data or with *ab initio* results (e.g. PM7 method). The parameters in the PM7 method were calibrated to obtain results consistent with experimental and *ab initio*

data for more than 9000 compounds. The accuracy of the PM7 method is close to that of the *ab initio* and DFT methods used with the 6-31G(d) basis set.

The main differences between the classical MM/MD, semi-empirical PM7, *ab initio* and DFT methods are due to the way in which the contributions of electrons are taken into account. The contribution of all electrons is taken into account in *ab initio* and DFT with self-consistent field (SCF); only valence electrons are considered in semi-empirical quantum-chemical methods (QCMs) with SCF, and no electrons *per se* are considered in classical MM/MD methods without SCF.

A new continuum solvation model based on the quantum mechanical charge density of a solute molecule interacting with a continuum description of a solvent was named the SMD (*D* stands for density which refers to the full solute electron density) model. The term continuum indicates that the solvent is represented as a dielectric medium with surface tension at the solute-solvent boundary. The SMD model was parameterized with a training set of almost three thousand solvation data.

In the case of modelling of the transient processes, the Dynamic Reaction Coordinates (DRC) method has been widely used. The key concept of this method is the Dynamic Reaction Coordinate which is the path followed by all the atoms in a system assuming the conservation of energy. In contrast to conventional molecular dynamic (MD) approaches, the contributions of the processes at the electronic level are taken into account.

The models described in this section have been implemented in a number of known programs, including Gaussian 09, WinGAMESS 2013 R1, and MOPAC2012. Some results of their applications, using these three programs, are summarised in the following sections.

5.3.2. Evaporation rate

To the best of our knowledge, the first attempt to perform a quantum chemical study of the processes during the evaporation of real-life Diesel fuel droplets was described in [103]. The composition of Diesel fuel used in their analysis is shown in Fig. 7, while the analysis focused on the evaporation from the surface of a Diesel fuel droplet into a vacuum, described by the evaporation rate:

$$\gamma = \left(\frac{1}{t}\right) \ln \left(\frac{n_{\text{ev}}(t)}{n_0}\right), \quad (92)$$

where $n_{\text{ev}}(t)$ is the time dependent number of molecules leaving the droplet, n_0 is the initial number of molecules, t is the duration of the process. Considering the evaporation rate of the i th-molecule from a cluster (or nanodroplet) $i + j$ ($\gamma_{i(i+j)}$), the value of $\gamma_{i(i+j)}$ was estimated as [134, 135]:

$$\gamma_{i(i+j)} = b_{ij} \frac{p}{k_B T n_0} \exp \left(\frac{\Delta G_{i+j} - \Delta G_i - \Delta G_j}{k_B T} \right), \quad (93)$$

where ΔG_{i+j} , ΔG_i , and ΔG_j are the Gibbs free energies of formation of the molecules (clusters/nanodroplets) from monomers (molecules) at the reference pressure p . An additional assumption that clusters or nanodroplets are so small that their interaction with molecules can be described by the kinetic gas theory was made for the estimation of b_{ij} .

Although these assumptions are rather restrictive for practical engineering applications, they allowed the authors of [103] to gain insight into the physics of some of the processes at the surface of the droplets. The SMD/HF or SMD/DFT models with the same 6-31G(d,p) basis set were used to estimate changes in the Gibbs free energy during the transfer of a molecule from a liquid medium into a gas phase. Such solvents as n-dodecane, tetraline, benzene, and isopropyltoluene were used to analyse the effects of surroundings on the evaporation rate of the components of Diesel fuel: normal, iso and cyclic alkanes, 1-3 ring aromatics, tetralines and indanes (in the C₁₂-C₂₀ range). It was shown that compounds C₁₄-C₁₆ make the main contribution to the Diesel fuel under consideration. An increase in the molecular size of alkanes from n-octane to n-heptacosane or in the aromaticity of compounds resulted in a strong decrease in the values of the evaporation rate.

In contrast to [103], the analysis of [130] focused only on alkanes as the main components of Diesel fuels, and particularly on n-dodecane, the component widely used as a representative of this fuel. The evaporation rate was shown to decrease with increasing cluster/nanodroplet diameter and decreasing temperature. The relative number of evaporated molecules, however, did not depend on cluster/nanodroplet diameters, and increased with increasing temperature. At certain temperatures, the clusters/nanodroplets were expected to fully evaporate. The relative number of residual molecules in clusters/nanodroplets for n-alkanes in the range C₈-C₂₇ was shown to increase with temperature and with the carbon numbers in the molecules. Thus the evaporation process of a mixture of n-alkanes was expected to lead to increased concentration of heavy n-alkanes in droplets, which is consistent with the results presented in Section 4.

Steady-state evaporation from a liquid surface into a vacuum was also modelled in [136] by non-equilibrium molecular dynamics simulations of a Lennard-Jones fluid, without taking into account quantum chemical effects.

5.3.3. *Interaction between molecules and clusters/nanodroplets*

The analysis described in Section 5.3.2 referred to the integral characteristics of the processes at the surface of the droplets. In this section, the details of the analysis of the collision processes between n-dodecane molecules and clusters/nanodroplets, based on the Dynamic Reaction Coordinate (DRC) method, are described, following [130] and [133]. These processes are expected to lead to scattering or sticking of the molecules. In the DRC calculations, the total kinetic energy includes the kinetic energy of random thermal bond vibrations and rotations and the kinetic energy of the translational motion of the whole molecules. In the above-mentioned papers, the DRC method was applied to study the dependence of sticking/scattering of n-dodecane molecules on their angles of attack, temperature, and cluster/nanodroplet size. The DRC calculations were performed for molecules interacting with a cluster (7 molecules) or a nanodropletlet (64 or 128 molecules) of n-dodecane molecules. The results are shown in Fig. 18.

From Fig. 18, at large angles of attack, absorption of a molecule by a cluster or nanodrop of relatively small size ($d = 2-7$ nm) can be clearly seen if the kinetic energy is low and the attacking molecule is not oriented exactly towards one of the surface molecules. At $\Theta \approx 1^\circ$ an almost perfectly elastic collision is observed if the molecule has relatively high kinetic energy (~ 10 kJ/mol or larger) and is oriented directly towards one of the surface molecules. In the DRC calculations the kinetic energy of the molecules in the clusters or nanodroplets was low and thermal vibrations and bond rotations corresponded to 300-400 K. The kinetic energy of the attacking molecule was high (its effective temperature was in the range 500-1200 K).

Further analyses, similar to those shown in Fig. 18, allowed the authors of [130] and [133] to conclude that the probability of the attacking molecule sticking to a droplet is maximal if the molecular plane is parallel or almost parallel to the droplet surface. This corresponds to multi-point interactions of relatively long n-dodecane molecules with the droplet surface. If the kinetic energy of the attacking molecules is greater than that of boiling temperature then it is expected that they will scatter and be removed from the cluster/nanodroplet surface. Molecule-nanodroplet interaction results (sticking

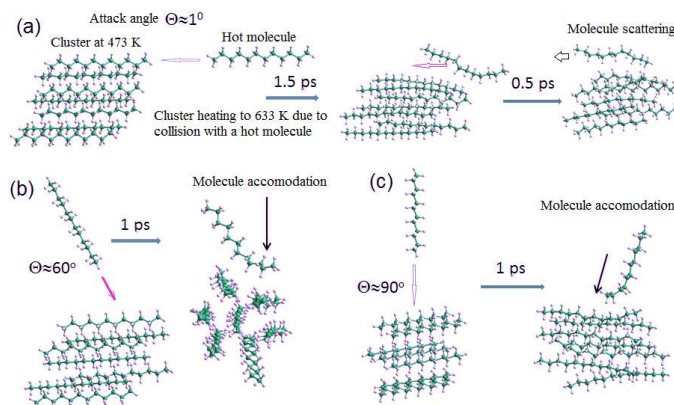


Figure 18: Interaction of an n-dodecane molecule (hot, temperature ~ 1100 K) with a cluster of seven n-dodecane molecules (initial temperature 473 K; it increases due to the interaction with a hot molecule) at the angles of attack $\Theta \approx$ (a) 1° , (b) 60° and (c) 90° . The results were obtained using the DFT B3LYP. Reprinted from Fuel, Volume 165, Sazhin et al., Quantum-chemical analysis of the processes at the surfaces of Diesel fuel droplets, Pages 405-412, Copyright Elsevier (2016).

or scattering) depend on the kinetic energy and orientations of the attacking and surface molecules. It was shown that the mechanisms of evaporation of microdroplets and nanodroplets are likely to involve rather different processes. In the case of microdroplets, individual carbon molecules are evaporated from their surfaces, while nanodroplets are expected to disintegrate into clusters and individual molecules.

The decrease in the likelihood of evaporation/condensation with temperature, predicted by the analysis presented above, agrees with the prediction of the classical theory based on the MD simulations of n-dodecane molecules (see [128]). At the same time, the analysis of this section does not allow us to predict the evaporation coefficient, as was done in [128]) using the classical FF analysis. The analysis of each collision process, shown in Fig. 18, required a powerful PC. To study these processes using DFT/DRC methods for larger systems with dozens or hundreds of molecules, a supercomputer would be needed. The latter was used for some calculations to study the conformerisation effects for n-dodecane (95 conformers). To quantify the values of the evaporation/condensation coefficient, using the above-mentioned analysis, one would need to repeat these calculations for a wide range of angles of attack, orientation of molecules and energies for various conformers and

various conditions of clusters and nanodroplets (the effects of the size of the clusters/nanodroplets would need to be investigated as well). Since this does not look feasible at the moment, an alternative approach to calculating the above-mentioned evaporation/condensation coefficient, taking into account quantum chemical effects, is described in Section 5.3.4, following [131] and [133].

5.3.4. Estimation of the evaporation/condensation coefficient

The analysis of [131] was based on the transition state theory (TST) and quantum chemical DFT methods. These were applied to several ensembles of n-dodecane conformers. There was similarity between the approach used in [131] and the one used previously (see [2]). In contrast to the previous studies, however, in the analysis of [131] the TST was based on a QC DFT approach taking into account the conformerisation of n-dodecane molecules (considered as a representative of Diesel fuel). It was shown that the most accurate expression for the condensation coefficient is the one averaged over the states of various conformers transferred between two phases and given by the following formula [131]:

$$\langle \beta_V \rangle = \left\{ 1 - \left[\frac{\rho_g}{\rho_l} \exp \frac{\langle \Delta G_{g \rightarrow l} \rangle}{RT} \right]^{1/3} \right\} \exp \left\{ -0.5 \left[\left[\frac{\rho_g}{\rho_l} \exp \frac{\langle \Delta G_{g \rightarrow l} \rangle}{RT} \right]^{1/3} - 1 \right]^{-1} \right\}, \quad (94)$$

where R is the universal gas constant, $\rho_{g(l)}$ is the gas (liquid) density, $\Delta G_{g \rightarrow l}$ is the change in the Gibbs free energy during the condensation process, subscript V indicates that the expression for β explicitly depends on the specific volumes, $\langle \rangle$ indicates averaging over the states of various conformers transferred between two phases. It was assumed that the process under consideration is quasi-steady-state and the condensation coefficient is equal to the evaporation coefficient.

The effects of both the conformerisation and cross-conformerisation (changes in conformer state during transfer into another phase) of n-dodecane molecules (CDM effects), which can contribute to the Gibbs free energies of evaporation and solvation, were taken into account. Ninety-five stable conformers were selected based on the changes in the Gibbs free energy.

A comparison between the results of calculations of β based on Expression (94) and those obtained previously is shown in Fig. 19. As one can see from this figure, taking into account the QC effects leads to marginal modifi-

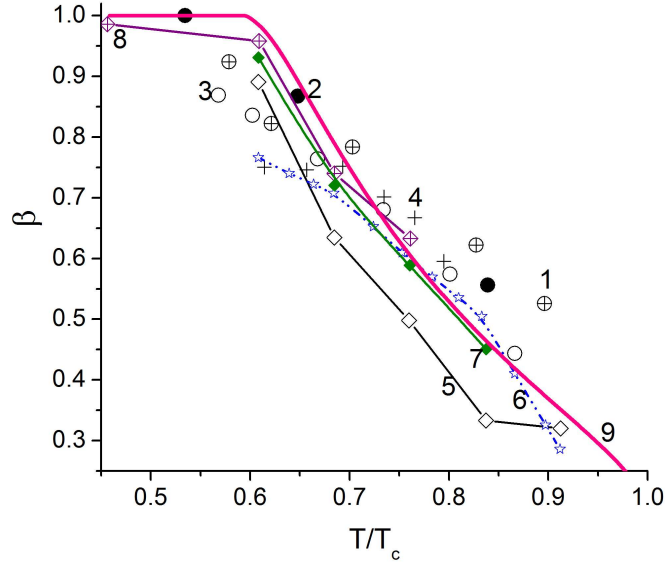


Figure 19: Comparison of the values of the evaporation coefficient β , predicted by MD, FF (symbols 1-4, curves 5-8) and Expression (94) (curve 9), versus normalised temperature (T/T_c , where T_c is the critical temperature). Symbols (1-4) refer to the models for structureless LJ fluids with various input parameters [137, 138], curves 5 and 7 refer to the results obtained based on the United Atom Model reported in [139, 128], respectively, curve 6 refers to the results of calculations based on the TST model reproduced from [139], curve 8 is based on the results of calculations using the model described by Mizuguchi et al. [138]. QC calculations were performed using DFT ω B97X-D/cc-pVTZ and SMD/ ω B97X-D/cc-pVTZ. Reprinted from Fuel, Volume 165, Sazhin et al., Quantum-chemical analysis of the processes at the surfaces of Diesel fuel droplets, Pages 405-412, Copyright Elsevier (2016).

cations of the predicted evaporation/condensation coefficient, except at temperatures close to the critical temperature (where this modification turned out to be significant). Thus, although the analysis of the QC effects takes into account many new effects ignored in the conventional FF approach, the contribution of these effects to the values of the evaporation/condensation coefficient turned out to be marginal, unless temperatures close to the critical temperature were considered.

6. Unsolved problems

Although the results summarised early in this review show noticeable progress in the development of the models of droplet heating and evaporation, many important problems in this area are still not resolved. The focus of this section will be on some of these unsolved problems. This list is certainly not complete. The selection of unsolved problems is rather subjective, and has been motivated by the author's personal research interests. There will be some overlap between the discussion of unsolved problems below and the one presented in [140].

6.1. *Non-spherical droplets*

Most of the models discussed so far are applicable only to spherical droplets, while the shapes of most of the droplets observed in various environmental and engineering applications, including those in internal combustion engines, are far from spherical [61, 141]. Some preliminary results referring to the modelling of heating and evaporation of spheroidal droplets are discussed in Section 3.3. The main limitation of the approach discussed in this section is that it is applicable only to weakly deformed spherical droplets. Even in this case, however, it was not possible to develop models as elegant as the ones developed for spherical droplets. The perturbation methods might be used if the deviation of the shape of the droplets from the spherical is very small, or these shapes can be approximated by long cylinders. In the general case, however, these problems would most likely need to be analysed using complex and CPU intensive numerical methods, which are still to be developed.

6.2. *Limitations of the ETC/ED model*

The application of analytical models for moving spherical droplets has been based on the assumption that the Effective Thermal Conductivity/Effective

Diffusivity (ETC/ED) model is valid. The validity of this model was investigated based on the direct comparison of the predictions of this model and the prediction of a more general vortex model for a limited range of parameters (see this comparison for the ETC model presented in [11, 13]). The applicability of the model outside this range is not at all obvious. In any case, the errors linked with the application of this model could only be estimated based on a direct comparison between its predictions and the predictions of the vortex model for a wider range of parameters. This has not yet been done. Another problem with the application of the ETC/ED model lies in the assumption that a realistic inhomogeneous distribution of surface temperatures in moving droplets can be approximated by the homogeneous distribution in the analysis of droplet heating and evaporation. The limits of applicability of this assumption would require special investigation.

6.3. Effects of the interaction between droplets

As demonstrated in a number of recent papers summarised in [2], even in the simple case of droplets moving in tandem the effect of interaction between droplets on their heating and evaporation cannot be ignored when the distance parameter (ratio of the distance between droplets and their diameter) is less than about 10 (see [142] for further discussions of this issue). Various semi-empirical formulae taking into account these interactions have been suggested. In realistic internal combustion engines, however, the mutual positions of moving droplets are quite complex [61, 141]. Also, the number of droplets affecting any particular droplet in a dense spray can be rather large. It is not clear how this complex interaction between droplets can be taken into account when modelling individual droplet heating and evaporation. In a number of papers, including [143], it was demonstrated that increasing the number of droplets per unit volume reduces the evaporation rate.

6.4. Droplet heating and evaporation in near- and super-critical conditions

Most of the models described in [2] and in this review have been developed for those cases when both temperature and pressure do not approach the critical point. This restriction of these models have turned out to be crucial for many engineering applications including those in realistic Diesel engine conditions, where both temperature and pressure are likely to reach and exceed critical values. Taking pressure as an example, Diesel and biodiesel fuels are injected into a cylinder pressurised to about 25 atm, which may then

increase to more than 60 atm after ignition. At the same time, critical pressure for most hydrocarbon fuels is expected to be in the range of 15-30 atm. Therefore fuel spray processes, including droplet heating and evaporation, occur under near-, trans- and super-critical regimes. Under these regimes, the properties of liquid fuels change significantly. (1) The latent heat of evaporation becomes zero; as a consequence, the solubility of one fluid into the other, instead of evaporation, becomes important [144]; (2) The sharp distinction between the liquid and gas phase disappears, and thus the surface tension vanishes; (3) Transport and thermodynamic properties may vary significantly even with small changes in temperature and pressure due to strong thermodynamic nonideality and nonlinearity [144].

6.5. Effects of the moving interface due to evaporation

The effects of the moving interface due to evaporation on droplet heating and diffusion of species inside droplets, discussed in [2], look rather unexpected from the point of view of the physical background of the problem. From the point of view of classical mechanics, one would expect that the exchange of energy between a lorry, and a ball hitting the back of that lorry, would decrease in the case when the lorry moves away from the approaching ball, compared with the case of a stationary lorry. The same decrease in energy is predicted by the model described in [2]. The problem, however, lies in the quantification of this effect. Since the velocity of the moving interface due to evaporation is many orders of magnitude less than the velocity of molecules, this effect would be expected to be negligibly small in contrast to the prediction of the model. Hence, the investigation of the physical background of this effect still needs to be performed. Also, the analysis of droplet heating and evaporation in the presence of the moving interface, described in [2], did not take into account the effect of thermal radiation. We do not anticipate any serious difficulties in taking into account this effect, if we assume that droplets are semi-transparent and the radiative heating is spherically symmetric (cf. the effect of thermal radiation on droplet heating in the case of a stationary boundary [2]).

6.6. Complex multi-component droplets

We believe that the development of the Multi-dimensional Quasi-discrete model (MDQDM), described in Sections 4.3 and 4.4, was a considerable step forward in the development of a model for heating and evaporation of complex multi-component droplets (Diesel and gasoline fuel droplets). The version of

this model described in these sections, however, can be considered a preliminary one. The choice of quasi-components and components in this model was based on trial and error and no ‘universal’ algorithm for their selection was developed. As in the case of the Discrete Component Model, the MDQDM was based on the assumption that the diffusion coefficient of all species is the same and is controlled only by the composition of the droplet. This assumption introduces errors which are impossible to quantify at present. The corrections of the liquid diffusion coefficient due to droplet motion were estimated based on the average composition of droplets. The validity of this assumption has never been investigated to the best of my knowledge. Finally, this model was developed for modelling heating and evaporation of spherical droplets. Its generalisation to the case of non-spherical droplets (even slightly deformed spheres) has not been investigated to the best of my knowledge.

6.7. Advanced kinetic and molecular dynamics models

Recent progress in the development of advanced kinetic and molecular dynamics models was summarised in Section 5. The effect of the complexity of Diesel fuel composition was taken into account by approximating this fuel with a mixture of n-dodecane and p-dipropylbenzene. Crude estimates of quantum chemical effects on the value of the evaporation coefficient of n-dodecane droplets were made, and these effects were shown to be small except at temperatures close to the critical temperature. Despite the above-mentioned progress in the development of these models, there are a number of issues which have still to be addressed. The approximation of Diesel fuel by just two components is certainly too crude even for engineering applications. We cannot use the 98 component approximation, developed in the Multi-dimensional Quasi-discrete model, in kinetic modelling, but it would be essential to take into account the heaviest components of this fuel which are the dominant components at the final stage of Diesel fuel droplet heating and evaporation. If this is not done then errors due to ignoring the kinetic effects altogether could be less than those due to the simplified approximation of Diesel fuel. Despite our early conclusion that quantum-chemical effects on the values of the evaporation coefficient are weak, this issue cannot be considered closed. Firstly this conclusion was drawn based on the application of a rather simplistic model. The quantum-chemical effects on the values of the evaporation coefficient, analysed more advanced models (e.g. the models considered in Section 5.3.3) are still to be investigated. Also, the quantum-chemical effects on the evaporation coefficient for realistic multi-

component Diesel fuel droplets have not been investigated at all to the best of my knowledge.

6.8. Effective approximation of the kinetic effects

As mentioned in [2], the only feasible way to apply the results of kinetic modelling to the analysis of Diesel fuel droplet heating and evaporation within CFD codes would be to approximate these results using simple approximate analytical formulae. The first attempt to do this was made in [145] (this paper is discussed in [2]), where simple approximate formulae describing the temporal evolution of Diesel fuel droplet radii and temperatures predicted by the kinetic model are suggested. These formulae, however, are valid for a rather limited range of gas temperatures and fixed values of initial droplet radii, or for a limited range of initial droplet radii and fixed values of gas temperature. A more general approximation of these results has yet to be found. An alternative approach to approximating the kinetic results was suggested in [129]. This approach was based on the approximation of the vapour density and temperature at the outer boundary of the kinetic region, rather than on the direct approximation of the values of the droplet radii and surface temperatures. The applicability of the approach suggested in [129] to engineering CFD modelling is still to be investigated.

Acknowledgements

The author is grateful to EPSRC (grants EP/K005758/1 and EP/M002608/1) for their financial support.

References

- [1] S. S. Sazhin, Advanced models of fuel droplet heating and evaporation, *Progress in Energy and Combustion Science* 32 (2006) 162–214.
- [2] S. S. Sazhin, *Droplets and Sprays*, Springer, Heidelberg, 2014.
- [3] J. B. Heywood, *Internal combustion engines fundamentals*, McGraw-Hill, New York, 1988.
- [4] M. Rahman, M. Saghir, Thermodiffusion or Soret effect: Historical review, *International Journal of Heat and Mass Transfer* 73 (2014) 693 – 705. doi:<http://dx.doi.org/10.1016/j.ijheatmasstransfer.2014.02.057>. URL <http://www.sciencedirect.com/science/article/pii/S0017931014001859>

- [5] W. A. Sirignano, Advances in droplet array combustion theory and modeling, *Progress in Energy and Combustion Science* 42 (2014) 54 – 86. doi:<http://dx.doi.org/10.1016/j.pecs.2014.01.002>.
URL <http://www.sciencedirect.com/science/article/pii/S0360128514000033>
- [6] S. K. Aggarwal, Single droplet ignition: Theoretical analyses and experimental findings, *Progress in Energy and Combustion Science* 45 (2014) 79 – 107. doi:<http://dx.doi.org/10.1016/j.pecs.2014.05.002>.
URL <http://www.sciencedirect.com/science/article/pii/S0360128514000276>
- [7] H. Olguin, E. Gutheil, Influence of evaporation on spray flamelet structures, *Combustion and Flame* 161 (4) (2014) 987 – 996. doi:<http://dx.doi.org/10.1016/j.combustflame.2013.10.010>.
URL <http://www.sciencedirect.com/science/article/pii/S0010218013003842>
- [8] O. Rybdylova, M. Al Qubeissi, M. Braun, C. Crua, J. Manin, L. M. Pickett, G. de Sercey, E. M. Sazhina, S. S. Sazhin, M. Heikal, A model for droplet heating and its implementation into ANSYS Fluent, *International Communications in Heat and Mass Transfer*.
- [9] A. Aissa, M. Abdelouahab, A. Nouredine, M. El Ganaoui, B. Pateyron, Ranz and Marcschall correlations limits on heat flow between a sphere and its surrounding gas at high temperature, *Thermal Science* 19 (5) (2015) 1521–1528.
- [10] R. Clift, J. R. Grace, M. E. Weber, *Bubbles, Drops and Particles*, Academic Press, New York, 1978.
- [11] B. Abramzon, W. A. Sirignano, Droplet vaporization model for spray combustion calculations, *International Journal of Heat and Mass Transfer* 32 (1989) 1605–1618.
- [12] C. Yin, Modelling of heating and evaporation of n-heptane droplets: Towards a generic model for fuel droplet/particle conversion, *Fuel* 141 (2015) 64 – 73. doi:<http://dx.doi.org/10.1016/j.fuel.2014.10.031>.
URL <http://www.sciencedirect.com/science/article/pii/S0016236114010266>
- [13] B. Abramzon, S. S. Sazhin, Convective vaporization of fuel droplets with thermal radiation absorption, *Fuel* 85 (2006) 32–46.

- [14] G. Gouesbet, G. Grehan, Generalized Lorenz-Mie theories, Springer, Berlin, 2011.
- [15] M. Brewster, Evaporation and condensation of water mist/cloud droplets with thermal radiation, International Journal of Heat and Mass Transfer 88 (2015) 695 – 712.
doi:<http://dx.doi.org/10.1016/j.ijheatmasstransfer.2015.03.055>.
URL <http://www.sciencedirect.com/science/article/pii/S0017931015003130>
- [16] M. Brewster, Corrigendum to evaporation and condensation of water mist/cloud droplets with thermal radiation [int. j. heat mass transfer 88 (2015) 695712], International Journal of Heat and Mass Transfer 96 (2016) 703 – 704.
doi:<http://dx.doi.org/10.1016/j.ijheatmasstransfer.2015.08.073>.
URL <http://www.sciencedirect.com/science/article/pii/S0017931015303227>
- [17] G. J. Brereton, A discrete multicomponent temperature-dependent model for the evaporation of spherical droplets, International Journal of Heat and Mass Transfer 60 (2013) 512–522.
- [18] A. Y. Snegirev, Transient temperature gradient in a single-component vaporizing droplet, International Journal of Heat and Mass Transfer 65 (2013) 80–94.
- [19] H. Xiao, L. Zhao, Z. Li, W. M., G. G., Development of a simplified model for droplet vaporization, Thermal Science 20 (1) (2016) 337–345.
- [20] V. R. Subramanian, V. D. Diwakar, D. Tapriyal, Efficient macro-micro scale coupled modeling of batteries, Journal of the Electrochemical Society 152 (10) (2005) A2002–A2008.
- [21] A. Snegirev, V. A. Talalov, A. S. Tsoi, S. S. Sazhin, C. Crua, Advancement in turbulent spray modeling: the effect of internal temperature gradient in droplets, Proceedings of International Symposium on Advances in Computational Heat Transfer (16 July Bath, 2012, UK) CHT12-MP09.
- [22] T. J. Moore, M. R. Jones, Solving nonlinear heat transfer problems using variation of parameters, International Journal of Thermal Sciences 93 (2015) 29 – 35.

doi:<http://dx.doi.org/10.1016/j.ijthermalsci.2015.02.002>.

URL <http://www.sciencedirect.com/science/article/pii/S1290072915000538>

- [23] M. Mierzwiczak, W. Chen, Z.-J. Fu, The singular boundary method for steady-state nonlinear heat conduction problem with temperature-dependent thermal conductivity, *International Journal of Heat and Mass Transfer* 91 (2015) 205 – 217. doi:<http://dx.doi.org/10.1016/j.ijheatmasstransfer.2015.07.051>. URL <http://www.sciencedirect.com/science/article/pii/S0017931015007711>
- [24] J. Hristov, An approximate analytical (integral-balance) solution to a non-linear heat diffusion equation, *Thermal Science* 19 (2) (2015) 723–733.
- [25] S. Feng, X. Cui, A. Li, Fast and efficient analysis of transient nonlinear heat conduction problems using combined approximations (ca) method, *International Journal of Heat and Mass Transfer* 97 (2016) 638 – 644. doi:<http://dx.doi.org/10.1016/j.ijheatmasstransfer.2016.02.061>. URL <http://www.sciencedirect.com/science/article/pii/S0017931015316550>
- [26] D. Sarkar, A. Haji-Sheikh, A. Jain, Thermal conduction in an orthotropic sphere with circumferentially varying convection heat transfer, *International Journal of Heat and Mass Transfer* 96 (2016) 406 – 412. doi:<http://dx.doi.org/10.1016/j.ijheatmasstransfer.2016.01.027>. URL <http://www.sciencedirect.com/science/article/pii/S0017931015302891>
- [27] H. Qi, X. Guo, Transient fractional heat conduction with generalized cattaneo model, *International Journal of Heat and Mass Transfer* 76 (2014) 535 – 539. doi:<http://dx.doi.org/10.1016/j.ijheatmasstransfer.2013.12.086>. URL <http://www.sciencedirect.com/science/article/pii/S0017931014003858>
- [28] R. Khayat, J. deBruyn, M. Niknami, D. Stranges, R. Khorasany, Non-Fourier effects in macro- and micro-scale non-isothermal flow of liquids and gases. review, *International Journal of Thermal Sciences* 97 (2015) 163 – 177. doi:<http://dx.doi.org/10.1016/j.ijthermalsci.2015.06.007>. URL <http://www.sciencedirect.com/science/article/pii/S1290072915001726>
- [29] L. Zhang, X. Shang, Analytical solution to non-Fourier heat conduction as a laser beam irradiating on local surface of a semi-infinite medium,

- International Journal of Heat and Mass Transfer 85 (2015) 772 – 780.
doi:<http://dx.doi.org/10.1016/j.ijheatmasstransfer.2015.02.024>.
URL <http://www.sciencedirect.com/science/article/pii/S0017931015001878>
- [30] V. Borukhov, G. Zayats, Identification of a time-dependent source term in nonlinear hyperbolic or parabolic heat equation, International Journal of Heat and Mass Transfer 91 (2015) 1106 – 1113.
doi:<http://dx.doi.org/10.1016/j.ijheatmasstransfer.2015.07.066>.
URL <http://www.sciencedirect.com/science/article/pii/S0017931015007863>
- [31] K. Zhukovsky, Exact solution of Guyer-Krumhansl type heat equation by operational method, International Journal of Heat and Mass Transfer 96 (2016) 132 – 144.
doi:<http://dx.doi.org/10.1016/j.ijheatmasstransfer.2016.01.005>.
URL <http://www.sciencedirect.com/science/article/pii/S0017931015315611>
- [32] K. Zhukovsky, Violation of the maximum principle and negative solutions for pulse propagation in Guyer-Krumhansl model, International Journal of Heat and Mass Transfer 98 (2016) 523 – 529.
doi:<http://dx.doi.org/10.1016/j.ijheatmasstransfer.2016.03.021>.
URL <http://www.sciencedirect.com/science/article/pii/S0017931016301971>
- [33] S.-N. Li, B.-Y. Cao, On defects of taylor series approximation in heat conduction models, International Journal of Heat and Mass Transfer 98 (2016) 824 – 832.
doi:<http://dx.doi.org/10.1016/j.ijheatmasstransfer.2016.03.067>.
URL <http://www.sciencedirect.com/science/article/pii/S001793101531749X>
- [34] C. Niven, On the conduction of heat in ellipsoids of revolution, Philosophical Transactions of the Royal Society London 171 (1880) 117–151.
- [35] S. Tonini, G. E. Cossali, An analytical model of liquid drop evaporation in gaseous environment, International Journal of Thermal Sciences 57 (2012) 45–53.
- [36] W. Gao, W. Sun, K. Anderson, Y. Cheng, A. Li, Investigation on temperature distribution of flash evaporation of licl droplets released into vacuum, International Journal of Heat and Mass Transfer 74 (2014) 414 – 420. doi:<http://dx.doi.org/10.1016/j.ijheatmasstransfer.2014.03.043>.
URL <http://www.sciencedirect.com/science/article/pii/S001793101400249X>

- [37] W. long Cheng, H. Chen, L. Hu, W. wei Zhang, Effect of droplet flash evaporation on vacuum flash evaporation cooling: Modeling, *International Journal of Heat and Mass Transfer* 84 (2015) 149 – 157.
doi:<http://dx.doi.org/10.1016/j.ijheatmasstransfer.2014.12.078>.
URL <http://www.sciencedirect.com/science/article/pii/S0017931015000095>
- [38] H. Schlichting, K. Gersten, *Boundary-Layer Theory*, Springer, Berlin, 2000.
- [39] G. F. Yao, S. I. Abdel-Khalik, S. M. Ghiaasiaan, An investigation of simple evaporation models used in spray simulations, *ASME Journal of Heat Transfer* 125 (2003) 179–182.
- [40] A. E. Elwardany, I. G. Gusev, G. Castanet, F. Lemoine, S. S. Sazhin, Mono- and multi-component droplet cooling/heating and evaporation: comparative analysis of numerical models, *Atomization and Sprays* 21 (2011) 907–931.
- [41] P. Ghose, J. Patra, A. Datta, A. Mukhopadhyay, Effect of air flow distribution on soot formation and radiative heat transfer in a model liquid fuel spray combustor firing kerosene, *International Journal of Heat and Mass Transfer* 74 (2014) 143 – 155.
doi:<http://dx.doi.org/10.1016/j.ijheatmasstransfer.2014.03.001>.
URL <http://www.sciencedirect.com/science/article/pii/S0017931014002051>
- [42] G. Borghesi, E. Mastorakos, Spontaneous ignition of isolated n-heptane droplets at low, intermediate, and high ambient temperatures from a mixture-fraction perspective, *Combustion and Flame* 162 (6) (2015) 2544 – 2560.
doi:<http://dx.doi.org/10.1016/j.combustflame.2015.03.003>.
URL <http://www.sciencedirect.com/science/article/pii/S0010218015000784>
- [43] F. Snchez, A. Kaiser, B. Zamora, J. Ruiz, M. Lucas, Prediction of the lifetime of droplets emitted from mechanical cooling towers by numerical investigation, *International Journal of Heat and Mass Transfer* 89 (2015) 1190 – 1206.
doi:<http://dx.doi.org/10.1016/j.ijheatmasstransfer.2015.06.014>.
URL <http://www.sciencedirect.com/science/article/pii/S0017931015006365>

- [44] P. Wongsarivej, W. Tanthapanichakoon, A model for a non-uniform spray evaporator taking into account the effect of non-isothermal polydisperse droplets, *International Journal of Heat and Mass Transfer* 90 (2015) 1170 – 1177. doi:<http://dx.doi.org/10.1016/j.ijheatmasstransfer.2015.07.035>. URL <http://www.sciencedirect.com/science/article/pii/S0017931015007449>
- [45] H. A. El-Asrag, M. Braun, Effect of turbulence non-isotropy modeling on spray dynamics for an evaporating acetone spray jet, *International Journal of Multiphase Flow* 68 (2015) 100 – 120. doi:<http://dx.doi.org/10.1016/j.ijmultiphaseflow.2014.10.009>. URL <http://www.sciencedirect.com/science/article/pii/S0301932214001979>
- [46] S. Gavhane, S. Pati, S. Som, Evaporation of multicomponent liquid fuel droplets: Influences of component composition in droplet and vapor concentration in free stream ambience, *International Journal of Thermal Sciences* 105 (2016) 83 – 95. doi:<http://dx.doi.org/10.1016/j.ijthermalsci.2016.03.003>. URL <http://www.sciencedirect.com/science/article/pii/S1290072916302460>
- [47] D. Nguyen, J. Soria, D. Honnery, Efficiency of the lumped parameter concept and the role of liquid properties in modelling microdroplet evaporation, *Fuel* 166 (2016) 86 – 95. doi:<http://dx.doi.org/10.1016/j.fuel.2015.10.097>. URL <http://www.sciencedirect.com/science/article/pii/S0016236115011114>
- [48] B. Helgans, D. H. Richter, Turbulent latent and sensible heat flux in the presence of evaporative droplets, *International Journal of Multiphase Flow* 78 (2016) 1 – 11. doi:<http://dx.doi.org/10.1016/j.ijmultiphaseflow.2015.09.010>. URL <http://www.sciencedirect.com/science/article/pii/S0301932215002086>
- [49] H. L. Rehman, J. Weiss, P. Seers, Effect of heat conduction on droplet life time and evaporation rate under forced convection at low temperatures, *Experimental Thermal and Fluid Science* 72 (2016) 59 – 66. doi:<http://dx.doi.org/10.1016/j.expthermflusci.2015.10.030>. URL <http://www.sciencedirect.com/science/article/pii/S0894177715003064>
- [50] B. Helgans, D. H. Richter, Turbulent latent and sensible heat flux in the presence of evaporative droplets, In-

- ternational Journal of Multiphase Flow 78 (2016) 1 – 11.
doi:<http://dx.doi.org/10.1016/j.ijmultiphaseflow.2015.09.010>.
URL <http://www.sciencedirect.com/science/article/pii/S0301932215002086>
- [51] M. H. Azami, M. Savill, Modelling of spray evaporation and penetration for alternative fuels, Fuel 180 (2016) 514 – 520.
doi:<http://dx.doi.org/10.1016/j.fuel.2016.04.050>.
URL <http://www.sciencedirect.com/science/article/pii/S0016236116302150>
- [52] M. M. Yasin, R. Cant, C. Chong, S. Hochgreb, Discrete multicomponent model for biodiesel spray combustion simulation, Fuel 126 (2014) 44 – 54. doi:<http://dx.doi.org/10.1016/j.fuel.2014.02.020>.
URL <http://www.sciencedirect.com/science/article/pii/S0016236114001537>
- [53] O. Rybdylova, A. N. Osipov, S. S. Sazhin, S. Begg, M. Heikal, A combined viscous-vortex, thermal-blob and Lagrangian method for non-isothermal, two-phase flow modelling, International Journal of Heat and Fluid Flow 58 (2016) 93 – 102.
doi:<http://dx.doi.org/10.1016/j.ijheatfluidflow.2015.12.003>.
URL <http://www.sciencedirect.com/science/article/pii/S0142727X15001538>
- [54] P. Keller, T. Knorsch, M. Wensing, C. Hasse, Experimental and numerical analysis of iso-octane/ethanol sprays under gasoline engine conditions, International Journal of Heat and Mass Transfer 84 (2015) 497 – 510. doi:<http://dx.doi.org/10.1016/j.ijheatmasstransfer.2015.01.011>.
URL <http://www.sciencedirect.com/science/article/pii/S0017931015000186>
- [55] S. S. Sazhin, M. Al Qubeissi, J.-F. Xie, Two approaches to modelling the heating of evaporated droplets, International Communications in Heat and Mass Transfer 57 (2014) 353–356.
- [56] A. E. Elwardany, S. S. Sazhin, A quasi-discrete model for droplet heating and evaporation: Application to diesel and gasoline fuels, Fuel 97 (2012) 685–694.
- [57] S. S. Sazhin, P. A. Krutitskii, I. G. Gusev, M. Heikal, Transient heating of an evaporating droplet with presumed time evolution of its radius, International Journal of Heat and Mass Transfer 54 (2011) 1278–1288.
- [58] B. Sobac, P. Talbot, B. Haut, A. Rednikov, P. Colinet, A comprehensive analysis of the evaporation of a liquid spherical drop,

Journal of Colloid and Interface Science 438 (2015) 306 – 317.

doi:<http://dx.doi.org/10.1016/j.jcis.2014.09.036>.

URL <http://www.sciencedirect.com/science/article/pii/S0021979714006857>

- [59] P. Talbot, B. Sobac, A. Rednikov, P. Colinet, B. Haut, Thermal transients during the evaporation of a spherical liquid drop, International Journal of Heat and Mass Transfer 97 (2016) 803 – 817. doi:<http://dx.doi.org/10.1016/j.ijheatmasstransfer.2015.12.075>. URL <http://www.sciencedirect.com/science/article/pii/S001793101530569X>
- [60] E. Michaelides, Particles, Bubbles and Drops, World Scietific, New Jersey, 2006.
- [61] C. Crua, T. Shoba, M. Heikal, M. Gold, C. Higham, High-speed microscopic imaging of the initial stage of diesel spray formation and primary breakup, SAE International 2010-01-2247.
- [62] M. A. Jog, H. M. A., Transient heat transfer to a spheroidal liquid drop suspended in an electric field, International Journal of Heat and Fluid Flow 18 (1997) 411–418.
- [63] D. R. Lima, S. N. Farias, G. B. Lima, Mass transport in spheroids using the galerkin method, Brazilian Journal of Chemical Engineering 21 (2004) 667–680.
- [64] R. S. Alassar, Forced convection past an oblate spheroid at low to moderate reynolds numbers, ASME Journal of Heat Transfer 127 (2005) 1062–1070.
- [65] A. Richter, P. A. Nikrityuk, Drag forces and heat transfer coefficients for spherical, cuboidal and ellipsoidal particles in cross flow at sub-critical reynolds numbers, International Journal of Heat and Mass Transfer 55 (2012) 1343–1354.
- [66] N. Kishore, S. Gu, Momentum and heat transfer phenomena of spheroid particles at moderate reynolds and prandtl numbers, International Journal of Heat Mass Transfer 55 (2011) 2595–2601.
- [67] B. Sreenivasulu, B. Srinivas, K. Ramesh, Forced convection heat transfer from a spheroid to a power law fluid, International Journal of Heat and Mass Transfer 70 (2014) 71 – 80.

doi:<http://dx.doi.org/10.1016/j.ijheatmasstransfer.2013.10.065>.

URL <http://www.sciencedirect.com/science/article/pii/S0017931013009253>

- [68] B. Sreenivasulu, B. Srinivas, Mixed convection heat transfer from a spheroid to a newtonian fluid, *International Journal of Thermal Sciences* 87 (2015) 1 – 18.
doi:<http://dx.doi.org/10.1016/j.ijthermalsci.2014.08.002>.
URL <http://www.sciencedirect.com/science/article/pii/S1290072914002270>
- [69] G. Juncu, Unsteady heat transfer from an oblate/prolate spheroid, *International Journal of Heat Mass Transfer* 53 (2010) 3483–3494.
- [70] D. A. Grow, Heat and mass transfer to an elliptical particle, *Combustion and Flame* 80 (1990) 209–213.
- [71] S. Tonini, G. E. Cossali, An exact solution of the mass transport equations for spheroidal evaporating drops, *International Journal of Heat and Mass Transfer* 60 (2013) 236–240.
- [72] J. Li, J. Zhang, A theoretical study of the spheroidal droplet evaporation in forced convection, *Physics Letters A* 378 (47) (2014) 3537 – 3543. doi:<http://dx.doi.org/10.1016/j.physleta.2014.10.020>.
URL <http://www.sciencedirect.com/science/article/pii/S037596011401038X>
- [73] S. Tonini, G. Cossali, An evaporation model for oscillating spheroidal drops, *International Communications in Heat and Mass Transfer* 51 (2014) 18 – 24.
doi:<http://dx.doi.org/10.1016/j.icheatmasstransfer.2013.12.001>.
URL <http://www.sciencedirect.com/science/article/pii/S0735193313002388>
- [74] F. Mashayek, Dynamics of evaporating drops. part ii: free oscillations, *International Journal of Heat and Mass Transfer* 44 (8) (2001) 1527–1541.
- [75] S. Tonini, G. Cossali, One-dimensional analytical approach to modelling evaporation and heating of deformed drops, *International Journal of Heat and Mass Transfer* 97 (2016) 301 – 307.
doi:<http://dx.doi.org/10.1016/j.ijheatmasstransfer.2016.02.004>.
URL <http://www.sciencedirect.com/science/article/pii/S0017931015317415>

- [76] C. Sasmal, N. Nirmalkar, Momentum and heat transfer characteristics from heated spheroids in water based nanofluids, *International Journal of Heat and Mass Transfer* 96 (2016) 582 – 601. doi:<http://dx.doi.org/10.1016/j.ijheatmasstransfer.2016.01.054>. URL <http://www.sciencedirect.com/science/article/pii/S0017931015307225>
- [77] B. Samareh, J. Mostaghimi, C. Moreau, Thermocapillary migration of a deformable droplet, *International Journal of Heat and Mass Transfer* 73 (2014) 616 – 626. doi:<http://dx.doi.org/10.1016/j.ijheatmasstransfer.2014.02.022>. URL <http://www.sciencedirect.com/science/article/pii/S0017931014001392>
- [78] N. Ghata, B. D. Shaw, Computational modeling of the effects of support fibers on evaporation of fiber-supported droplets in reduced gravity, *International Journal of Heat and Mass Transfer* 77 (2014) 22 – 36. doi:<http://dx.doi.org/10.1016/j.ijheatmasstransfer.2014.04.074>. URL <http://www.sciencedirect.com/science/article/pii/S0017931014003925>
- [79] D. L. Albernaz, G. Amberg, M. Do-Quang, Simulation of a suspended droplet under evaporation with Marangoni effects, *International Journal of Heat and Mass Transfer* 97 (2016) 853 – 860. doi:<http://dx.doi.org/10.1016/j.ijheatmasstransfer.2016.02.073>. URL <http://www.sciencedirect.com/science/article/pii/S0017931015314228>
- [80] E. Wenzel, F. Kulacki, S. Garrick, Modeling and simulation of liquidliquid droplet heating in a laminar boundary layer, *International Journal of Heat and Mass Transfer* 97 (2016) 653 – 661. doi:<http://dx.doi.org/10.1016/j.ijheatmasstransfer.2016.02.067>. URL <http://www.sciencedirect.com/science/article/pii/S0017931015303598>
- [81] P. Yi, W. Long, M. Jia, J. Tian, B. Li, Development of a quasi-dimensional vaporization model for multi-component fuels focusing on forced convection and high temperature conditions, *International Journal of Heat and Mass Transfer* 97 (2016) 130 – 145. doi:<http://dx.doi.org/10.1016/j.ijheatmasstransfer.2016.01.075>. URL <http://www.sciencedirect.com/science/article/pii/S0017931015308760>
- [82] S. S. Sazhin, A. Elwardany, E. M. Sazhina, M. R. Heikal, A quasi-discrete model for heating and evaporation of complex multicompo-

nent hydrocarbon fuel droplets, *International Journal of Heat and Mass Transfer* 54 (2011) 4325–4332.

- [83] L. Chen, Z. Liu, Y. Lin, C. Zhang, Different spray droplet evaporation models for non-ideal multi-component fuels with experimental validation, *International Journal of Heat and Mass Transfer* 94 (2016) 292 – 300. doi:<http://dx.doi.org/10.1016/j.ijheatmasstransfer.2015.11.017>. URL <http://www.sciencedirect.com/science/article/pii/S0017931015310504>
- [84] T. Kitano, J. Nishio, R. Kurose, S. Komori, Evaporation and combustion of multicomponent fuel droplets, *Fuel* 136 (2014) 219 – 225. doi:<http://dx.doi.org/10.1016/j.fuel.2014.07.045>. URL <http://www.sciencedirect.com/science/article/pii/S0016236114006966>
- [85] E. Tolonen, W. L. Hallett, C. M. Monreal, Droplet evaporation behaviour of a liquid fuel from chicken litter, *Fuel* 139 (2015) 26 – 34. doi:<http://dx.doi.org/10.1016/j.fuel.2014.08.017>. URL <http://www.sciencedirect.com/science/article/pii/S0016236114007868>
- [86] J. Quio, T. Hellwig, M. Griesing, W. Pauer, H.-U. Moritz, S. Will, A. Braeuer, One-dimensional Raman spectroscopy and shadowgraphy for the analysis of the evaporation behavior of acetone/water drops, *International Journal of Heat and Mass Transfer* 89 (2015) 406 – 413. doi:<http://dx.doi.org/10.1016/j.ijheatmasstransfer.2015.05.053>. URL <http://www.sciencedirect.com/science/article/pii/S0017931015005475>
- [87] M. Manjunath, V. Raghavan, P. S. Mehta, Vaporization characteristics of suspended droplets of biodiesel fuels of indian origin and their diesel blends an experimental study, *International Journal of Heat and Mass Transfer* 88 (2015) 28 – 41. doi:<http://dx.doi.org/10.1016/j.ijheatmasstransfer.2015.04.052>. URL <http://www.sciencedirect.com/science/article/pii/S0017931015004202>
- [88] W. J. Gerken, A. V. Thomas, N. Koratkar, M. A. Oehlschlaeger, Nanofluid pendant droplet evaporation: Experiments and modeling, *International Journal of Heat and Mass Transfer* 74 (2014) 263 – 268. doi:<http://dx.doi.org/10.1016/j.ijheatmasstransfer.2014.03.031>. URL <http://www.sciencedirect.com/science/article/pii/S0017931014002373>

- [89] S. Basu, A. Miglani, Combustion and heat transfer characteristics of nanofluid fuel droplets: A short review, *International Journal of Heat and Mass Transfer* 96 (2016) 482 – 503. doi:<http://dx.doi.org/10.1016/j.ijheatmasstransfer.2016.01.053>. URL <http://www.sciencedirect.com/science/article/pii/S0017931015311601>
- [90] Y. Wei, W. Deng, R.-H. Chen, Effects of insoluble nanoparticles on nanofluid droplet evaporation, *International Journal of Heat and Mass Transfer* 97 (2016) 725 – 734. doi:<http://dx.doi.org/10.1016/j.ijheatmasstransfer.2016.02.052>. URL <http://www.sciencedirect.com/science/article/pii/S0017931015313764>
- [91] H. Grosshans, M. Griesing, M. Mnckedieck, T. Hellwig, B. Walther, S. R. Gopireddy, R. Sedelmayer, W. Pauer, H.-U. Moritz, N. A. Urbanetz, E. Gutheil, Numerical and experimental study of the drying of bi-component droplets under various drying conditions, *International Journal of Heat and Mass Transfer* 96 (2016) 97 – 109. doi:<http://dx.doi.org/10.1016/j.ijheatmasstransfer.2015.12.062>. URL <http://www.sciencedirect.com/science/article/pii/S001793101501087X>
- [92] G. V. Kuznetsov, M. V. Piskunov, P. A. Strizhak, Evaporation, boiling and explosive breakup of heterogeneous droplet in a high-temperature gas, *International Journal of Heat and Mass Transfer* 92 (2016) 360 – 369. doi:<http://dx.doi.org/10.1016/j.ijheatmasstransfer.2015.08.061>. URL <http://www.sciencedirect.com/science/article/pii/S0017931015303069>
- [93] G. J. Oberman, T. W. Farrell, Modelling of the evaporation of a droplet suspended in a binary atmosphere, *International Journal of Heat and Mass Transfer* 92 (2016) 381 – 393. doi:<http://dx.doi.org/10.1016/j.ijheatmasstransfer.2015.08.080>. URL <http://www.sciencedirect.com/science/article/pii/S0017931015009254>
- [94] M. Sadafi, I. Jahn, A. Stilgoe, K. Hooman, A theoretical model with experimental verification for heat and mass transfer of saline water droplets, *International Journal of Heat and Mass Transfer* 81 (2015) 1 – 9. doi:<http://dx.doi.org/10.1016/j.ijheatmasstransfer.2014.10.005>. URL <http://www.sciencedirect.com/science/article/pii/S0017931014008904>
- [95] D. Tarlet, E. Mura, C. Josset, J. Bellettre, C. Allouis, P. Massoli, Distribution of thermal energy of child-droplets

- issued from an optimal micro-explosion, *International Journal of Heat and Mass Transfer* 77 (2014) 1043 – 1054.
doi:<http://dx.doi.org/10.1016/j.ijheatmasstransfer.2014.06.054>.
URL <http://www.sciencedirect.com/science/article/pii/S0017931014005262>
- [96] J. Shinjo, J. Xia, L. C. Ganippa, A. Megaritis, Physics of puffing and microexplosion of emulsion fuel droplets, *Physics of Fluids* 26 (10).
doi:<http://dx.doi.org/10.1063/1.4897918>.
URL <http://scitation.aip.org/content/aip/journal/pof2/26/10/10.1063/1.4897918>
- [97] D. Tarlet, C. Josset, J. Bellettre, Comparison between unique and coalesced water drops in micro-explosions scanned by differential calorimetry, *International Journal of Heat and Mass Transfer* 95 (2016) 689 – 692. doi:<http://dx.doi.org/10.1016/j.ijheatmasstransfer.2015.12.054>.
URL <http://www.sciencedirect.com/science/article/pii/S0017931015310814>
- [98] M. M. Avulapati, L. C. Ganippa, J. Xia, A. Megaritis, Puffing and micro-explosion of dieselbiodieselethanol blends, *Fuel* 166 (2016) 59 – 66. doi:<http://dx.doi.org/10.1016/j.fuel.2015.10.107>.
URL <http://www.sciencedirect.com/science/article/pii/S0016236115011217>
- [99] S. S. Sazhin, M. Al Qubeissi, R. Kolodnytska, A. Elwardany, R. Nasiri, M. Heikal, Modelling of biodiesel fuel droplet heating and evaporation, *Fuel* 115 (2014) 559–572.
- [100] M. A. Qubeissi, S. S. Sazhin, C. Crua, J. Turner, M. R. Heikal, Modelling of biodiesel fuel droplet heating and evaporation: Effects of fuel composition, *Fuel* 154 (2015) 308 – 318. doi:<http://dx.doi.org/10.1016/j.fuel.2015.03.051>.
URL <http://www.sciencedirect.com/science/article/pii/S0016236115003476>
- [101] N. Hashimoto, H. Nomura, M. Suzuki, T. Matsumoto, H. Nishida, Y. Ozawa, Evaporation characteristics of a palm methyl ester droplet at high ambient temperatures, *Fuel* 143 (2015) 202 – 210. doi:<http://dx.doi.org/10.1016/j.fuel.2014.11.057>.
URL <http://www.sciencedirect.com/science/article/pii/S0016236114011612>
- [102] S. S. Sazhin, M. Al Qubeissi, R. Nasiri, V. M. Gunko, A. E. Elwardany, F. Lemoine, F. Grisch, M. R. Heikal, A multi-dimensional quasi-discrete model for the analysis of diesel fuel droplet heating and evaporation, *Fuel* 129 (2014) 238–266.

- [103] V. M. Gunko, R. Nasiri, S. S. Sazhin, F. Lemoine, F. Grisch, A quantum chemical study of the processes during the evaporation of real-life diesel fuel droplets, *Fluid Phase Equilibria* 356 (2013) 146–156.
- [104] S. Bair, The pressure and temperature dependence of volume and viscosity of four diesel fuels, *Fuel* 135 (2014) 112 – 119. doi:<http://dx.doi.org/10.1016/j.fuel.2014.06.035>. URL <http://www.sciencedirect.com/science/article/pii/S0016236114006012>
- [105] M. A. Qubeissi, S. S. Sazhin, J. Turner, S. Begg, C. Crua, M. Heikal, Modelling of gasoline fuel droplets heating and evaporation, *Fuel* 159 (2015) 373–384.
- [106] A. E. Elwardany, S. S. Sazhin, A. Farooq, Modelling of heating and evaporation of gasoline fuel droplets: a comparative analysis of approximations, *Fuel* 111 (2013) 643–647.
- [107] L. Cai, H. Pitsch, Optimized chemical mechanism for combustion of gasoline surrogate fuels, *Combustion and Flame* 162 (5) (2015) 1623 – 1637. doi:<http://dx.doi.org/10.1016/j.combustflame.2014.11.018>. URL <http://www.sciencedirect.com/science/article/pii/S0010218014003721>
- [108] Y. Chang, M. Jia, Y. Li, Y. Liu, M. Xie, H. Wang, R. D. Reitz, Development of a skeletal mechanism for diesel surrogate fuel by using a decoupling methodology, *Combustion and Flame* 162 (10) (2015) 3785 – 3802. doi:<http://dx.doi.org/10.1016/j.combustflame.2015.07.016>. URL <http://www.sciencedirect.com/science/article/pii/S0010218015002175>
- [109] Y. Ra, R. D. Reitz, A combustion model for multi-component fuels using a physical surrogate group chemistry representation (psgcr), *Combustion and Flame* 162 (10) (2015) 3456 – 3481. doi:<http://dx.doi.org/10.1016/j.combustflame.2015.05.014>. URL <http://www.sciencedirect.com/science/article/pii/S0010218015001522>
- [110] J. Yu, Y. Ju, X. Gou, Surrogate fuel formulation for oxygenated and hydrocarbon fuels by using the molecular structures and functional groups, *Fuel* 166 (2016) 211 – 218. doi:<http://dx.doi.org/10.1016/j.fuel.2015.10.085>. URL <http://www.sciencedirect.com/science/article/pii/S0016236115010959>

- [111] H. M. Poon, K. M. Pang, H. K. Ng, S. Gan, J. Schramm, Development of multi-component diesel surrogate fuel models part ii: Validation of the integrated mechanisms in 0-d kinetic and 2-d {CFD} spray combustion simulations, *Fuel* 181 (2016) 120 – 130. doi:<http://dx.doi.org/10.1016/j.fuel.2016.04.114>. URL <http://www.sciencedirect.com/science/article/pii/S0016236116302794>
- [112] A. E. Elwardany, S. S. Sazhin, H. G. Im, A new formulation of physical surrogates of FACE a gasoline fuel based on heating and evaporation characteristics, *Fuel* 176 (2016) 56 – 62. doi:<http://dx.doi.org/10.1016/j.fuel.2016.02.041>. URL <http://www.sciencedirect.com/science/article/pii/S0016236116001629>
- [113] O. S. Abianeh, M. A. Oehlschlaeger, C.-J. Sung, A surrogate mixture and kinetic mechanism for emulating the evaporation and autoignition characteristics of gasoline fuel, *Combustion and Flame* 162 (10) (2015) 3773 – 3784. doi:<http://dx.doi.org/10.1016/j.combustflame.2015.07.015>. URL <http://www.sciencedirect.com/science/article/pii/S0010218015002163>
- [114] M. Su, C. Chen, Heating and evaporation of a new gasoline surrogate fuel: A discrete multicomponent modeling study, *Fuel* 161 (2015) 215 – 221. doi:<http://dx.doi.org/10.1016/j.fuel.2015.08.048>. URL <http://www.sciencedirect.com/science/article/pii/S0016236115008571>
- [115] P. Yi, W. Long, M. Jia, L. Feng, J. Tian, Development of an improved hybrid multi-component vaporization model for realistic multi-component fuels, *International Journal of Heat and Mass Transfer* 77 (2014) 173 – 184. doi:<http://dx.doi.org/10.1016/j.ijheatmasstransfer.2014.05.008>. URL <http://www.sciencedirect.com/science/article/pii/S0017931014004086>
- [116] S. Tonini, G. E. Cossali, A novel formulation of multi-component drop evaporation models for spray applications, *International Journal of Thermal Sciences* 89 (2015) 245 – 253. doi:<http://dx.doi.org/10.1016/j.ijthermalsci.2014.10.016>. URL <http://www.sciencedirect.com/science/article/pii/S1290072914003007>
- [117] S. Tonini, G. Cossali, A multi-component drop evaporation model based on analytical solution of stefanmaxwell equations, *Interna-*

- tional Journal of Heat and Mass Transfer 92 (2016) 184 – 189.
doi:<http://dx.doi.org/10.1016/j.ijheatmasstransfer.2015.08.014>.
URL <http://www.sciencedirect.com/science/article/pii/S0017931015301551>
- [118] X. Ma, F. Zhang, K. Han, G. Song, Numerical modeling of acetone-butanol-ethanol and diesel blends droplet evaporation process, Fuel 174 (2016) 206 – 215. doi:<http://dx.doi.org/10.1016/j.fuel.2016.01.091>.
URL <http://www.sciencedirect.com/science/article/pii/S0016236116001125>
- [119] G. Brenn, L. J. Deviprasath, F. Durstb, C. Finkc, Evaporation of acoustically levitated multi-component liquid droplets, International Journal of Heat and Mass Transfer 50 (25-26) (2007) 5073–5086.
- [120] N. Padoin, A. T. D. Toe, L. P. Rangel, K. Ropelato, C. Soares, Heat and mass transfer modeling for multicomponent multiphase flow with CFD, International Journal of Heat and Mass Transfer 73 (2014) 239 – 249. doi:<http://dx.doi.org/10.1016/j.ijheatmasstransfer.2014.01.075>.
URL <http://www.sciencedirect.com/science/article/pii/S0017931014001161>
- [121] G. Jarvas, J. Kontos, J. Hancsok, A. Dallos, Modeling ethanolblended gasoline droplet evaporation using COSMO-RS theory and computation fluid dynamics, International Journal of Heat and Mass Transfer 84 (2015) 1019 – 1029. doi:<http://dx.doi.org/10.1016/j.ijheatmasstransfer.2014.12.046>.
URL <http://www.sciencedirect.com/science/article/pii/S0017931014011545>
- [122] A. T. O. D. Toe, N. Padoin, K. Ropelato, C. Soares, Cross diffusion effects in the interfacial mass and heat transfer of multicomponent droplets, International Journal of Heat and Mass Transfer 85 (2015) 830 – 840. doi:<http://dx.doi.org/10.1016/j.ijheatmasstransfer.2015.01.131>.
URL <http://www.sciencedirect.com/science/article/pii/S0017931015001490>
- [123] R. B. Bird, W. E. Stewart, E. N. Lightfoot, Transport Phenomena, John Wiley & Sons, Inc., New York, 2002.
- [124] M. Arias-Zugasti, P. L. Garcia-Ybarra, J. L. Castillo, Efficient calculation of multicomponent diffusion fluxes based on kinetic theory, Combustion and Flame 163 (2016) 540 – 556. doi:<http://dx.doi.org/10.1016/j.combustflame.2015.10.033>.
URL <http://www.sciencedirect.com/science/article/pii/S0010218015003892>

- [125] Y. Xin, W. Liang, W. Liu, T. Lu, C. K. Law, A reduced multicomponent diffusion model, *Combustion and Flame* 162 (1) (2015) 68 – 74.
doi:<http://dx.doi.org/10.1016/j.combustflame.2014.07.019>.
URL <http://www.sciencedirect.com/science/article/pii/S0010218014002144>
- [126] N. A. Fuchs, *Evaporation and Droplet Growth in Gaseous Media*, Pergamon Press, London, 1959.
- [127] R. Payri, J. P. Viera, Y. Pei, S. Som, Experimental and numerical study of lift-off length and ignition delay of a two-component diesel surrogate, *Fuel* 158 (2015) 957 – 967.
doi:<http://dx.doi.org/10.1016/j.fuel.2014.11.072>.
URL <http://www.sciencedirect.com/science/article/pii/S0016236114011764>
- [128] J.-F. Xie, S. S. Sazhin, B.-Y. Cao, Molecular dynamics study of the processes in the vicinity of the n-dodecane vapour/liquid interface, *Physics of Fluids* 23 (11) (2011) 112104.
- [129] S. S. Sazhin, I. N. Shishkova, M. Al Qubeissi, A self-consistent kinetic model for droplet heating and evaporation, *International Journal of Heat and Mass Transfer* 93 (2016) 1206–1217.
- [130] V. M. Gunko, R. Nasiri, S. S. Sazhin, A study of the evaporation and condensation of n-alkane clusters and nanodroplets using quantum chemical methods, *Fluid Phase Equilibria* 366 (2014) 99–107.
- [131] V. M. Gunko, R. Nasiri, S. S. Sazhin, Effects of the surroundings and conformerisation of n-dodecane molecules on evaporation/condensation processes, *Journal of Chemical Physics* 142 (3) (2015) 034502.
- [132] R. Nasiri, V. M. Gunko, S. S. Sazhin, The effects of internal molecular dynamics on the evaporation/condensation of n-dodecane, *Theoretical Chemistry Accounts* 134 (2015) N83.
- [133] S. S. Sazhin, V. M. Gunko, R. Nasiri, Quantum-chemical analysis of the processes at the surfaces of diesel fuel droplets, *Fuel* 165 (2016) 405–412.
- [134] I. K. Ortega, O. Kupiainen, T. Kurtén, T. Olenius, O. Wilkman, M. J. McGrath, V. Loukonen, H. Vehkamäki, From quantum chemical formation free energies to evaporation rates, *Atmospheric Chemistry and Physics* 12 (2012) 225–235.

- [135] O. Kupiainen, I. K. Ortega, T. Kurtén, , H. Vehkamäki, Amine substitution into sulfuric acid - ammonia clusters, *Atmospheric Chemistry and Physics* 12 (2012) 3591–3599.
- [136] A. Lotfi, J. Vrabec, J. Fischer, Evaporation from a free liquid surface, *International Journal of Heat and Mass Transfer* 73 (2014) 303 – 317.
doi:<http://dx.doi.org/10.1016/j.ijheatmasstransfer.2014.02.010>.
URL <http://www.sciencedirect.com/science/article/pii/S0017931014001276>
- [137] A. Lotfi, J. Vrabec, J. Fischer, Evaporation from a free liquid surface, *International Journal of Heat and Mass Transfer* 73 (2014) 303–317.
- [138] H. Mizuguchi, G. Nagayama, T. Tsuruta, Molecular dynamics study on evaporation coefficient of biodiesel fuel, *Seventh International Conference on Flow Dynamics* (2010) 386.
- [139] B.-Y. Cao, J.-F. Xie, S. S. Sazhin, Molecular dynamics study on evaporation and condensation of n-dodecane at liquid-vapor phase equilibria, *AIP The Journal of Chemical Physics* 134 (16) (2011) 164309.
- [140] S. S. Sazhin, M. R. Heikal, Droplet heating and evaporation - recent results and unsolved problems, *Computational Thermal Sciences* 4 (6) (2012) 485–496.
- [141] C. Crua, M. R. Heikal, M. R. Gold, Microscopic imaging of the initial stage of diesel spray formation, *Fuel* 157 (2015) 140 – 150.
doi:<http://dx.doi.org/10.1016/j.fuel.2015.04.041>.
URL <http://www.sciencedirect.com/science/article/pii/S0016236115004391>
- [142] G. Castanet, L. Perrin, O. Caballina, F. Lemoine, Evaporation of closely-spaced interacting droplets arranged in a single row, *International Journal of Heat and Mass Transfer* 93 (2016) 788 – 802.
doi:<http://dx.doi.org/10.1016/j.ijheatmasstransfer.2015.09.064>.
URL <http://www.sciencedirect.com/science/article/pii/S0017931015301782>
- [143] R. Volkov, G. Kuznetsov, P. Strizhak, Influence of droplet concentration on evaporation in a high-temperature gas, *International Journal of Heat and Mass Transfer* 96 (2016) 20 – 28.
doi:<http://dx.doi.org/10.1016/j.ijheatmasstransfer.2016.01.029>.
URL <http://www.sciencedirect.com/science/article/pii/S0017931015315970>

- [144] K. G. M., F. G. K., Thermodynamic Models for Industrial Applications, John Wiley & Sons, Inc., New York, 2010.
- [145] S. S. Sazhin, I. N. Shishkova, M. R. Heikal, Kinetic modelling of fuel droplet heating and evaporation: calculations and approximations, International J of Engineering Systems Modelling and Simulation 2 (3) (2010) 169–176.